Solid Earth, 11, 437–467, 2020
https://doi.org/10.5194/se-11-437-2020


Solid Earth
Open Access
EGU

# Cenozoic deformation in the Tauern Window (Eastern Alps) constrained by in situ Th-Pb dating of fissure monazite

**Emmanuelle Ricchi[1], Christian A. Bergemann[2], Edwin Gnos[3], Alfons Berger[4], Daniela Rubatto[4,5], Martin J. Whitehouse[6], and Franz Walter[7]**

[1]Department of Earth Sciences, University of Geneva, Rue des Maraîchers 13, 1205 Geneva, Switzerland
[2]Institute of Geosciences, Heidelberg University, Im Neuenheimer Feld 236, 69120 Heidelberg, Germany
[3]Natural History Museum of Geneva, Route de Malagnou 1, 1208 Geneva, Switzerland
[4]Institute of Geological Sciences, University of Bern, Baltzerstrasse 1+3, 3012 Bern, Switzerland
[5]Institute of Earth Sciences, University of Lausanne, Geopolis, 1015 Lausanne, Switzerland
[6]Swedish Museum of Natural History, P.O. Box 50007, 104-05 Stockholm, Sweden
[7]Institut für Erdwissenschaften, Karl-Franzens-Universität, Universitätsplatz 2, 8010 Graz, Austria

**Correspondence:** Emmanuelle Ricchi (emmanuelle.ricchi@unige.ch)

Received: 21 October 2019 – Discussion started: 30 October 2019
Revised: 14 February 2020 – Accepted: 24 February 2020 – Published: 3 April 2020

**Abstract.** Thorium–lead (Th-Pb) crystallization ages of hydrothermal monazites from the western, central and eastern Tauern Window provide new insights into Cenozoic tectonic evolution of the Tauern metamorphic dome. Growth domain crystallization ages range from $21.7 \pm 0.4$ to $10.0 \pm 0.2$ Ma. Three major periods of monazite growth are recorded between ~22–20 (peak at 21 Ma), 19–15 (major peak at 17 Ma) and 14–10 Ma (major peak around 12 Ma), respectively, interpreted to be related to prevailing N–S shortening, in association with E–W extension, beginning strike-slip movements and reactivation of strike-slip faulting. Fissure monazite ages largely overlap with zircon and apatite fission track data. Besides tracking the thermal evolution of the Tauern dome, monazite dates reflect episodic tectonic movement along major shear zones that took place during the formation of the dome. Geochronological and structural data from the Pfitschtal area in the western Tauern Window show the existence of two cleft generations separated in time by 4 Ma and related to strike-slip to oblique-slip faulting. Moreover, these two phases overprint earlier phases of fissure formation.

**Highlights.**

- In situ dating of hydrothermal monazite-(Ce).
- New constraints on the exhumation of the Tauern metamorphic dome.
- Distinct tectonic pulses recorded from east to west.

## 1 Introduction

In situ thorium–lead (Th-Pb) dating of hydrothermal fissure monazite-(Ce) (in the following simply monazite) has recently been demonstrated to be a reliable method for dating tectonic activity under retrograde metamorphic conditions (Bergemann et al., 2017, 2018, 2019, 2020; Berger et al., 2013; Fitz-Diaz et al., 2019; Gasquet et al., 2010; Gnos et al., 2015; Grand'Homme et al., 2016a; Janots et al., 2012; Ricchi et al., 2019). These studies conducted through the entire Alpine orogenic belt allowed constraining tectonic activity in relation with exhumation and fault activity under retrograde lower greenschist to sub-greenschist facies metamorphic conditions.

Hydrothermal fissure monazite, concentrating light rare earth elements (LREE), Th and U, generally crystallizes in Ca-poor lithologies, outside the stability field of titanite or epidote / allanite. However, once formed, hydrothermal processes may cause dissolution–reprecipitation events leading to resetting of the monazite Th-Pb decay

Published by Copernicus Publications on behalf of the European Geosciences Union.

system in parts of the crystal. Chemically and isotopically homogeneous crystals indicate a single, rapid growth episode (e.g. Grand'Homme et al., 2016a). However, crystals showing different growth domains indicative of successive growth episodes are more common. In other cases, parts of, or entire, grains display a patchy zoning due to dissolution–reprecipitation processes (e.g. Ayers et al., 1999; Grand'Homme et al., 2016b). These processes involve element fractionation resulting in crystal zones with often distinct Th/U values (Seydoux-Guillaume et al., 2012).

The advantage of using hydrothermal monazite for dating tectonic activity is related to the high closure temperature of monazite of > 800 °C, implying that diffusion in monazite is negligible (Cherniak et al., 2004; Gardés et al., 2006, 2007) under $P$–$T$ conditions at or below 450–500 °C and 0.3–0.4 GPa (e.g. Mullis et al., 1994; Mullis, 1996; Sharp et al., 2005) where hydrothermal fissures form. Fissure monazites date crystallization following chemical disequilibrium within a fissure. This causes a dissolution–precipitation cycle that may include dissolution or partial dissolution of existing fissure monazite. This has the consequence that late dissolution–precipitation steps may be well recorded, whereas earlier growth domains may be completely destroyed. Thus, monazite crystallization due to chemical disequilibrium is interpreted as being related to tectonic activity (e.g. volume change, fissure propagation, exposure of fresh host rock, delamination of fissure wall, seismic activity, fluid loss or gain).

Recent studies have shown that fissure monazite typically forms between generally lower to higher 200–400 °C (Gnos et al., 2015; Janots et al., 2019). For this reason, fissure monazite ages are generally interpreted as dating crystallization or re-crystallization. Monazite geochronology can thus be utilized to constrain shear and damage zone activity under greenschist and very low-grade metamorphic conditions at least down to 200 °C (e.g. Bergemann et al., 2017, 2018; Gnos et al., 2015).

Fissures and clefts develop close to the brittle–ductile transition (< 450 °C; Mullis, 1996) and are usually oriented perpendicular to the foliation and lineation of the host rock (Gnos et al., 2015). Fissures are generally straight when they form and either became enlarged by subsequent tectonic activity to form fluid-filled decimetre- to metre-sized clefts, displaying a more open shape with rounded surfaces (e.g. Ricchi et al., 2019) when the stress field retains the same orientation, or become completely filled to form mineral veins. However, they may show a complex shape when the stress field direction changes during deformation. Fluid inclusion studies (e.g. Mullis, 1996) show that clefts generally suffered several deformation episodes.

Interaction of the fluid that fills the fissures with the surrounding rock leads to dissolution of minerals in the wall rock and mineral precipitation in the fissure. As long as deformation continues, fluid-filled clefts will react to deformation via dissolution–precipitation cycles due to disequilibrium between fluid, rock wall and mineral assemblage within the cleft (e.g. Putnis, 2009). Thus, hydrothermal minerals like monazite do not only grow following the initial fissure formation but form, continue to grow or dissolve during subsequent deformation stages. The timing of these growth or alteration stages may not always be resolvable with the precision of currently available geochronological methods, but different growth stages may be distinguishable through differences in the chemical composition (Grand'Homme et al., 2018). In contrast to the surrounding country rock, the fissures and clefts remain highly reactive at low temperature due to the presence of fluids. For this reasons, deformation steps during brittle deformation may be registered through mineral growth or recrystallization in clefts (e.g. Berger et al., 2013) down to conditions where clay minerals form in fault gauges.

The Tauern Window (TW) is a thermal and structural dome of the eastern Alps (Fig. 1) exhumed over a period of about 30 Ma starting from the Early Oligocene (e.g. Rosenberg et al., 2018; Schmid et al., 2013). Previous monazite crystallization ages obtained in the eastern subdome of the TW record tectonic activity between $19.0 \pm 0.5$ and $15.0 \pm 0.5$ Ma (Gnos et al., 2015). In the current study, monazite geochronology is extended to the entire TW in order to investigate its Cenozoic deformation history. We particularly aim to establish a chronological record for the younger exhumation history recorded by fissure monazite crystallization, to be compared with known deformation phases.

A total of 23 monazite grains together with provenance data, and in some cases host-rock information, were dated (Table 1). Seven grains come from the western limb of the TW (INNB1 ZEI1, SCHR1, MAYR4, PFIT1, BURG2 and PLAN1; samples 1–7; Fig. 1), another seven grains come from the eastern border of the western subdome (central TW; SCHEI1, HOPF2, GART1, NOWA3, GART3, STEI2 and KNOR1; samples 8–14; Fig. 1), and nine grains were collected in the eastern subdome (KAIS6, SALZ18, LOHN4, ORT1, EUKL2, HOAR1, MOKR1, SAND1 and REIS1; samples 15–25; Fig. 1, Table 1). In order to capture at best the tectonic activity during the exhumation of the TW, the investigated samples were selected in a way that gives priority to sample localities in regions affected by major fault zones and at lithological boundaries. In the following, we will discuss the ages in terms of sample ID numbers (1–25) provided in Table 1.

## 2 Geologic settings

In the largest tectonic window of the Austroalpine nappe stack, the TW, Penninic (Glockner nappe system and Matrei zone; Fig. 1) and Subpenninic nappes (mainly the Venediger Duplex) are exposed (e.g. Schmid et al., 2013; Fig. 1). The TW metamorphic and structural dome consists of two subdomes, with E–W-striking upright folds in the internal parts

**Table 1.** Summary of monazite samples investigated in this study and by Gnos et al. (2015). Samples name, number, location, host-rock lithology, metamorphic degree and fissure mineral association are provided. Samples with approximate finding location are marked with "approx.".

| Locality | Sample | No. | Latitude (° N) | Longitude (° E) | Remark | Host rock | Host rock Alpine met. | Fissure mineral association | Reference | Ion probe |
|---|---|---|---|---|---|---|---|---|---|---|
| Western Tauern Window | | | | | | | | | | |
| Innerböden, Zillertal, Tyrol, Austria | INNB1 | 1 | 47°05.850′ | 011°47.667′ | approx. | gneiss | AM | Qtz, Adl, Chl | this study | SwissSIMS |
| Zeischalm, Valsertal, Tyrol, Austria | ZEI1 | 2 | 47°01.400′ | 011°35.767′ | approx. | gneiss | AM | Qtz, Adl, Chl | this study | SwissSIMS |
| Schrammacher, Zillertal, Tyrol, Italy | SCHR1 | 3 | 47°01.47′ | 011°38.60′ | approx. | gneiss | AM | Qtz, Chl, Adl, Rt, Snt | this study | NordSIMS |
| Kluppen, Pfitschtal, South Tyrol, Italy | MAYR4 | 4 | 47°00.400′ | 011°36.217′ | approx. | gneiss | AM | Qtz, Adl, Ant, Cc, Rt, Xnt | this study | SwissSIMS |
| Pfitscherjoch, Tyrol, Austria | PFIT1 | 5 | 46°59.65′ | 011°39.60′ | | mica schist | AM | Qtz, Hm, Adl, Trm, Rt, Brk, Ant, Syn, Asc | this study | NordSIMS |
| Burgumalpe, Pfitschtal, South Tyrol, Italy[a] | BURG2 | 6 | 46°55.217′ | 011°33.350′ | approx. | serpentinite | GAT | Ilm, Rt, Cc | this study | SwissSIMS |
| Schwarzenbach, Ahrntal, South Tyrol, Italy | PLAN1 | 7 | 46°58.641′ | 011°53.302′ | approx. | gneiss | AM | Qtz, Adl | this study | SwissSIMS |
| Central Tauern Window | | | | | | | | | | |
| Scheissgraben (Kotriesen), Habachtal, Salzburg, Austria | SCHEI1 | 8 | 47°14.483′ | 012°18.667′ | | mica schist | UGS | Qtz, Ab, Ant, Ank, Rt | this study | SwissSIMS |
| Hopffeldboden, Obersulzbachtal, Salzburg, Austria | HOPF2 | 9 | 47°12.278′ | 012°14.844′ | | gneiss | GAT | Qtz, Ilm, Rt, Ant, Brk, Asc, Syn, Ap, Chl, Lm | this study | NordSIMS |
| Hopffeldgraben, Obersulzbachtal, Salzburg, Austria | GART1 | 10 | 47°12.100′ | 012°14.167′ | | gneiss | GAT | Qtz, Adl, Ant, Rtl, Asc + Bt and Chl from EDS analyses | this study | SwissSIMS |
| Wildenkarer Wald, Habachtal, Salzburg, Austria | NOWA3 | 11 | 47°12.633′ | 012°20.000′ | approx. | gneiss | GAT | Qtz, Ab, Adl | this study | SwissSIMS |
| Beryller, Untersulzbachtal, Salzburg, Austria | GART3 | 12 | 47°11.250′ | 012°18.517′ | approx. | gneiss | AM | Qtz, Adl | this study | SwissSIMS |
| Sattelkar, Obersulzbachtal, Salzburg, Austria | STEI2 | 13 | 47°09.783′ | 012°17.250′ | approx. | gneiss | AM | Qtz, Adl, Rt, Chl | this study | SwissSIMS |
| Innerer Knorrkogel, East Tyrol, Austria | KNOR1 | 14 | 47°06.117′ | 012°25.183′ | | gneiss | AM | Adl, Qtz, Chl | this study | NordSIMS |
| Eastern Tauern Window | | | | | | | | | | |
| Kaiserer Steinbruch, Hüttwinkeltal, Rauris, Salzburg, Austria[b] | KAIS6 | 15 | 47°07.787′ | 012°58.708′ | | meta-arenite | GAT | Qtz, Adl, Trm, Cc, Hm, Rt, Chl | this study | NordSIMS |
| Lohninger Quarry, Hüttwinkeltal, Rauris, Salzburg, Austria[b] | SALZ18 | 16a | 47°07.20′ | 012°59.33′ | | meta-arenite | GAT | Qtz, Adl, Trm, Cc, Hm, Rt, Chl | this study | NordSIMS |
| Lohninger Quarry, Hüttwinkeltal, Rauris, Salzburg, Austria[b] | T3 | 16b | 47°07.20′ | 012°59.33′ | | meta-arenite | GAT | Alb, Qtz, Trm, Hm, Rt | Gnos et al. (2015) | NordSIMS |
| Lohninger Quarry, Hüttwinkeltal, Rauris, Salzburg, Austria[b] | LOHN4 | 17 | 47°07.20′ | 012°59.33′ | | meta-arenite | GAT | Qtz, Adl, Trm, Cc, Hm, Rt, Chl | this study | NordSIMS |
| Ortberg bei Böckstein, Salzburg, Austria | ORT1 | 18 | 47°05.150′ | 013°04.217′ | | granitic gneiss | GAT | Qtz, Adl, Rt, Chl, Ap | this study | SwissSIMS |
| Euklaskluft, Griesswies, Salzburg, Austria | EUKL2 | 19a | 47°04.683′ | 012°57.250′ | | Bt-Mu schist | GAT | Alb, Pyr, Qtz, Rt, Chl, euclase, Xnt, goethite–todorokite–nordstrandite | this study | NordSIMS |
| Euklaskluft, Griesswies, Salzburg, Austria | T2 | 19b | 47°04.683′ | 012°57.250′ | | Bt-Mu schist | GAT | Alb, Pyr, Qtz, Rt, Chl, euclase, Xnt, goethite-todorokite-nordstrandite | Gnos et al. (2015) | NordSIMS |
| Hocharn, Kärnten, Austria | HOAR1 | 20 | 47°04.500′ | 012°56.083′ | | granitic gneiss | GAT | Qtz, Ab, Rt | this study | SwissSIMS |
| Erfurter Steig, Rauris, Salzburg, Austria | T1 | 21 | 47°04.133′ | 012°57.917′ | | Bt-Mu schist | GAT | Qtz, Ab, Adl, phenakite, Rt, Cc | Gnos et al. (2015) | NordSIMS |
| Gjaidtroghöhe, Grosses Fleisstal, Kärnten, Austria | T4 | 22 | 47°03.783′ | 012°54.650′ | | gneiss | GAT | Qtz, Ab, Ant/Rt, Chl, Cc | Gnos et al. (2015) | NordSIMS |
| Mokritzen, Kleines Fleisstal, Kärnten, Austria | MOKR1 | 23 | 47°03.033′ | 012°53.983′ | | graphite-bearing schist | GAT | Qtz, Sid | this study | SwissSIMS |
| Sandkopf, Grosses Zirknitztal, Kärnten, Austria | SAND1 | 24 | 47°01.983′ | 012°56.05′ | | banded gneiss | GAT | Qtz, Adl, Chl, Sid, Ant | this study | SwissSIMS |
| Kleiner Reisseck, Reisseckgruppe, Kärnten, Austria | REIS1 | 25 | 46°56.950′ | 013°22.433′ | | banded gneiss | AM | Qtz, Ant, Ab, Chl | this study | SwissSIMS |

Ab – albite; Adl – adularia; Ank – ankerite; Ant – anatase; Ap – fluorapatite; Asc – aeschynite; Brk – brookite; Cc – calcite; Chl – chlorite; Clc – clinochlore; Hm – hematite; Ilm – ilmenite; Lm – limonite; Pyr – pyrite; Qtz – quartz; Rt – rutile; Sd – siderite; Snt – senaite; Str – strontianite; Syn – synchisite; Trm – tourmaline; Xnt – xenotime; Alpine metamorphism: AM (amphibolite facies), GAT (greenschist–amphibolite transition), UGS (upper greenschist facies). [a] Bloc in glacial moraine. [b] Bloc in rock slide.

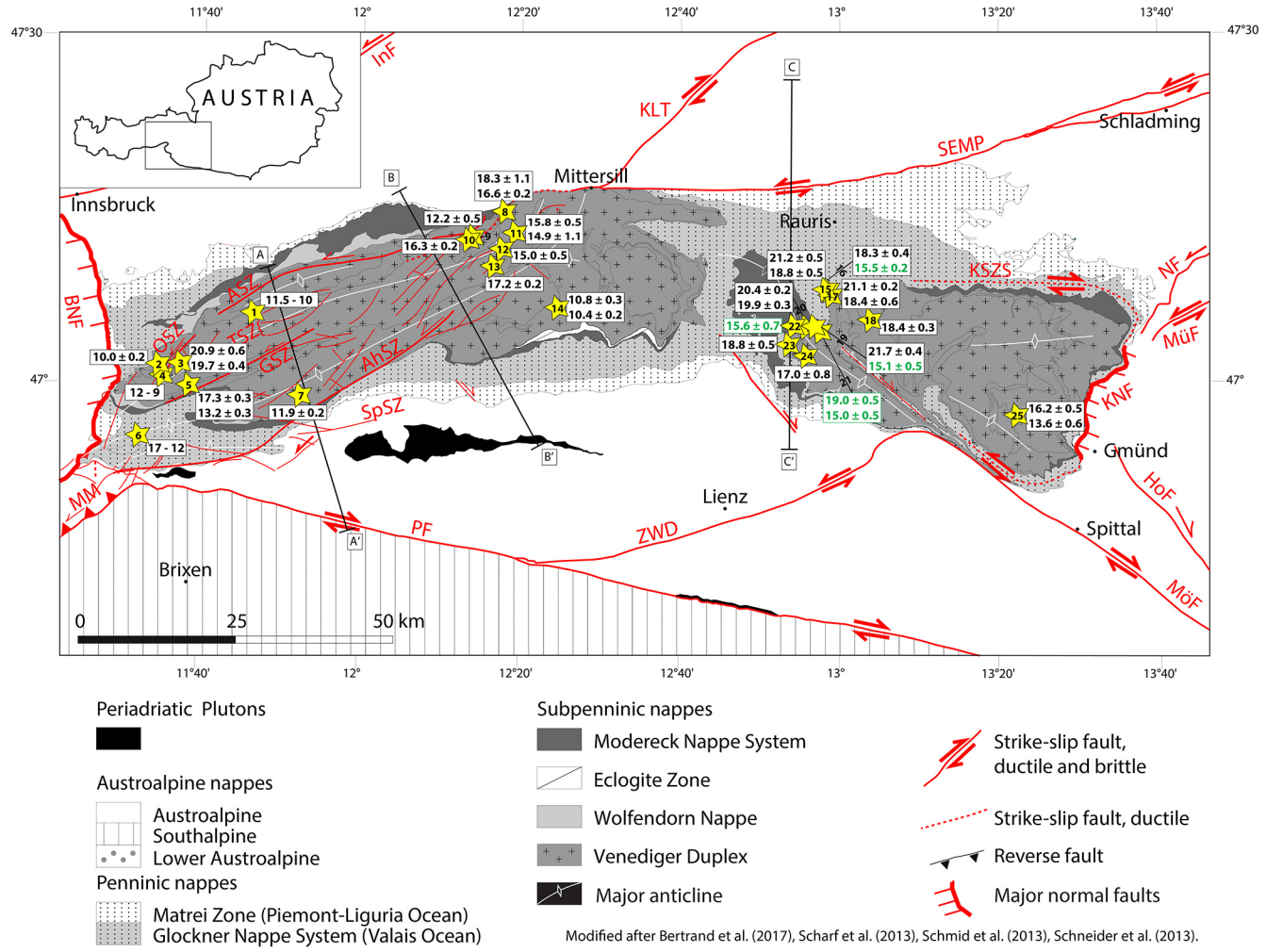


**Figure 1.** Tectonic map of the TW dome modified after Bertrand et al. (2017), Scharf et al. (2013), Schmid et al. (2013) and Schneider et al. (2013). Yellow stars on the map represent sample locations, and numbers inside the stars refer to samples listed in Table 1. Range of weighted mean growth domain ages are indicated for each grain from this study and Gnos et al. (2015), labelled in black and green, respectively, on the map (see Table 4 for an exhaustive summary of all the ages). Only the spot date range is indicated for grains 1, 4 and 6. Locations of AA', BB' and CC' cross sections are indicated by black lines, and individual cross sections are presented in Fig. 6 together with monazite crystallization ages. Two normal faults delimit the western and eastern borders of the TW, the Brenner normal fault (BNF) and the Katschberg normal fault (KNF), respectively. Note that the KNF prolongation results in dextral and sinistral strike slips in the north and south, respectively (KSZS: Katschberg shear zone system). Several sinistral strike-slip faults (AhSZ: Ahrntal shear zone; ASZ: Ahorn shear zone; DAV: Defereggen–Antholz–Vals fault; GSZ: Greiner shear zone; InF: Inntal fault; MüF: Mur–Mürz fault; NF: Niedere Tauern southern fault; OSZ: Olperer shear zone; SEMP: Salzach–Ennstal–Mariazell–Puchberg fault; SpSZ: Speikboden shear zone; TSZ: Tuxer shear zones; ZWD: Zwischenbergen–Wöllatratten and Drautal faults), dextral shear zones (HoF: Hochstuhl fault; IsF: Iseltal fault; KLT: Königsee–Lammertal–Traunsee fault; Mölltal fault (MöF); PF: Pustertal fault) and a reverse fault (MM: Meran–Mauls fault) are also visible in red on the map.

and bordered by two major normal faults, the Katschberg normal fault (KNF) in the east and the Brenner normal fault (BNF) in the west (Fig. 1). The western subdome is dissected by numerous sinistral shear zones (Ahorn shear zone (ASZ), Olperer shear zone (OSZ), Tuxer shear zones (TSZ), Greiner shear zone (GSZ) and Ahrntal shear zone (AhSZ)) and is bordered by the Salzach–Ennstal–Mariazell–Puchberg fault (SEMP) in the north (Fig. 1). The eastern subdome is bordered to the east by the Katschberg normal fault (KNF), continuing to the north into the dextral Katschberg shear zone system (KSZS) and to the south into an unnamed sinistral shear zone and oriented parallel to the Mölltal fault (MöF). The deformation history of these fault complexes will be discussed later.

The Alpine evolution of the TW started in the Early Paleocene with the accretion and subduction of the Piemonte–

**Table 2.** Summary of deformation phases in the Tauern metamorphic dome.

| Age (Ma) | Phase | Fault | Domain | Characteristics | Ref. | Remarks |
|---|---|---|---|---|---|---|
| Estimated peaks of deformation | | | | | | |
| ∼ 65 | D1 | | Penninic nappes | Accretion and subduction of Piemonte–Liguria Ocean | E | |
| ∼ 41 | D2 | | Penninic and Subpenninic nappes | Subduction of Valais Ocean and parts of the distal European margin | E | |
| ∼ 35 | D3 | | Central TW | Exhumation of high-pressure units | E | Folding of D2 thrust, decompression |
| ∼ 29 | D4 | | Subpenninic nappes | European slab break-off, Venediger Duplex formation and "Tauernkristallisation" | E | Contemporaneous intrusion of Periadriatic plutons and incipient NE-wards subduction of the Adriatic slab |
| ∼ 23–21 | | | East of the Giudicarie belt | Incipient indentation of the southern alpine units in the Eastern Alps | D, E | |
| ∼ 17 | D5 | | TW | Indentation, doming and lateral extrusion | E | |
| Faults' motion | | | | | | |
| 33–15 | | ASZ | Western TW | Sinistral ductile shear | F, G | Ductile continuation of the SEMP fault |
| 24–12 | | TSZ | Western TW | Sinistral ductile shear | B, F | |
| 20–7 | | GSZ | Western TW | Sinistral ductile shear | F | |
| 21–10 | | BNF | Western TW | Normal fault | C | |
| 22–13 | | KNF | Eastern TW | Normal fault | C | |

A: Bertrand et al. (2017, 2015); B: Blanckenburg et al. (1989); C: Favaro et al. (2017); D: Scharf et al. (2013); E: Schmid et al. (2013); F: Schneider et al. (2013); G: Rosenberg and Schneider (2008). ASZ: Ahorn shear zone, BNF: Brenner normal fault, GSZ: Greiner shear zone, KNF: Katschberg normal fault, SEMP: Salzach–Ennstal–Mariazell–Puchberg fault, TSZ: Tuxer shear zones.

Liguria Ocean (Matrei zone; Fig. 1) under the Apulian margin (Austroalpine nappe stack; e.g. Schmid et al., 2004, 2013; D1 deformation of Schmid et al., 2013; Fig. 1, Table 2). In the Middle Eocene, the Valais Ocean and parts of the distal European margin (Glockner nappe system, Eclogite zone and parts of the Modereck nappe system; Fig. 1) were equally subducted below the Austroalpine nappe stack and the Matrei zone accreted during D1 deformation (D2 deformation of Schmid et al., 2013; Table 2). In the Late Eocene, exhumation was achieved by extrusion of the high-pressure units that went together with major folding of the D2 thrust formed between the subducted Glockner nappe system and Modereck nappe system (D3 deformation of Schmid et al., 2013; Table 2). In the Early Oligocene, nearly contemporaneous break-off of the subducting European slab and formation of the Venediger Duplex (crustal-scale duplex structure) occurred, followed by the "Tauernkristallisation" (reheating of the whole nappe stack to amphibolite facies conditions) (D4 deformation of Schmid et al., 2013; Table 2). This was followed by an inversion of subduction polarity at ∼ 23 to 21 Ma (e.g. Rosenberg et al., 2018; Scharf et al., 2013; Schmid et al., 2013; Table 2). The following exhumation of the TW started in the Early to Middle Miocene by Alpine N–S collisional shortening and E–W orogen-parallel extension leading to folding, erosion and lateral extrusion through shear zone development (e.g. Luth and Willingshofer, 2008; Rosenberg and Berger, 2009; Rosenberg and Garcia, 2011; Schmid et al., 2004, 2013; Selverstone, 1988; D5 deformation of Schmid et al., 2013). Previous shear zone age dating in the TW was achieved using different geochronometers: Rb-Sr whole-rock–phengite dating (20 Ma; Blanckenburg et al., 1989), Rb-Sr whole-rock–white mica dating (39–16 Ma; Glodny et al., 2008), Sm-Nd dating on garnet (27.5–20 Ma; Pollington and Baxter, 2010, 2011) and $^{40}Ar/^{39}Ar$ dating on mica (35–28 Ma; Urbanek et al., 2002). A recent detailed study by Schneider et al. (2013) using texturally controlled in situ $^{40}Ar/^{39}Ar$ dating of syn-kinematic phengite and K-feldspar returned ages of 33–15, 24–12 and 20–7 Ma. They were interpreted as recording deformation along three major shear zones (ASZ, TSZ and GSZ, respectively) of the western subdome.

## Sample location

Fissure monazite is rare and difficult to find, meaning that this study could not have been conducted without the help of crystal searchers who provided samples. Fissure monazites were selected to cover all parts of the TW areas with known shear zones within it. It was, however, unfortunately not possible to obtain exact coordinates for all of the samples (Table 1). This is due to the rarity of fissure monazite, so that

some samples were obtained from old finds or collections. In other cases, the crystal searcher could not anymore precisely identify the fissure in which the monazite was found. These samples are marked with "approx." in Table 1. We could therefore only revisit some of the sample locations in order to add structural information. Experience from other parts of the Alps (e.g. Bergemann et al., 2017, 2019; Ricchi et al., 2019) shows that fissure monazite sampled within the damage or central zones of a shear zone generally records shear zone activity well. Information on the source localities, host rocks, degree of alpine metamorphism and mineral associations is in Table 1.

## 3 Methods

The crystals were polished individually on a lapidary disc and embedded in epoxy together with the monazite standard "44069" (425 Ma, Aleinikoff et al., 2006), following the same procedure as that in Bergemann et al. (2017). Backscatter electron (BSE) images were acquired in order to investigate the internal textural features of each grain (e.g. zoning, evidence of alteration) using an energy dispersive spectrometer (EDS)-equipped JEOL JSM7001F and a Zeiss DSM940A electron microscope at the University of Geneva with a beam current of 3.5 nA and acceleration voltage of 15 kV. BSE images helped in the selection of secondary-ion mass spectrometry (SIMS) spot analysis points, carefully placed in chemically distinct domains.

Ion probe U-Th-Pb analyses of 15 monazite crystals were conducted at the SwissSIMS ion microprobe facility, University of Lausanne, Switzerland, and analyses of another eight crystals were performed at the NordSIMS facility, Swedish Museum of Natural History, Stockholm (Tables 1 and 3). Both laboratories are equipped with a Cameca IMS 1280-HR instrument. The instruments were run following the procedure of Janots et al. (2012), applying a $-13$ kV $O^{2-}$ primary beam, an intensity of $\sim 3$ and 6 nA focused on the sample (SwissSIMS and NordSIMS, respectively) to produce a spot of 15–20 µm in diameter. A mass resolution of 4300–5000 ($M/\Delta M$, $^{208}Pb\,/\,^{232}Th$ at 10 % peak height) and an energy window at 40 eV were applied, with data collection in peak hopping mode using an ion-counting electron multiplier. All the unknowns were standardized to 44069 (425 Ma; Aleinikoff et al., 2006) monazite, and the uncertainty on the standard $^{208}Pb\,/\,^{232}Th$-ThO / Th calibration in each session was 1.7 % on average.

A $^{207}Pb$ and $^{204}Pb$ common lead (Pbc) correction calculated at time zero was applied to the data acquired at the SwissSIMS and NordSIMS (Table 3) using the terrestrial Pb evolution model of Stacey and Kramers (1975). Cameca customizable ion probe software (CIPS) was used for data reduction. $^{204}Pb$- and $^{207}Pb$-corrected ages agree within uncertainty (Table 3), but we preferred to discuss $^{207}Pb$-corrected ages because they are more robust and consistent (better statistics and less scatter in the data). Calculation of weighted mean ages, based on $^{207}Pb$ correction, and plotting was carried out using the IsoPlot Ex 4.1 programme (Ludwig, 2003). Single and weighted mean ages (or average ages) are quoted at the $1\sigma$ and at the 95 % confidence level in the text, respectively.

Weighted mean $^{208}Pb\,/\,^{232}Th$ ages were calculated for each growth domain following the approach of Bergemann et al. (2017, 2018, 2019, 2020) and Ricchi et al. (2019). Distinct chemical and textural domains were carefully defined in each grain based on Th concentrations as function of U concentrations and BSE image information. Since fissure monazite is dissolved and re-precipitated under changing chemical conditions (e.g. Grand'Homme et al., 2018), spot analyses affected by Pbc (resulting in older dates directly related to higher Pbc, i.e. positive age-f208 correlation), inclusions or those with high uncertainty ($1\sigma > 1$ abs.) were removed from the dataset and marked in italic in Table 3. However, spot dates located on dissolution trails, generally providing younger dates, were considered in the age ranges because they likely record a later phase of monazite crystallization.

## 4 Results

### 4.1 Field observations

An example of deformed fissures and different stages of fissure formation is well exposed in outcrops along the road leading to Pfitscherjoch (in proximity to the PFIT1 sample locality 5, western TW; Table 1), where two fissure generations are present (Fig. 2a and b). In this outcrop, an earlier fissure generation ($C_2$, green ellipses) is partly deformed during subsequent deformation, and a younger generation of fissures ($C_3$, blue ellipses) is also present. Subhorizontal fissures ($C_3$) seem linked to a strongly inclined lineation ($L_3$, blue arrows), whereas older subvertical fissures ($C_2$) seem related to a weakly inclined strike-slip lineation ($L_2$, green arrows). The older fissures are wider and sigmoidal in shape and contain muscovite which is not found in the younger fissures. In some cases, younger fissures crosscut older ones (Fig. 2b). Moreover, the orientation of the foliation ($S_{2,3}$; Fig. 2c) of these two fissure generations ($C_2$ and $C_3$) is different from the foliation ($S_1$; Fig. 2c) of early fissure formation mainly observed in the eastern part of the TW ($C_1$, Fig. 2c, discussed below). This suggests that, in the Pfitscherjoch area, early fissures $C_1$ were overprinted by younger tectonic movements.

The large majority of the fissures present in all the investigated localities are oriented subvertically ($C_1$ and $C_2$ type in Fig. 2c), roughly striking NE–SW. For $C_2$, this would indicate a similar direction of extension for the development of this fissure type, which is in line with palaeostress orientations provided by Bertrand et al. (2015). However, even if all subvertical fissures are subparallel, at least two generations exist. (i) Early subvertical fissures ($C_1$, Fig. 2c) are re-

**Table 3.** Th-U-Pb analyses of monazite by ion microprobe (SwissSIMS and NordSIMS). Analyses resulting in unreliable dates (e.g. presence of cracks, affected by Pbc causing high uncertainty) were not considered and are written in italic.

| | | | | | | | | | | | | 204-corr | | 204-corr spot ages | | 207-corr | | 207-corr spot ages | |
|---|---|---|---|---|---|---|---|---|---|---|---|---|---|---|---|---|---|---|---|
| Groups | Analysis ID | U (ppm) | Th (ppm) | Th / U | $^{208}Pb/^{204}Pb$ | 1σ (%) | $^{207}Pb/^{206}Pb$ | 1σ (%) | $^{208}Pb/^{232}Th$ | 1σ (%) | f208 from 207 (%) | $^{208}Pb/^{232}Th$ | 1σ (%) | $^{208}Pb/^{232}Th$ Age (Ma) | 1σ (abs.) | $^{208}Pb/^{232}Th$ | 1σ (%) | $^{208}Pb/^{232}Th$ Age (Ma) | 1σ (abs.) |
| Western Tauern Window | | | | | | | | | | | | | | | | | | | |
| | INNB1@01 | 258 | 8810 | 34 | 180 | 11 | 0.359 | 3.0 | 0.000621 | 1.4 | 13 | 0.000514 | 2.7 | 10.39 | 0.29 | 0.000543 | 1.5 | 10.97 | 0.16 |
| | INNB1@02 | 397 | 26461 | 67 | 497 | 10 | 0.253 | 2.8 | 0.000592 | 1.6 | 4 | 0.000560 | 1.7 | 11.32 | 0.19 | 0.000570 | 1.6 | 11.52 | 0.18 |
| | INNB1@03 | 341 | 19205 | 56 | 421 | 11 | 0.280 | 3.0 | 0.000589 | 1.4 | 5 | 0.000547 | 1.6 | 11.05 | 0.18 | 0.000561 | 1.4 | 11.34 | 0.16 |
| | INNB1@04 | 1098 | 8717 | 8 | 202 | 12 | 0.158 | 2.7 | 0.000607 | 1.6 | 12 | 0.000536 | 2.8 | 10.83 | 0.31 | 0.000534 | 1.6 | 10.80 | 0.18 |
| | INNB1@05 | 924 | 23297 | 25 | 421 | 10 | 0.216 | 2.3 | 0.000552 | 1.8 | 7 | 0.000518 | 1.9 | 10.47 | 0.20 | 0.000516 | 1.8 | 10.43 | 0.18 |
| | INNB1@06 | 883 | 24902 | 28 | 364 | 9 | 0.215 | 2.3 | 0.000557 | 1.4 | 6 | 0.000514 | 1.7 | 10.39 | 0.17 | 0.000521 | 1.4 | 10.54 | 0.15 |
| | INNB1@07 | 923 | 10635 | 12 | 200 | 11 | 0.194 | 2.6 | 0.000594 | 1.6 | 12 | 0.000508 | 2.6 | 10.26 | 0.27 | 0.000521 | 1.6 | 10.53 | 0.17 |
| | *INNB1@08* | *1217* | *15622* | *13* | *283* | *13* | *0.228* | *2.7* | *0.000466* | *5.1* | *13* | *0.000433* | *5.1* | *8.74* | *0.45* | *0.000406* | *5.1* | *8.21* | *0.42* |
| A | ZEI1@01 | 84 | 2630 | 31 | 393 | 21 | 0.202 | 5.2 | 0.000515 | 2.6 | 6 | 0.000465 | 3.1 | 9.39 | 0.29 | 0.000485 | 2.7 | 9.80 | 0.26 |
| | ZEI1@04 | 75 | 2041 | 27 | 408 | 25 | 0.196 | 5.8 | 0.000509 | 3.0 | 6 | 0.000475 | 3.8 | 9.60 | 0.36 | 0.000477 | 3.0 | 9.65 | 0.29 |
| | ZEI1@06 | 147 | 2086 | 14 | 251 | 18 | 0.185 | 4.2 | 0.000558 | 2.6 | 9 | 0.000485 | 3.6 | 9.79 | 0.36 | 0.000505 | 2.7 | 10.20 | 0.28 |
| | ZEI1@07 | 185 | 2785 | 15 | 547 | 24 | 0.159 | 4.4 | 0.000524 | 2.6 | 7 | 0.000503 | 3.2 | 10.16 | 0.32 | 0.000487 | 2.7 | 9.84 | 0.26 |
| | ZEI1@08 | 189 | 2292 | 12 | 316 | 21 | 0.185 | 4.2 | 0.000519 | 2.7 | 10 | 0.000456 | 3.5 | 9.21 | 0.32 | 0.000465 | 2.7 | 9.39 | 0.26 |
| | ZEI1@10 | 198 | 3078 | 16 | 421 | 20 | 0.143 | 4.0 | 0.000542 | 2.7 | 7 | 0.000493 | 3.0 | 9.96 | 0.30 | 0.000505 | 2.7 | 10.21 | 0.27 |
| | ZEI1@11 | 107 | 1820 | 17 | 298 | 20 | 0.180 | 4.6 | 0.000546 | 2.6 | 9 | 0.000475 | 3.5 | 9.60 | 0.34 | 0.000496 | 2.7 | 10.03 | 0.27 |
| | ZEI1@13 | 230 | 5870 | 26 | 559 | 15 | 0.163 | 3.2 | 0.000558 | 2.6 | 5 | 0.000519 | 2.6 | 10.49 | 0.28 | 0.000532 | 2.6 | 10.75 | 0.28 |
| | ZEI1@14 | 226 | 4846 | 21 | 532 | 18 | 0.153 | 3.8 | 0.000542 | 2.6 | 5 | 0.000509 | 2.8 | 10.29 | 0.29 | 0.000514 | 2.6 | 10.38 | 0.27 |
| | ZEI1@15 | 284 | 4694 | 16 | 412 | 16 | 0.204 | 3.4 | 0.000523 | 2.7 | 8 | 0.000474 | 2.8 | 9.58 | 0.27 | 0.000482 | 2.7 | 9.75 | 0.26 |
| | ZEI1@16 | 192 | 3057 | 16 | 422 | 18 | 0.158 | 3.7 | 0.000553 | 2.6 | 7 | 0.000506 | 2.9 | 10.23 | 0.30 | 0.000513 | 2.7 | 10.37 | 0.28 |
| | ZEI1@17 | 200 | 3756 | 19 | 282 | 14 | 0.234 | 3.1 | 0.000561 | 2.7 | 11 | 0.000484 | 3.0 | 9.79 | 0.30 | 0.000500 | 2.7 | 10.11 | 0.28 |
| | ZEI1@19 | 325 | 1152 | 4 | 188 | 22 | 0.114 | 3.8 | 0.000622 | 3.3 | 18 | 0.000495 | 5.2 | 10.00 | 0.52 | 0.000513 | 3.6 | 10.37 | 0.38 |
| | ZEI1@20 | 391 | 2715 | 7 | 485 | 27 | 0.094 | 4.6 | 0.000533 | 2.8 | 6 | 0.000491 | 3.3 | 9.91 | 0.33 | 0.000499 | 2.8 | 10.09 | 0.28 |
| | ZEI1@21 | 115 | 7335 | 64 | 555 | 15 | 0.219 | 4.3 | 0.000509 | 2.6 | 3 | 0.000476 | 2.7 | 9.62 | 0.26 | 0.000492 | 2.6 | 9.95 | 0.26 |
| | ZEI1@22 | 74 | 9153 | 124 | 780 | 15 | 0.281 | 4.0 | 0.000509 | 2.8 | 3 | 0.000484 | 2.7 | 9.78 | 0.27 | 0.000495 | 2.8 | 10.01 | 0.28 |
| | ZEI1@24 | 58 | 4809 | 82 | 617 | 19 | 0.235 | 4.7 | 0.000523 | 2.2 | 3 | 0.000491 | 2.4 | 9.91 | 0.24 | 0.000507 | 2.2 | 10.24 | 0.23 |
| | ZEI1@25 | 60 | 5152 | 86 | 670 | 21 | 0.230 | 4.8 | 0.000485 | 2.3 | 3 | 0.000459 | 2.5 | 9.28 | 0.23 | 0.000470 | 2.3 | 9.49 | 0.22 |
| | ZEI1@26 | 70 | 8182 | 117 | 609 | 18 | 0.255 | 4.8 | 0.000499 | 2.3 | 3 | 0.000468 | 2.4 | 9.45 | 0.23 | 0.000486 | 2.3 | 9.81 | 0.22 |
| | ZEI1@27 | 207 | 6179 | 30 | 565 | 21 | 0.109 | 4.4 | 0.000485 | 2.3 | 3 | 0.000455 | 2.6 | 9.19 | 0.24 | 0.000471 | 2.3 | 9.52 | 0.22 |
| B | ZEI1@02 | 99 | 2499 | 25 | 352 | 23 | 0.194 | 6.0 | 0.000451 | 2.8 | 6 | 0.000402 | 3.6 | 8.12 | 0.29 | 0.000423 | 2.8 | 8.56 | 0.24 |
| | ZEI1@03 | 130 | 2246 | 17 | 663 | 41 | 0.177 | 7.7 | 0.000378 | 2.7 | 6 | 0.000356 | 3.5 | 7.19 | 0.25 | 0.000355 | 2.8 | 7.18 | 0.20 |
| | ZEI1@05 | 45 | 2301 | 51 | 447 | 26 | 0.286 | 5.9 | 0.000468 | 3.1 | 7 | 0.000434 | 3.7 | 8.78 | 0.33 | 0.000436 | 3.2 | 8.82 | 0.28 |
| | ZEI1@09 | 325 | 2860 | 9 | 615 | 35 | 0.127 | 6.4 | 0.000429 | 2.7 | 6 | 0.000402 | 3.4 | 8.12 | 0.27 | 0.000403 | 2.8 | 8.15 | 0.22 |
| | ZEI1@12 | 117 | 1943 | 17 | 312 | 24 | 0.139 | 5.4 | 0.000394 | 2.7 | 8 | 0.000352 | 3.9 | 7.12 | 0.28 | 0.000361 | 2.7 | 7.30 | 0.20 |
| | ZEI1@18 | 258 | 3058 | 12 | 393 | 25 | 0.127 | 5.0 | 0.000398 | 2.6 | 8 | 0.000365 | 3.5 | 7.37 | 0.26 | 0.000365 | 2.7 | 7.38 | 0.20 |
| | ZEI1@23 | 78 | 6403 | 82 | 744 | 20 | 0.307 | 4.7 | 0.000464 | 2.6 | 4 | 0.000440 | 2.7 | 8.89 | 0.24 | 0.000447 | 2.6 | 9.03 | 0.24 |
| A | SCHR1@01 | 423 | 37708 | 89 | 1766 | 6 | 0.126 | 2.4 | 0.001025 | 2.19 | 1 | 0.001011 | 2.2 | 20.42 | 0.44 | 0.001016 | 2.2 | 20.53 | 0.45 |
| | SCHR1@02 | 499 | 36495 | 73 | 2194 | 8 | 0.124 | 2.7 | 0.001012 | 2.51 | 1 | 0.001004 | 2.5 | 20.29 | 0.51 | 0.001004 | 2.5 | 20.28 | 0.51 |
| | SCHR1@03 | 417 | 45163 | 108 | 1969 | 5 | 0.132 | 2.2 | 0.001090 | 2.18 | 1 | 0.001079 | 2.2 | 21.80 | 0.47 | 0.001082 | 2.2 | 21.85 | 0.48 |
| | SCHR1@04 | 438 | 43245 | 99 | 1960 | 6 | 0.142 | 2.3 | 0.001048 | 2.18 | 1 | 0.001038 | 2.2 | 20.97 | 0.45 | 0.001039 | 2.2 | 20.98 | 0.46 |
| | SCHR1@05 | 465 | 37059 | 80 | 2172 | 7 | 0.126 | 2.5 | 0.001016 | 2.18 | 1 | 0.001006 | 2.2 | 20.32 | 0.44 | 0.001007 | 2.2 | 20.35 | 0.44 |
| | SCHR1@06 | 443 | 46170 | 104 | 1859 | 5 | 0.137 | 2.3 | 0.001064 | 2.20 | 1 | 0.001051 | 2.2 | 21.24 | 0.46 | 0.001056 | 2.2 | 21.33 | 0.47 |
| B | SCHR1@07 | 509 | 24001 | 47 | 1168 | 6 | 0.160 | 2.0 | 0.001037 | 2.18 | 2 | 0.001009 | 2.1 | 20.38 | 0.43 | 0.001013 | 2.2 | 20.47 | 0.45 |
| | SCHR1@08 | 482 | 25025 | 52 | 1167 | 6 | 0.158 | 2.0 | 0.001060 | 2.20 | 2 | 0.001033 | 2.2 | 20.88 | 0.45 | 0.001037 | 2.2 | 20.95 | 0.46 |
| | SCHR1@09 | 478 | 26320 | 55 | 1119 | 6 | 0.167 | 1.9 | 0.001040 | 2.19 | 2 | 0.001012 | 2.1 | 20.44 | 0.44 | 0.001016 | 2.2 | 20.54 | 0.45 |
| | SCHR1@10 | 510 | 28255 | 55 | 1211 | 6 | 0.168 | 2.0 | 0.001051 | 2.17 | 2 | 0.001026 | 2.1 | 20.72 | 0.44 | 0.001030 | 2.2 | 20.81 | 0.45 |
| | SCHR1@11 | 465 | 26453 | 57 | 1145 | 6 | 0.169 | 1.8 | 0.001076 | 2.18 | 2 | 0.001053 | 2.1 | 21.28 | 0.46 | 0.001052 | 2.2 | 21.25 | 0.46 |
| | SCHR1@12 | 331 | 27180 | 82 | 1099 | 6 | 0.212 | 2.0 | 0.001043 | 2.18 | 2 | 0.001018 | 2.1 | 20.57 | 0.44 | 0.001020 | 2.2 | 20.60 | 0.45 |
| | SCHR1@13 | 312 | 28957 | 93 | 1243 | 6 | 0.233 | 2.0 | 0.001052 | 2.19 | 2 | 0.001028 | 2.1 | 20.76 | 0.44 | 0.001027 | 2.2 | 20.75 | 0.45 |
| | SCHR1@14 | 316 | 29632 | 94 | 1200 | 6 | 0.239 | 2.1 | 0.001031 | 2.22 | 2 | 0.001004 | 2.2 | 20.29 | 0.44 | 0.001008 | 2.2 | 20.37 | 0.45 |
| | SCHR1@15 | 331 | 31105 | 94 | 1151 | 5 | 0.247 | 2.1 | 0.001016 | 2.21 | 2 | 0.000993 | 2.2 | 20.05 | 0.43 | 0.000993 | 2.2 | 20.07 | 0.44 |
| | SCHR1@16 | 471 | 25641 | 54 | 1676 | 7 | 0.132 | 2.3 | 0.001020 | 2.19 | 1 | 0.001004 | 2.2 | 20.27 | 0.44 | 0.001005 | 2.2 | 20.31 | 0.44 |
| | SCHR1@17 | 477 | 28482 | 60 | 1358 | 6 | 0.151 | 2.3 | 0.001020 | 2.20 | 2 | 0.001001 | 2.2 | 20.23 | 0.44 | 0.001005 | 2.2 | 20.30 | 0.45 |
| | SCHR1@18 | 480 | 18234 | 38 | 1599 | 9 | 0.119 | 2.5 | 0.000998 | 2.21 | 2 | 0.000976 | 2.2 | 19.72 | 0.43 | 0.000981 | 2.2 | 19.83 | 0.44 |
| | SCHR1@19 | 492 | 18252 | 37 | 1339 | 8 | 0.116 | 2.5 | 0.001004 | 2.21 | 2 | 0.000981 | 2.2 | 19.81 | 0.43 | 0.000988 | 2.2 | 19.95 | 0.44 |
| | SCHR1@20 | 506 | 18432 | 36 | 1461 | 8 | 0.117 | 2.5 | 0.000992 | 2.25 | 2 | 0.000973 | 2.2 | 19.66 | 0.44 | 0.000976 | 2.3 | 19.72 | 0.44 |
| | SCHR1@21 | 443 | 21802 | 49 | 1500 | 8 | 0.134 | 2.4 | 0.000997 | 2.19 | 2 | 0.000979 | 2.2 | 19.78 | 0.43 | 0.000980 | 2.2 | 19.81 | 0.43 |
| | SCHR1@22 | 453 | 24816 | 55 | 1475 | 7 | 0.149 | 2.4 | 0.001007 | 2.18 | 2 | 0.000991 | 2.2 | 20.03 | 0.43 | 0.000991 | 2.2 | 20.01 | 0.44 |

**Table 3.** Continued.

| Groups | Analysis ID | U (ppm) | Th (ppm) | Th / U | $^{208}Pb/^{204}Pb$ | 1σ (%) | $^{207}Pb/^{206}Pb$ | 1σ (%) | $^{208}Pb/^{232}Th$ | 1σ (%) | f208 from 207 (%) | 204-corr | | 204-corr spot ages | | 207-corr | | 207-corr spot ages | |
|---|---|---|---|---|---|---|---|---|---|---|---|---|---|---|---|---|---|---|---|
| | | | | | | | | | | | | $^{208}Pb/^{232}Th$ | 1σ (%) | $^{208}Pb/^{232}Th$ Age (Ma) | 1σ (abs.) | $^{208}Pb/^{232}Th$ | 1σ (%) | $^{208}Pb/^{232}Th$ Age (Ma) | 1σ (abs.) |
| Western Tauern Window | | | | | | | | | | | | | | | | | | | |
| C | SCHR1@23 | 211 | 16187 | 77 | 921 | 7 | 0.323 | 2.4 | 0.000994 | 2.42 | 4 | 0.000957 | 2.3 | 19.34 | 0.45 | 0.000954 | 2.4 | 19.27 | 0.47 |
| | SCHR1@24 | 306 | 17861 | 58 | 513 | 5 | 0.371 | 2.0 | 0.001025 | 2.39 | 6 | 0.000960 | 2.3 | 19.39 | 0.44 | 0.000963 | 2.4 | 19.45 | 0.47 |
| | SCHR1@25 | 363 | 17322 | 48 | 546 | 6 | 0.370 | 2.3 | 0.001036 | 2.65 | 6 | 0.000968 | 2.5 | 19.55 | 0.49 | 0.000975 | 2.7 | 19.70 | 0.52 |
| | SCHR1@26 | 447 | 17105 | 38 | 1579 | 11 | 0.168 | 3.8 | 0.001047 | 3.28 | 2 | 0.001027 | 3.2 | 20.74 | 0.67 | 0.001029 | 3.3 | 20.78 | 0.68 |
| | SCHR1@27 | 351 | 18354 | 52 | 1635 | 10 | 0.177 | 3.3 | 0.000973 | 2.75 | 2 | 0.000954 | 2.7 | 19.28 | 0.52 | 0.000955 | 2.8 | 19.30 | 0.53 |
| | SCHR1@28 | 499 | 18145 | 36 | 1394 | 11 | 0.215 | 3.5 | 0.001031 | 3.21 | 3 | 0.001006 | 3.1 | 20.33 | 0.64 | 0.001004 | 3.2 | 20.28 | 0.65 |
| | MAYR4@01 | 259 | 5113 | 20 | 514 | 18 | 0.127 | 3.3 | 0.000567 | 1.3 | 4 | 0.000527 | 1.8 | 10.65 | 0.19 | 0.000542 | 1.3 | 10.95 | 0.14 |
| | MAYR4@02 | 340 | 3449 | 10 | 341 | 19 | 0.120 | 3.5 | 0.000527 | 1.5 | 6 | 0.000468 | 2.5 | 9.45 | 0.23 | 0.000493 | 1.5 | 9.96 | 0.15 |
| | MAYR4@03 | 336 | 3763 | 11 | 305 | 17 | 0.109 | 3.6 | 0.000541 | 1.5 | 5 | 0.000476 | 2.5 | 9.62 | 0.24 | 0.000512 | 1.5 | 10.35 | 0.15 |
| | MAYR4@04 | 368 | 3691 | 10 | 424 | 21 | 0.114 | 3.8 | 0.000496 | 1.6 | 6 | 0.000451 | 2.4 | 9.12 | 0.22 | 0.000467 | 1.7 | 9.44 | 0.16 |
| | MAYR4@05 | 311 | 2301 | 7 | 246 | 17 | 0.135 | 3.0 | 0.000636 | 1.9 | 11 | 0.000536 | 3.1 | 10.84 | 0.34 | 0.000565 | 2.0 | 11.41 | 0.23 |
| | MAYR4@06 | 385 | 1190 | 3 | 189 | 21 | 0.097 | 3.2 | 0.000618 | 2.3 | 15 | 0.000504 | 4.8 | 10.19 | 0.49 | 0.000524 | 2.6 | 10.58 | 0.28 |
| | MAYR4@07 | 136 | 6949 | 51 | 411 | 13 | 0.294 | 2.8 | 0.000601 | 1.2 | 7 | 0.000544 | 1.6 | 10.99 | 0.18 | 0.000561 | 1.2 | 11.33 | 0.13 |
| | MAYR4@08 | 192 | 5038 | 26 | 370 | 15 | 0.224 | 2.9 | 0.000599 | 1.2 | 8 | 0.000536 | 1.9 | 10.84 | 0.21 | 0.000553 | 1.3 | 11.17 | 0.14 |
| | MAYR4@09 | 201 | 4829 | 24 | 293 | 13 | 0.233 | 2.7 | 0.000602 | 1.4 | 9 | 0.000522 | 2.1 | 10.55 | 0.22 | 0.000547 | 1.4 | 11.06 | 0.16 |
| | MAYR4@10 | 251 | 4665 | 19 | 427 | 16 | 0.139 | 3.2 | 0.000600 | 1.2 | 5 | 0.000553 | 1.9 | 11.17 | 0.21 | 0.000568 | 1.3 | 11.48 | 0.15 |
| | MAYR4@11 | 334 | 1748 | 5 | 300 | 24 | 0.103 | 3.4 | 0.000511 | 2.2 | 14 | 0.000446 | 3.7 | 9.00 | 0.33 | 0.000442 | 2.4 | 8.93 | 0.21 |
| | MAYR4@12 | 295 | 2169 | 7 | 229 | 18 | 0.112 | 3.5 | 0.000582 | 2.0 | 9 | 0.000491 | 3.5 | 9.92 | 0.35 | 0.000531 | 2.1 | 10.72 | 0.22 |
| | MAYR4@13 | 81 | 5010 | 62 | 404 | 16 | 0.335 | 3.4 | 0.000627 | 1.3 | 7 | 0.000574 | 1.9 | 11.60 | 0.23 | 0.000584 | 1.3 | 11.80 | 0.15 |
| | MAYR4@14 | 103 | 5475 | 53 | 381 | 14 | 0.289 | 3.3 | 0.000602 | 1.2 | 6 | 0.000541 | 1.8 | 10.92 | 0.20 | 0.000564 | 1.2 | 11.39 | 0.13 |
| | MAYR4@15 | 94 | 6085 | 65 | 457 | 15 | 0.274 | 3.6 | 0.000545 | 1.4 | 5 | 0.000499 | 1.8 | 10.09 | 0.18 | 0.000519 | 1.4 | 10.48 | 0.15 |
| | MAYR4@16 | 122 | 6082 | 50 | 486 | 15 | 0.236 | 3.5 | 0.000546 | 1.0 | 4 | 0.000503 | 1.5 | 10.16 | 0.15 | 0.000522 | 1.0 | 10.56 | 0.11 |
| | MAYR4@17 | 134 | 5776 | 43 | 381 | 14 | 0.270 | 3.1 | 0.000553 | 0.9 | 6 | 0.000497 | 1.6 | 10.04 | 0.16 | 0.000519 | 1.0 | 10.50 | 0.10 |
| | MAYR4@18 | 180 | 4227 | 23 | 351 | 14 | 0.200 | 3.0 | 0.000603 | 1.1 | 7 | 0.000543 | 1.9 | 10.96 | 0.21 | 0.000561 | 1.1 | 11.34 | 0.12 |
| A | PFIT1@12 | 103 | 11683 | 114 | 554 | 6 | 0.387 | 2.6 | 0.000852 | 2.19 | 5 | 0.000809 | 2.1 | 16.34 | 0.35 | 0.000813 | 2.2 | 16.42 | 0.36 |
| | PFIT1@13 | 112 | 18466 | 165 | 580 | 5 | 0.450 | 2.4 | 0.000891 | 2.29 | 4 | 0.000845 | 2.2 | 17.06 | 0.38 | 0.000852 | 2.3 | 17.21 | 0.39 |
| | PFIT1@14 | 117 | 13986 | 120 | 569 | 5 | 0.413 | 2.4 | 0.000918 | 2.31 | 5 | 0.000868 | 2.2 | 17.54 | 0.39 | 0.000874 | 2.3 | 17.66 | 0.41 |
| | PFIT1@15 | 104 | 13449 | 130 | 473 | 5 | 0.430 | 2.3 | 0.000895 | 2.41 | 5 | 0.000835 | 2.3 | 16.87 | 0.39 | 0.000849 | 2.4 | 17.15 | 0.41 |
| | PFIT1@16 | 65 | 15956 | 244 | 629 | 5 | 0.497 | 2.8 | 0.000913 | 2.26 | 4 | 0.000877 | 2.2 | 17.72 | 0.39 | 0.000881 | 2.3 | 17.80 | 0.40 |
| | PFIT1@17 | 78 | 13368 | 171 | 586 | 7 | 0.506 | 3.3 | 0.000877 | 2.25 | 4 | 0.000833 | 2.2 | 16.82 | 0.37 | 0.000843 | 2.3 | 17.03 | 0.38 |
| | PFIT1@18 | 79 | 12054 | 153 | 662 | 7 | 0.365 | 3.6 | 0.000892 | 2.40 | 3 | 0.000859 | 2.4 | 17.35 | 0.41 | 0.000866 | 2.4 | 17.49 | 0.42 |
| | PFIT1@19 | 121 | 9937 | 82 | 697 | 10 | 0.328 | 4.6 | 0.000896 | 2.19 | 3 | 0.000856 | 2.2 | 17.29 | 0.38 | 0.000869 | 2.2 | 17.57 | 0.39 |
| | PFIT1@20 | 119 | 8358 | 70 | 871 | 11 | 0.287 | 4.9 | 0.000885 | 2.19 | 3 | 0.000853 | 2.2 | 17.23 | 0.37 | 0.000862 | 2.2 | 17.42 | 0.38 |
| | *PFIT1@01* | *30* | *5962* | *199* | *808* | *12* | *0.360* | *5.4* | *0.000658* | *2.29* | *3* | *0.000631* | *2.3* | *12.74* | *0.29* | *0.000640* | *2.3* | *12.94* | *0.30* |
| | *PFIT1@02* | *32* | *6627* | *209* | *723* | *10* | *0.350* | *5.0* | *0.000754* | *2.25* | *2* | *0.000721* | *2.2* | *14.57* | *0.32* | *0.000736* | *2.3* | *14.86* | *0.34* |
| | *PFIT1@03* | *13* | *5940* | *466* | *1033* | *11* | *0.414* | *6.9* | *0.000824* | *2.24* | *1* | *0.000808* | *2.2* | *16.33* | *0.37* | *0.000814* | *2.2* | *16.45* | *0.37* |
| | *PFIT1@04* | *36* | *6027* | *166* | *859* | *13* | *0.317* | *5.7* | *0.000705* | *2.28* | *3* | *0.000681* | *2.3* | *13.77* | *0.31* | *0.000687* | *2.3* | *13.88* | *0.32* |
| | *PFIT1@05* | *84* | *8610* | *102* | *1011* | *19* | *0.389* | *7.1* | *0.000710* | *3.39* | *4* | *0.000690* | *3.4* | *13.94* | *0.47* | *0.000685* | *3.4* | *13.84* | *0.47* |
| | *PFIT1@11* | *110* | *13146* | *119* | *548* | *6* | *0.428* | *2.7* | *0.000800* | *2.18* | *4* | *0.000756* | *2.1* | *15.28* | *0.32* | *0.000764* | *2.2* | *15.43* | *0.34* |
| B | PFIT1@06 | 245 | 5464 | 22 | 525 | 10 | 0.155 | 3.0 | 0.000697 | 2.20 | 6 | 0.000664 | 2.2 | 13.42 | 0.30 | 0.000658 | 2.2 | 13.30 | 0.29 |
| | PFIT1@07 | 336 | 4523 | 13 | 381 | 11 | 0.161 | 3.6 | 0.000706 | 2.33 | 6 | 0.000642 | 2.4 | 12.98 | 0.31 | 0.000661 | 2.3 | 13.35 | 0.31 |
| | PFIT1@08 | 347 | 3300 | 10 | 314 | 12 | 0.201 | 3.5 | 0.000728 | 2.21 | 11 | 0.000647 | 2.4 | 13.07 | 0.32 | 0.000648 | 2.3 | 13.09 | 0.30 |
| | PFIT1@09 | 383 | 3220 | 8 | 343 | 13 | 0.170 | 3.9 | 0.000704 | 2.21 | 9 | 0.000636 | 2.5 | 12.86 | 0.32 | 0.000638 | 2.3 | 12.89 | 0.29 |
| | PFIT1@10 | 388 | 2889 | 7 | 238 | 11 | 0.190 | 3.7 | 0.000740 | 2.33 | 12 | 0.000641 | 2.8 | 12.95 | 0.36 | 0.000650 | 2.4 | 13.13 | 0.32 |
| | BURG2@07 | 30 | 769 | 26 | 193 | 20 | 0.165 | 4.7 | 0.000732 | 2.3 | 10 | 0.000585 | 4.4 | 11.83 | 0.53 | 0.000659 | 2.4 | 13.32 | 0.31 |
| | BURG2@08 | 18 | 1014 | 57 | 219 | 16 | 0.306 | 3.6 | 0.000959 | 2.2 | 12 | 0.000790 | 3.4 | 15.97 | 0.54 | 0.000844 | 2.3 | 17.06 | 0.39 |
| | BURG2@09 | 53 | 626 | 12 | 275 | 24 | 0.087 | 5.1 | 0.000797 | 2.3 | 6 | 0.000685 | 3.9 | 13.85 | 0.54 | 0.000751 | 2.4 | 15.17 | 0.36 |
| | BURG2@10 | 30 | 1067 | 36 | 324 | 19 | 0.179 | 4.1 | 0.000878 | 2.3 | 7 | 0.000774 | 3.0 | 15.63 | 0.47 | 0.000818 | 2.3 | 16.53 | 0.38 |
| | BURG2@13 | 164 | 529 | 3 | 403 | 55 | 0.112 | 7.5 | 0.000683 | 2.3 | 12 | 0.000660 | 6.5 | 13.35 | 0.86 | 0.000600 | 2.8 | 12.12 | 0.33 |
| | *BURG2@12* | *52* | *2273* | *44* | *69* | *18* | *0.415* | *3.7* | *0.001048* | *8.6* | *46* | *0.000462* | *10.7* | *9.34* | *1.00* | *0.000571* | *9.5* | *11.53* | *1.10* |

**Table 3.** Continued.

| Groups | Analysis ID | U (ppm) | Th (ppm) | Th / U | $^{208}Pb/^{204}Pb$ | 1σ (%) | $^{207}Pb/^{206}Pb$ | 1σ (%) | $^{208}Pb/^{232}Th$ | 1σ (%) | f208 from 207 (%) | 204-corr | | 204-corr spot ages | | 207-corr | | 207-corr spot ages | |
|---|---|---|---|---|---|---|---|---|---|---|---|---|---|---|---|---|---|---|---|
| | | | | | | | | | | | | $^{208}Pb/^{232}Th$ | 1σ (%) | $^{208}Pb/^{232}Th$ Age (Ma) | 1σ (abs.) | $^{208}Pb/^{232}Th$ | 1σ (%) | $^{208}Pb/^{232}Th$ Age (Ma) | 1σ (abs.) |
| Western Tauern Window | | | | | | | | | | | | | | | | | | | |
| A | PLAN1@01 | 190 | 1647 | 9 | 56 | 9 | 0.577 | 2.2 | 0.001582 | 3.1 | 63 | 0.000706 | 6.9 | 14.27 | 0.98 | 0.000580 | 5.1 | 11.73 | 0.60 |
| | PLAN1@02 | 177 | 12498 | 71 | 284 | 11 | 0.361 | 2.9 | 0.000643 | 1.4 | 9 | 0.000585 | 2.1 | 11.81 | 0.25 | 0.000587 | 1.5 | 11.86 | 0.17 |
| | PLAN1@03 | 209 | 2322 | 11 | 56 | 8 | 0.620 | 1.9 | 0.001634 | 3.3 | 63 | 0.000578 | 5.5 | 11.67 | 0.64 | 0.000605 | 4.7 | 12.23 | 0.57 |
| | PLAN1@04 | 410 | 3160 | 8 | 101 | 12 | 0.269 | 2.8 | 0.000788 | 2.2 | 28 | 0.000583 | 5.4 | 11.78 | 0.63 | 0.000565 | 2.6 | 11.41 | 0.29 |
| | PLAN1@05 | 438 | 1542 | 4 | 59 | 11 | 0.261 | 2.7 | 0.001043 | 3.3 | 45 | 0.000489 | 7.9 | 9.88 | 0.78 | 0.000574 | 4.5 | 11.61 | 0.52 |
| | PLAN1@06 | 458 | 1687 | 4 | 58 | 10 | 0.377 | 2.4 | 0.001231 | 6.5 | 55 | 0.000575 | 8.0 | 11.62 | 0.93 | 0.000550 | 7.5 | 11.11 | 0.84 |
| | PLAN1@07 | 462 | 2662 | 6 | 90 | 12 | 0.284 | 2.5 | 0.000864 | 4.0 | 40 | 0.000635 | 6.3 | 12.83 | 0.81 | 0.000520 | 4.5 | 10.50 | 0.47 |
| | PLAN1@08 | 509 | 3332 | 7 | 104 | 14 | 0.242 | 3.3 | 0.000751 | 2.3 | 24 | 0.000607 | 6.0 | 12.26 | 0.74 | 0.000569 | 2.7 | 11.50 | 0.31 |
| | PLAN1@09 | 594 | 4167 | 7 | 101 | 12 | 0.238 | 2.9 | 0.000690 | 2.4 | 24 | 0.000501 | 5.1 | 10.12 | 0.51 | 0.000522 | 2.6 | 10.55 | 0.28 |
| | PLAN1@10 | 774 | 5878 | 8 | 148 | 12 | 0.190 | 2.8 | 0.000661 | 2.1 | 17 | 0.000557 | 3.9 | 11.26 | 0.44 | 0.000550 | 2.2 | 11.11 | 0.25 |
| | PLAN1@13 | 1215 | 1759 | 1 | 68 | 12 | 0.136 | 2.5 | 0.000967 | 5.4 | 41 | 0.000576 | 8.2 | 11.65 | 0.96 | 0.000567 | 6.6 | 11.45 | 0.75 |
| | PLAN1@14 | 589 | 4750 | 8 | 176 | 14 | 0.167 | 3.2 | 0.000680 | 1.5 | 15 | 0.000581 | 3.7 | 11.73 | 0.43 | 0.000579 | 1.6 | 11.71 | 0.19 |
| | PLAN1@15 | 424 | 3653 | 9 | 98 | 11 | 0.233 | 2.9 | 0.000783 | 1.8 | 22 | 0.000624 | 5.1 | 12.61 | 0.65 | 0.000610 | 2.0 | 12.32 | 0.25 |
| | PLAN1@16 | 448 | 3567 | 8 | 86 | 10 | 0.288 | 2.4 | 0.000869 | 2.9 | 30 | 0.000596 | 5.2 | 12.04 | 0.63 | 0.000611 | 3.2 | 12.35 | 0.39 |
| | PLAN1@17 | 454 | 3815 | 8 | 108 | 11 | 0.198 | 3.0 | 0.000744 | 1.9 | 18 | 0.000566 | 4.7 | 11.44 | 0.54 | 0.000608 | 2.1 | 12.28 | 0.26 |
| | PLAN1@18 | 443 | 4422 | 10 | 161 | 13 | 0.250 | 2.7 | 0.000763 | 3.9 | 21 | 0.000670 | 4.9 | 13.53 | 0.67 | 0.000600 | 4.0 | 12.13 | 0.48 |
| | PLAN1@19 | 365 | 10351 | 28 | 214 | 10 | 0.305 | 2.7 | 0.000685 | 1.8 | 11 | 0.000596 | 2.5 | 12.04 | 0.31 | 0.000609 | 1.8 | 12.30 | 0.22 |
| | PLAN1@20 | 467 | 8041 | 17 | 153 | 9 | 0.359 | 2.1 | 0.000751 | 1.5 | 22 | 0.000606 | 2.8 | 12.25 | 0.34 | 0.000588 | 1.6 | 11.88 | 0.20 |
| | PLAN1@21 | 627 | 6050 | 10 | 103 | 9 | 0.322 | 2.0 | 0.000836 | 2.0 | 28 | 0.000577 | 3.7 | 11.66 | 0.43 | 0.000600 | 2.2 | 12.12 | 0.27 |
| | PLAN1@23 | 373 | 4646 | 12 | 715 | 17 | 0.102 | 2.9 | 0.000645 | 2.6 | 4 | 0.000611 | 2.7 | 12.34 | 0.33 | 0.000617 | 2.7 | 12.46 | 0.33 |
| | PLAN1@24 | 390 | 4664 | 12 | 677 | 18 | 0.090 | 3.5 | 0.000610 | 2.6 | 4 | 0.000576 | 2.7 | 11.63 | 0.31 | 0.000588 | 2.7 | 11.89 | 0.32 |
| | PLAN1@25 | 359 | 5180 | 14 | 519 | 17 | 0.121 | 3.0 | 0.000639 | 2.7 | 6 | 0.000591 | 2.8 | 11.94 | 0.33 | 0.000598 | 2.7 | 12.09 | 0.32 |
| | PLAN1@26 | 365 | 4817 | 13 | 401 | 15 | 0.116 | 3.0 | 0.000627 | 2.6 | 6 | 0.000570 | 2.8 | 11.52 | 0.32 | 0.000588 | 2.7 | 11.88 | 0.32 |
| | PLAN1@27 | 476 | 3538 | 7 | 541 | 19 | 0.101 | 2.9 | 0.000650 | 2.7 | 8 | 0.000603 | 2.8 | 12.19 | 0.35 | 0.000601 | 2.7 | 12.14 | 0.33 |
| | PLAN1@28 | 564 | 8192 | 15 | 460 | 11 | 0.125 | 2.3 | 0.000660 | 2.6 | 6 | 0.000604 | 2.6 | 12.21 | 0.32 | 0.000622 | 2.6 | 12.56 | 0.33 |
| | PLAN1@29 | 620 | 14199 | 23 | 619 | 10 | 0.130 | 2.1 | 0.000637 | 2.6 | 4 | 0.000598 | 2.6 | 12.09 | 0.31 | 0.000609 | 2.6 | 12.32 | 0.33 |
| | PLAN1@30 | 528 | 8241 | 16 | 420 | 13 | 0.127 | 2.7 | 0.000632 | 2.7 | 6 | 0.000574 | 2.7 | 11.60 | 0.31 | 0.000595 | 2.7 | 12.02 | 0.32 |
| | PLAN1@31 | 1028 | 1527 | 1 | 124 | 12 | 0.090 | 2.0 | 0.000802 | 3.1 | 26 | 0.000552 | 4.4 | 11.16 | 0.49 | 0.000595 | 3.8 | 12.02 | 0.45 |
| | PLAN1@32 | 1152 | 1721 | 1 | 227 | 19 | 0.066 | 2.7 | 0.000661 | 2.7 | 12 | 0.000548 | 4.0 | 11.08 | 0.44 | 0.000579 | 3.1 | 11.70 | 0.36 |
| | PLAN1@33 | 926 | 4303 | 5 | 361 | 14 | 0.085 | 2.2 | 0.000642 | 2.7 | 8 | 0.000573 | 2.8 | 11.57 | 0.33 | 0.000588 | 2.8 | 11.87 | 0.33 |
| | PLAN1@34 | 623 | 7966 | 13 | 483 | 12 | 0.125 | 2.3 | 0.000669 | 2.6 | 7 | 0.000615 | 2.6 | 12.43 | 0.32 | 0.000624 | 2.6 | 12.61 | 0.33 |
| | PLAN1@35 | 408 | 6529 | 16 | 185 | 8 | 0.307 | 1.7 | 0.000746 | 3.1 | 19 | 0.000592 | 3.0 | 11.97 | 0.36 | 0.000605 | 3.2 | 12.22 | 0.39 |
| | PLAN1@36 | 304 | 7521 | 25 | 427 | 13 | 0.182 | 2.7 | 0.000646 | 2.6 | 7 | 0.000587 | 2.7 | 11.87 | 0.31 | 0.000603 | 2.6 | 12.19 | 0.32 |
| | PLAN1@38 | 580 | 9607 | 17 | 525 | 14 | 0.112 | 2.4 | 0.000626 | 2.2 | 5 | 0.000580 | 2.3 | 11.73 | 0.27 | 0.000596 | 2.2 | 12.05 | 0.27 |
| | PLAN1@39 | 331 | 10707 | 32 | 497 | 13 | 0.164 | 2.7 | 0.000628 | 2.2 | 4 | 0.000581 | 2.3 | 11.74 | 0.27 | 0.000600 | 2.2 | 12.12 | 0.27 |
| | PLAN1@40 | 344 | 2342 | 7 | 311 | 21 | 0.143 | 2.9 | 0.000698 | 2.3 | 15 | 0.000612 | 3.3 | 12.36 | 0.41 | 0.000593 | 2.5 | 11.98 | 0.30 |
| | PLAN1@41 | 487 | 10698 | 22 | 360 | 11 | 0.172 | 2.1 | 0.000654 | 2.2 | 7 | 0.000584 | 2.3 | 11.80 | 0.27 | 0.000608 | 2.3 | 12.28 | 0.28 |
| B | PLAN1@11 | 1410 | 6659 | 5 | 175 | 20 | 0.204 | 4.3 | 0.000568 | 2.5 | 18 | 0.000578 | 6.4 | 11.69 | 0.74 | 0.000464 | 2.8 | 9.38 | 0.26 |
| | PLAN1@12 | 1310 | 7371 | 6 | 160 | 23 | 0.206 | 5.3 | 0.000467 | 2.1 | 18 | 0.000509 | 7.9 | 10.28 | 0.81 | 0.000384 | 2.5 | 7.75 | 0.19 |
| | PLAN1@37 | 619 | 3146 | 5 | 312 | 20 | 0.085 | 2.7 | 0.000555 | 2.6 | 11 | 0.000493 | 3.5 | 9.96 | 0.34 | 0.000492 | 2.7 | 9.94 | 0.27 |
| | *PLAN1@22* | *733* | *1514* | *2* | *52* | *9* | *0.291* | *2.1* | *0.001227* | *7.7* | *60* | *0.000544* | *8.3* | *10.99* | *0.92* | *0.000491* | *9.1* | *9.91* | *0.90* |
| Central Tauern Window | | | | | | | | | | | | | | | | | | | |
| A | SCHEI1@16 | 408 | 58860 | 144 | 1205 | 6 | 0.181 | 1.8 | 0.000876 | 2.6 | 1 | 0.000849 | 2.6 | 17.14 | 0.44 | 0.000864 | 2.6 | 17.46 | 0.46 |
| | SCHEI1@17 | 304 | 61361 | 202 | 1483 | 7 | 0.210 | 1.9 | 0.000939 | 2.6 | 1 | 0.000915 | 2.6 | 18.49 | 0.48 | 0.000928 | 2.6 | 18.75 | 0.50 |
| | SCHEI1@18 | 265 | 60179 | 227 | 1432 | 6 | 0.235 | 1.9 | 0.000949 | 2.6 | 1 | 0.000924 | 2.6 | 18.66 | 0.48 | 0.000937 | 2.6 | 18.93 | 0.50 |
| | SCHEI1@20 | 311 | 62554 | 201 | 1416 | 7 | 0.222 | 2.0 | 0.000906 | 2.7 | 1 | 0.000881 | 2.6 | 17.81 | 0.46 | 0.000893 | 2.7 | 18.05 | 0.48 |
| B | SCHEI1@11 | 394 | 53473 | 136 | 780 | 7 | 0.309 | 2.0 | 0.000868 | 1.4 | 3 | 0.000829 | 1.4 | 16.75 | 0.23 | 0.000842 | 1.4 | 17.02 | 0.23 |
| | SCHEI1@12 | 434 | 47204 | 109 | 857 | 9 | 0.268 | 2.2 | 0.000886 | 1.4 | 3 | 0.000855 | 1.4 | 17.28 | 0.24 | 0.000862 | 1.4 | 17.41 | 0.24 |
| | SCHEI1@13 | 360 | 50556 | 140 | 639 | 8 | 0.349 | 2.1 | 0.000907 | 1.4 | 3 | 0.000861 | 1.4 | 17.39 | 0.24 | 0.000876 | 1.4 | 17.71 | 0.24 |
| | SCHEI1@14 | 321 | 53530 | 167 | 655 | 7 | 0.402 | 1.9 | 0.000911 | 1.4 | 4 | 0.000863 | 1.4 | 17.45 | 0.24 | 0.000876 | 1.4 | 17.69 | 0.25 |
| | SCHEI1@32 | 291 | 55126 | 189 | 1026 | 6 | 0.303 | 1.5 | 0.000868 | 2.8 | 2 | 0.000836 | 2.7 | 16.88 | 0.46 | 0.000848 | 2.8 | 17.14 | 0.48 |

**Table 3.** Continued.

| Groups | Analysis ID | U (ppm) | Th (ppm) | Th / U | $^{208}Pb/^{204}Pb$ | 1σ (%) | $^{207}Pb/^{206}Pb$ | 1σ (%) | $^{208}Pb/^{232}Th$ | 1σ (%) | f208 from 207 (%) | 204-corr | | 204-corr spot ages | | 207-corr | | 207-corr spot ages | |
|---|---|---|---|---|---|---|---|---|---|---|---|---|---|---|---|---|---|---|---|
| | | | | | | | | | | | | $^{208}Pb/^{232}Th$ | 1σ (%) | $^{208}Pb/^{232}Th$ Age (Ma) | 1σ (abs.) | $^{208}Pb/^{232}Th$ | 1σ (%) | $^{208}Pb/^{232}Th$ Age (Ma) | 1σ (abs.) |
| Central Tauern Window | | | | | | | | | | | | | | | | | | | |
| C | SCHEI1@01 | 776 | 17285 | 22 | 303 | 8 | 0.196 | 2.1 | 0.000888 | 1.4 | 7 | 0.000802 | 1.7 | 16.20 | 0.27 | 0.000825 | 1.4 | 16.67 | 0.23 |
| | SCHEI1@02 | 485 | 32602 | 67 | 655 | 11 | 0.283 | 2.6 | 0.000843 | 1.4 | 4 | 0.000808 | 1.5 | 16.33 | 0.25 | 0.000808 | 1.4 | 16.33 | 0.24 |
| | SCHEI1@03 | 496 | 23525 | 47 | 411 | 9 | 0.285 | 2.2 | 0.000899 | 1.4 | 6 | 0.000826 | 1.6 | 16.70 | 0.26 | 0.000844 | 1.4 | 17.05 | 0.25 |
| | SCHEI1@04 | 619 | 20187 | 33 | 312 | 10 | 0.254 | 2.5 | 0.000862 | 1.5 | 7 | 0.000797 | 1.9 | 16.10 | 0.31 | 0.000802 | 1.5 | 16.21 | 0.25 |
| | SCHEI1@05 | 702 | 14215 | 20 | 252 | 9 | 0.255 | 2.1 | 0.000929 | 1.5 | 11 | 0.000806 | 1.9 | 16.29 | 0.32 | 0.000825 | 1.5 | 16.66 | 0.25 |
| | SCHEI1@06 | 831 | 11524 | 14 | 190 | 8 | 0.274 | 1.7 | 0.000974 | 1.8 | 18 | 0.000810 | 2.3 | 16.36 | 0.37 | 0.000800 | 1.8 | 16.16 | 0.30 |
| | SCHEI1@07 | 545 | 19842 | 36 | 279 | 8 | 0.383 | 1.9 | 0.000949 | 1.6 | 12 | 0.000839 | 1.8 | 16.95 | 0.31 | 0.000840 | 1.6 | 16.97 | 0.27 |
| | SCHEI1@08 | 902 | 10829 | 12 | 216 | 9 | 0.220 | 2.0 | 0.000979 | 1.4 | 14 | 0.000843 | 2.1 | 17.04 | 0.36 | 0.000843 | 1.5 | 17.03 | 0.25 |
| | SCHEI1@09 | 888 | 10863 | 12 | 239 | 11 | 0.212 | 2.3 | 0.000942 | 1.8 | 13 | 0.000809 | 2.4 | 16.35 | 0.39 | 0.000819 | 1.8 | 16.55 | 0.31 |
| | SCHEI1@10 | 1103 | 20671 | 19 | 314 | 11 | 0.206 | 2.6 | 0.000864 | 1.5 | 7 | 0.000791 | 2.0 | 15.98 | 0.31 | 0.000801 | 1.5 | 16.18 | 0.24 |
| | SCHEI1@15 | 427 | 31409 | 74 | 280 | 6 | 0.426 | 1.7 | 0.000933 | 1.6 | 9 | 0.000818 | 1.7 | 16.53 | 0.28 | 0.000851 | 1.6 | 17.19 | 0.28 |
| | SCHEI1@19 | 650 | 22198 | 34 | 1132 | 11 | 0.093 | 2.6 | 0.000890 | 2.6 | 1 | 0.000860 | 2.6 | 17.37 | 0.45 | 0.000878 | 2.6 | 17.73 | 0.47 |
| | SCHEI1@21 | 704 | 20090 | 29 | 1036 | 10 | 0.086 | 2.2 | 0.000849 | 2.6 | 2 | 0.000818 | 2.6 | 16.52 | 0.42 | 0.000836 | 2.6 | 16.89 | 0.44 |
| | SCHEI1@22 | 815 | 10348 | 13 | 1078 | 15 | 0.078 | 2.3 | 0.000846 | 2.6 | 3 | 0.000818 | 2.6 | 16.52 | 0.43 | 0.000825 | 2.6 | 16.66 | 0.44 |
| | SCHEI1@23 | 417 | 36731 | 88 | 1703 | 12 | 0.133 | 2.8 | 0.000865 | 2.6 | 1 | 0.000847 | 2.6 | 17.11 | 0.44 | 0.000855 | 2.6 | 17.28 | 0.45 |
| | SCHEI1@24 | 656 | 16727 | 25 | 1183 | 11 | 0.083 | 2.3 | 0.000848 | 2.6 | 2 | 0.000821 | 2.6 | 16.59 | 0.43 | 0.000834 | 2.6 | 16.86 | 0.44 |
| | SCHEI1@27 | 720 | 19708 | 27 | 976 | 10 | 0.108 | 2.0 | 0.000831 | 2.6 | 3 | 0.000798 | 2.6 | 16.13 | 0.41 | 0.000809 | 2.6 | 16.35 | 0.43 |
| | SCHEI1@28 | 420 | 36082 | 86 | 1062 | 9 | 0.169 | 2.4 | 0.000860 | 2.6 | 2 | 0.000829 | 2.6 | 16.76 | 0.43 | 0.000846 | 2.6 | 17.08 | 0.45 |
| | SCHEI1@29 | 513 | 37241 | 73 | 665 | 9 | 0.231 | 2.2 | 0.000854 | 2.6 | 4 | 0.000804 | 2.5 | 16.25 | 0.41 | 0.000823 | 2.6 | 16.64 | 0.44 |
| | SCHEI1@30 | 588 | 23098 | 39 | 738 | 10 | 0.122 | 2.3 | 0.000808 | 2.7 | 3 | 0.000765 | 2.6 | 15.46 | 0.40 | 0.000787 | 2.7 | 15.89 | 0.43 |
| | SCHEI1@31 | 435 | 37275 | 86 | 945 | 8 | 0.176 | 2.0 | 0.000817 | 2.6 | 2 | 0.000784 | 2.5 | 15.84 | 0.40 | 0.000800 | 2.6 | 16.16 | 0.43 |
| | SCHEI1@33 | 678 | 12021 | 18 | 1406 | 18 | 0.060 | 2.6 | 0.000800 | 2.2 | 1 | 0.000778 | 2.2 | 15.73 | 0.35 | 0.000792 | 2.2 | 16.00 | 0.36 |
| | SCHEI1@34 | 996 | 8782 | 9 | 2159 | 31 | 0.056 | 3.1 | 0.000807 | 2.3 | 1 | 0.000793 | 2.3 | 16.02 | 0.37 | 0.000796 | 2.3 | 16.08 | 0.37 |
| A | HOPF2@15 | 82 | 61530 | 749 | 720 | 4 | 0.611 | 2.2 | 0.000560 | 2.37 | 2 | 0.000542 | 2.3 | 10.94 | 0.25 | 0.000546 | 2.4 | 11.03 | 0.26 |
| | HOPF2@16 | 69 | 33784 | 490 | 619 | 4 | 0.641 | 2.6 | 0.000647 | 2.36 | 3 | 0.000620 | 2.3 | 12.54 | 0.29 | 0.000625 | 2.4 | 12.63 | 0.30 |
| | HOPF2@17 | 97 | 33439 | 343 | 972 | 7 | 0.571 | 3.6 | 0.000663 | 2.91 | 2 | 0.000643 | 2.8 | 13.00 | 0.37 | 0.000647 | 2.9 | 13.08 | 0.38 |
| | HOPF2@18 | 77 | 40713 | 530 | 274 | 3 | 0.761 | 1.5 | 0.000762 | 2.67 | 11 | 0.000667 | 2.4 | 13.48 | 0.32 | 0.000677 | 2.7 | 13.67 | 0.37 |
| | HOPF2@19 | 120 | 62586 | 520 | 840 | 5 | 0.572 | 2.8 | 0.000623 | 3.49 | 2 | 0.000605 | 3.4 | 12.23 | 0.42 | 0.000609 | 3.5 | 12.30 | 0.43 |
| | HOPF2@20 | 120 | 49522 | 413 | 853 | 7 | 0.590 | 3.7 | 0.000594 | 2.39 | 3 | 0.000571 | 2.3 | 11.54 | 0.27 | 0.000577 | 2.4 | 11.67 | 0.28 |
| | HOPF2@21 | 173 | 37157 | 215 | 1309 | 13 | 0.585 | 6.1 | 0.000683 | 2.78 | 2 | 0.000667 | 2.7 | 13.47 | 0.37 | 0.000667 | 2.8 | 13.47 | 0.38 |
| B | HOPF2@07 | 49 | 28763 | 591 | 480 | 5 | 0.735 | 2.5 | 0.000600 | 2.26 | 6 | 0.000559 | 2.1 | 11.29 | 0.24 | 0.000561 | 2.3 | 11.35 | 0.26 |
| | HOPF2@08 | 46 | 28779 | 627 | 495 | 5 | 0.740 | 2.3 | 0.000630 | 2.20 | 6 | 0.000593 | 2.1 | 11.98 | 0.25 | 0.000592 | 2.2 | 11.97 | 0.26 |
| | HOPF2@09 | 55 | 32338 | 593 | 429 | 4 | 0.721 | 1.9 | 0.000649 | 2.17 | 7 | 0.000603 | 2.1 | 12.18 | 0.25 | 0.000604 | 2.2 | 12.20 | 0.27 |
| | HOPF2@10 | 76 | 22645 | 296 | 595 | 9 | 0.714 | 4.1 | 0.000637 | 3.67 | 6 | 0.000597 | 3.5 | 12.06 | 0.42 | 0.000596 | 3.7 | 12.05 | 0.44 |
| | HOPF2@11 | 40 | 28273 | 701 | 140 | 3 | 0.810 | 1.2 | 0.000782 | 3.59 | 24 | 0.000580 | 2.8 | 11.72 | 0.32 | 0.000597 | 3.6 | 12.07 | 0.43 |
| | HOPF2@12 | 38 | 26357 | 689 | 346 | 4 | 0.780 | 2.1 | 0.000694 | 2.20 | 9 | 0.000628 | 2.1 | 12.68 | 0.26 | 0.000628 | 2.2 | 12.69 | 0.28 |
| | HOPF2@13 | 52 | 40578 | 775 | 305 | 3 | 0.777 | 1.7 | 0.000688 | 2.54 | 10 | 0.000615 | 2.3 | 12.43 | 0.29 | 0.000616 | 2.5 | 12.45 | 0.32 |
| | HOPF2@14 | 55 | 27790 | 505 | 261 | 3 | 0.773 | 1.6 | 0.000708 | 2.22 | 12 | 0.000614 | 2.0 | 12.41 | 0.25 | 0.000626 | 2.2 | 12.65 | 0.28 |
| C | HOPF2@01 | 40 | 23096 | 582 | 683 | 6 | 0.646 | 3.0 | 0.000591 | 2.20 | 4 | 0.000565 | 2.1 | 11.43 | 0.24 | 0.000567 | 2.2 | 11.45 | 0.25 |
| | HOPF2@02 | 42 | 25870 | 612 | 584 | 6 | 0.682 | 3.3 | 0.000619 | 2.23 | 4 | 0.000590 | 2.2 | 11.92 | 0.26 | 0.000594 | 2.2 | 11.99 | 0.27 |
| | HOPF2@03 | 45 | 29023 | 642 | 538 | 5 | 0.659 | 2.6 | 0.000647 | 2.27 | 4 | 0.000617 | 2.2 | 12.46 | 0.27 | 0.000619 | 2.3 | 12.50 | 0.28 |
| | HOPF2@04 | 50 | 30246 | 610 | 510 | 4 | 0.677 | 2.3 | 0.000656 | 2.35 | 5 | 0.000621 | 2.2 | 12.54 | 0.28 | 0.000622 | 2.3 | 12.58 | 0.30 |
| | HOPF2@05 | 57 | 32908 | 577 | 451 | 4 | 0.690 | 2.1 | 0.000670 | 2.48 | 6 | 0.000627 | 2.4 | 12.67 | 0.30 | 0.000629 | 2.5 | 12.70 | 0.32 |
| | HOPF2@06 | 58 | 28865 | 500 | 481 | 4 | 0.680 | 2.1 | 0.000642 | 2.18 | 6 | 0.000602 | 2.1 | 12.16 | 0.25 | 0.000602 | 2.2 | 12.17 | 0.27 |
| A | GART1@07 | 232 | 13668 | 59 | 1022 | 10 | 0.175 | 2.0 | 0.000830 | 2.3 | 2 | 0.000799 | 2.3 | 16.14 | 0.36 | 0.000811 | 2.3 | 16.38 | 0.38 |
| | GART1@08 | 302 | 9312 | 31 | 523 | 8 | 0.208 | 1.6 | 0.000831 | 2.3 | 6 | 0.000769 | 2.3 | 15.54 | 0.35 | 0.000785 | 2.3 | 15.85 | 0.37 |
| | GART1@09 | 206 | 14195 | 69 | 1054 | 9 | 0.173 | 2.0 | 0.000815 | 2.0 | 2 | 0.000785 | 2.0 | 15.86 | 0.31 | 0.000799 | 2.0 | 16.14 | 0.32 |
| | GART1@10 | 199 | 17962 | 90 | 716 | 7 | 0.192 | 2.1 | 0.000838 | 2.1 | 2 | 0.000793 | 2.1 | 16.01 | 0.33 | 0.000823 | 2.1 | 16.63 | 0.36 |
| | GART1@11 | 221 | 9789 | 44 | 881 | 12 | 0.162 | 2.5 | 0.000813 | 2.3 | 3 | 0.000778 | 2.3 | 15.71 | 0.36 | 0.000792 | 2.3 | 16.00 | 0.38 |
| | GART1@22 | 86 | 8047 | 93 | 412 | 8 | 0.321 | 1.8 | 0.000889 | 2.0 | 6 | 0.000806 | 2.0 | 16.29 | 0.32 | 0.000835 | 2.0 | 16.86 | 0.34 |
| | GART1@23 | 142 | 9137 | 65 | 454 | 8 | 0.317 | 1.8 | 0.000858 | 1.9 | 6 | 0.000786 | 1.9 | 15.88 | 0.29 | 0.000810 | 1.9 | 16.36 | 0.31 |
| | GART1@24 | 133 | 7292 | 55 | 371 | 8 | 0.322 | 1.8 | 0.000864 | 2.3 | 7 | 0.000774 | 2.2 | 15.64 | 0.35 | 0.000808 | 2.3 | 16.32 | 0.38 |
| | GART1@25 | 132 | 8048 | 61 | 435 | 9 | 0.318 | 2.0 | 0.000855 | 2.4 | 6 | 0.000779 | 2.3 | 15.74 | 0.37 | 0.000804 | 2.5 | 16.24 | 0.40 |
| | GART1@26 | 139 | 9550 | 69 | 512 | 8 | 0.328 | 1.8 | 0.000866 | 2.1 | 6 | 0.000800 | 2.1 | 16.17 | 0.33 | 0.000816 | 2.1 | 16.49 | 0.35 |

**Table 3.** Continued.

| Groups | Analysis ID | U (ppm) | Th (ppm) | Th / U | $^{208}Pb$ / $^{204}Pb$ | 1σ (%) | $^{207}Pb$ / $^{206}Pb$ | 1σ (%) | $^{208}Pb$ / $^{232}Th$ | 1σ (%) | f208 from 207 (%) | 204-corr $^{208}Pb$ / $^{232}Th$ | 204-corr 1σ (%) | 204-corr spot ages $^{208}Pb$ / $^{232}Th$ Age (Ma) | 204-corr spot ages 1σ (abs.) | 207-corr $^{208}Pb$ / $^{232}Th$ | 207-corr 1σ (%) | 207-corr spot ages $^{208}Pb$ / $^{232}Th$ Age (Ma) | 207-corr spot ages 1σ (abs.) |
|---|---|---|---|---|---|---|---|---|---|---|---|---|---|---|---|---|---|---|---|
| Central Tauern Window | | | | | | | | | | | | | | | | | | | |
| B | GART1@01 | 14 | 7467 | 551 | 446 | 9 | 0.626 | 2.3 | 0.000807 | 2.3 | 6 | 0.000737 | 2.3 | 14.89 | 0.34 | 0.000758 | 2.4 | 15.32 | 0.37 |
| | GART1@02 | 16 | 11180 | 718 | 285 | 14 | 0.707 | 3.8 | 0.000774 | 2.3 | 7 | 0.000669 | 2.7 | 13.51 | 0.37 | 0.000716 | 2.4 | 14.47 | 0.35 |
| | GART1@04 | 28 | 11198 | 401 | 967 | 11 | 0.299 | 3.0 | 0.000783 | 2.2 | 1 | 0.000752 | 2.2 | 15.19 | 0.33 | 0.000771 | 2.2 | 15.59 | 0.35 |
| | GART1@05 | 31 | 13066 | 424 | 1149 | 11 | 0.232 | 3.4 | 0.000731 | 3.0 | 1 | 0.000707 | 2.9 | 14.28 | 0.42 | 0.000724 | 3.0 | 14.64 | 0.44 |
| | GART1@17 | 86 | 22525 | 263 | 679 | 7 | 0.397 | 1.5 | 0.000854 | 1.8 | 4 | 0.000806 | 1.8 | 16.28 | 0.29 | 0.000820 | 1.8 | 16.56 | 0.30 |
| | GART1@18 | 110 | 23948 | 218 | 894 | 7 | 0.307 | 1.7 | 0.000820 | 1.8 | 2 | 0.000784 | 1.8 | 15.84 | 0.28 | 0.000799 | 1.8 | 16.15 | 0.30 |
| | GART1@19 | 14 | 7182 | 501 | 832 | 14 | 0.437 | 3.9 | 0.000778 | 2.2 | 2 | 0.000742 | 2.2 | 14.98 | 0.32 | 0.000763 | 2.2 | 15.42 | 0.34 |
| | GART1@20 | 108 | 19460 | 180 | 740 | 7 | 0.321 | 1.8 | 0.000828 | 2.0 | 3 | 0.000785 | 2.0 | 15.86 | 0.31 | 0.000805 | 2.0 | 16.26 | 0.33 |
| | GART1@21 | 106 | 23334 | 220 | 775 | 7 | 0.330 | 1.6 | 0.000839 | 2.0 | 3 | 0.000797 | 2.0 | 16.10 | 0.32 | 0.000816 | 2.0 | 16.48 | 0.34 |
| | *GART1@03* | *16* | *15175* | *927* | 53 | *3* | *0.802* | *0.8* | *0.001916* | *11.9* | *62* | *0.000516* | *4.1* | *10.43* | *0.43* | *0.000729* | *17.7* | *14.72* | *2.61* |
| | *GART1@04* | *19* | *13099* | *696* | 69 | *4* | *0.810* | *1.0* | *0.001303* | *7.8* | *48* | *0.000571* | *4.2* | *11.53* | *0.48* | *0.000679* | *12.9* | *13.72* | *1.76* |
| | *GART1@06* | *93* | *12315* | *133* | 2322 | *26* | *0.182* | *6.4* | *0.000453* | *4.0* | *1* | *0.000446* | *3.9* | *9.01* | *0.35* | *0.000450* | *4.0* | *9.09* | *0.36* |
| A | NOWA3@01 | 99 | 7183 | 73 | 397 | 10 | 0.433 | 2.1 | 0.000894 | 4.3 | 9 | 0.000807 | 4.0 | 16.31 | 0.65 | 0.000809 | 4.3 | 16.35 | 0.71 |
| | NOWA3@02 | 111 | 7973 | 72 | 205 | 7 | 0.569 | 1.8 | 0.000864 | 3.8 | 15 | 0.000704 | 3.4 | 14.23 | 0.48 | 0.000733 | 3.8 | 14.80 | 0.57 |
| | NOWA3@03 | 95 | 10612 | 112 | 506 | 9 | 0.474 | 2.1 | 0.000852 | 3.8 | 7 | 0.000787 | 3.6 | 15.90 | 0.57 | 0.000793 | 3.8 | 16.03 | 0.61 |
| | NOWA3@04 | 93 | 10175 | 109 | 103 | 5 | 0.724 | 1.2 | 0.001132 | 5.8 | 37 | 0.000707 | 4.1 | 14.29 | 0.58 | 0.000713 | 5.9 | 14.40 | 0.84 |
| | NOWA3@05 | 107 | 6658 | 62 | 94 | 5 | 0.695 | 1.4 | 0.001145 | 5.8 | 38 | 0.000674 | 4.1 | 13.62 | 0.56 | 0.000711 | 5.9 | 14.37 | 0.84 |
| | NOWA3@06 | 146 | 7715 | 53 | 176 | 9 | 0.606 | 2.0 | 0.000875 | 5.6 | 22 | 0.000683 | 4.8 | 13.80 | 0.66 | 0.000681 | 5.6 | 13.75 | 0.77 |
| | NOWA3@07 | 162 | 4216 | 26 | 137 | 7 | 0.461 | 1.6 | 0.001023 | 4.8 | 27 | 0.000734 | 4.0 | 14.84 | 0.59 | 0.000743 | 4.8 | 15.01 | 0.72 |
| | NOWA3@09 | 187 | 2571 | 14 | 81 | 7 | 0.445 | 1.7 | 0.001077 | 5.9 | 36 | 0.000565 | 4.4 | 11.42 | 0.50 | 0.000686 | 5.9 | 13.86 | 0.82 |
| | NOWA3@10 | 178 | 3925 | 22 | 124 | 7 | 0.478 | 1.5 | 0.001053 | 6.0 | 30 | 0.000726 | 4.6 | 14.68 | 0.68 | 0.000738 | 6.0 | 14.91 | 0.89 |
| | NOWA3@11 | 106 | 5924 | 56 | 188 | 7 | 0.477 | 1.8 | 0.000922 | 4.7 | 17 | 0.000732 | 4.0 | 14.80 | 0.59 | 0.000761 | 4.7 | 15.38 | 0.72 |
| | NOWA3@22 | 106 | 6470 | 61 | 1230 | 19 | 0.133 | 3.9 | 0.000837 | 1.2 | 2 | 0.000811 | 1.3 | 16.38 | 0.22 | 0.000824 | 1.2 | 16.65 | 0.20 |
| | NOWA3@23 | 94 | 9038 | 96 | 1036 | 14 | 0.300 | 2.7 | 0.000864 | 0.9 | 4 | 0.000832 | 1.0 | 16.81 | 0.18 | 0.000834 | 0.9 | 16.85 | 0.16 |
| | NOWA3@24 | 100 | 9053 | 90 | 896 | 14 | 0.265 | 3.1 | 0.000786 | 1.0 | 3 | 0.000752 | 1.2 | 15.19 | 0.18 | 0.000765 | 1.1 | 15.45 | 0.16 |
| | NOWA3@25 | 91 | 7689 | 84 | 1010 | 15 | 0.176 | 3.6 | 0.000857 | 0.9 | 2 | 0.000824 | 1.0 | 16.65 | 0.17 | 0.000842 | 0.9 | 17.01 | 0.15 |
| B | NOWA3@17 | 192 | 9482 | 50 | 555 | 10 | 0.290 | 1.7 | 0.000859 | 3.7 | 7 | 0.000799 | 3.5 | 16.15 | 0.57 | 0.000799 | 3.7 | 16.15 | 0.61 |
| | NOWA3@18 | 193 | 8656 | 45 | 388 | 8 | 0.288 | 1.7 | 0.000838 | 3.8 | 8 | 0.000755 | 3.5 | 15.24 | 0.53 | 0.000774 | 3.8 | 15.64 | 0.59 |
| | NOWA3@19 | 179 | 11023 | 62 | 531 | 9 | 0.286 | 1.7 | 0.000832 | 3.9 | 6 | 0.000771 | 3.7 | 15.58 | 0.57 | 0.000786 | 3.9 | 15.87 | 0.62 |
| | NOWA3@20 | 189 | 10600 | 56 | 451 | 8 | 0.278 | 1.7 | 0.000836 | 3.9 | 6 | 0.000765 | 3.6 | 15.45 | 0.56 | 0.000786 | 3.9 | 15.87 | 0.62 |
| | NOWA3@21 | 212 | 10750 | 51 | 225 | 13 | 0.368 | 2.5 | 0.000907 | 4.0 | 17 | 0.000752 | 4.0 | 15.18 | 0.60 | 0.000757 | 4.0 | 15.30 | 0.61 |
| C | NOWA3@12 | 50 | 12537 | 253 | 347 | 7 | 0.547 | 1.8 | 0.000868 | 3.9 | 8 | 0.000771 | 3.6 | 15.58 | 0.56 | 0.000796 | 3.9 | 16.08 | 0.63 |
| | NOWA3@13 | 34 | 9676 | 287 | 371 | 8 | 0.556 | 1.9 | 0.000839 | 3.8 | 8 | 0.000751 | 3.5 | 15.18 | 0.54 | 0.000773 | 3.8 | 15.62 | 0.60 |
| | NOWA3@14 | 39 | 10246 | 260 | 323 | 8 | 0.534 | 2.0 | 0.000783 | 3.9 | 8 | 0.000689 | 3.6 | 13.93 | 0.50 | 0.000723 | 3.9 | 14.61 | 0.58 |
| | NOWA3@15 | 48 | 11123 | 231 | 498 | 10 | 0.504 | 2.1 | 0.000777 | 3.8 | 7 | 0.000717 | 3.6 | 14.48 | 0.52 | 0.000726 | 3.8 | 14.66 | 0.56 |
| | NOWA3@16 | 48 | 10718 | 225 | 349 | 9 | 0.590 | 2.0 | 0.000745 | 4.4 | 9 | 0.000663 | 4.0 | 13.39 | 0.53 | 0.000677 | 4.4 | 13.68 | 0.60 |
| | *NOWA3@08* | *212* | *3097* | *15* | *123* | *8* | *0.375* | *1.7* | *0.001111* | *6.8* | *29* | *0.000763* | *5.3* | *15.41* | *0.81* | *0.000788* | *6.9* | *15.93* | *1.09* |
| A | GART3@13 | 85 | 8547 | 101 | 226 | 9 | 0.537 | 2.1 | 0.000901 | 2.6 | 14 | 0.000747 | 2.7 | 15.09 | 0.41 | 0.000775 | 2.6 | 15.65 | 0.41 |
| | GART3@14 | 112 | 9936 | 89 | 207 | 10 | 0.541 | 2.4 | 0.000879 | 2.8 | 14 | 0.000715 | 3.0 | 14.46 | 0.43 | 0.000760 | 2.9 | 15.36 | 0.44 |
| | GART3@15 | 95 | 9197 | 97 | 184 | 10 | 0.595 | 2.1 | 0.000969 | 3.9 | 19 | 0.000769 | 3.7 | 15.54 | 0.58 | 0.000781 | 3.9 | 15.78 | 0.62 |
| | GART3@16 | 94 | 9295 | 99 | 183 | 9 | 0.585 | 1.9 | 0.000917 | 3.2 | 20 | 0.000723 | 3.2 | 14.61 | 0.47 | 0.000733 | 3.3 | 14.82 | 0.48 |
| | GART3@17 | 159 | 9327 | 59 | 179 | 13 | 0.621 | 2.6 | 0.000881 | 2.9 | 25 | 0.000691 | 3.7 | 13.95 | 0.51 | 0.000662 | 3.0 | 13.38 | 0.40 |
| | GART3@18 | 161 | 8380 | 52 | 128 | 11 | 0.623 | 2.6 | 0.000904 | 2.9 | 25 | 0.000638 | 4.0 | 12.90 | 0.51 | 0.000676 | 3.0 | 13.65 | 0.41 |
| B | GART3@07 | 251 | 11739 | 47 | 318 | 10 | 0.312 | 2.1 | 0.000865 | 2.8 | 8 | 0.000760 | 2.7 | 15.36 | 0.41 | 0.000794 | 2.8 | 16.04 | 0.44 |
| | GART3@08 | 318 | 9593 | 30 | 219 | 11 | 0.374 | 2.3 | 0.000836 | 2.7 | 15 | 0.000689 | 3.0 | 13.92 | 0.41 | 0.000711 | 2.7 | 14.37 | 0.39 |
| | GART3@09 | 335 | 8995 | 27 | 220 | 11 | 0.379 | 2.2 | 0.000858 | 2.7 | 17 | 0.000711 | 3.0 | 14.37 | 0.44 | 0.000714 | 2.8 | 14.43 | 0.40 |
| | GART3@10 | 318 | 9819 | 31 | 221 | 11 | 0.377 | 2.2 | 0.000875 | 2.8 | 15 | 0.000722 | 3.0 | 14.58 | 0.44 | 0.000745 | 2.9 | 15.05 | 0.43 |
| | GART3@11 | 387 | 10683 | 28 | 244 | 13 | 0.326 | 2.8 | 0.000829 | 2.7 | 11 | 0.000703 | 3.1 | 14.20 | 0.44 | 0.000738 | 2.7 | 14.92 | 0.41 |
| | GART3@12 | 484 | 11366 | 24 | 210 | 13 | 0.388 | 3.1 | 0.000864 | 2.6 | 12 | 0.000712 | 3.3 | 14.38 | 0.47 | 0.000760 | 2.6 | 15.35 | 0.40 |
| | GART3@19 | 129 | 5307 | 41 | 100 | 7 | 0.543 | 1.7 | 0.001103 | 4.2 | 31 | 0.000681 | 3.9 | 13.75 | 0.53 | 0.000756 | 4.3 | 15.27 | 0.65 |
| | GART3@20 | 251 | 4358 | 17 | 122 | 10 | 0.408 | 2.1 | 0.000990 | 3.6 | 29 | 0.000676 | 4.1 | 13.65 | 0.56 | 0.000707 | 3.7 | 14.29 | 0.53 |
| | GART3@21 | 247 | 13787 | 56 | 218 | 8 | 0.411 | 1.9 | 0.000901 | 2.7 | 12 | 0.000742 | 2.7 | 14.99 | 0.40 | 0.000797 | 2.7 | 16.09 | 0.44 |
| | GART3@22 | 431 | 10631 | 25 | 215 | 13 | 0.466 | 2.5 | 0.000880 | 2.6 | 19 | 0.000734 | 3.3 | 14.83 | 0.49 | 0.000712 | 2.7 | 14.38 | 0.39 |
| | GART3@23 | 240 | 12846 | 54 | 247 | 10 | 0.414 | 2.2 | 0.000879 | 2.9 | 12 | 0.000745 | 2.9 | 15.05 | 0.44 | 0.000773 | 2.9 | 15.61 | 0.45 |
| C | GART3@01 | 114 | 7936 | 69 | 285 | 12 | 0.352 | 2.7 | 0.000762 | 2.6 | 10 | 0.000659 | 2.8 | 13.31 | 0.37 | 0.000689 | 2.6 | 13.92 | 0.36 |
| | GART3@03 | 183 | 3983 | 22 | 100 | 13 | 0.392 | 3.3 | 0.000778 | 2.9 | 23 | 0.000477 | 5.4 | 9.65 | 0.52 | 0.000602 | 3.1 | 12.17 | 0.37 |
| | GART3@04 | 176 | 3297 | 19 | 138 | 17 | 0.392 | 3.3 | 0.000802 | 2.9 | 26 | 0.000578 | 5.1 | 11.67 | 0.60 | 0.000595 | 3.1 | 12.02 | 0.37 |
| | GART3@05 | 123 | 4784 | 39 | 191 | 14 | 0.393 | 2.9 | 0.000770 | 2.8 | 17 | 0.000614 | 3.6 | 12.41 | 0.44 | 0.000639 | 2.8 | 12.92 | 0.36 |
| | GART3@06 | 166 | 4521 | 27 | 197 | 17 | 0.374 | 3.5 | 0.000763 | 2.6 | 17 | 0.000623 | 4.0 | 12.58 | 0.51 | 0.000630 | 2.7 | 12.72 | 0.34 |
| | *GART3@02* | *161* | *3479* | *22* | 109 | 12 | *0.449* | *2.6* | 0.000824 | 8.0 | *32* | *0.000531* | *6.8* | *10.73* | *0.73* | *0.000558* | *8.1* | *11.28* | *0.91* |

**Table 3.** Continued.

| Groups | Analysis ID | U (ppm) | Th (ppm) | Th / U | $^{208}Pb/^{204}Pb$ | 1σ (%) | $^{207}Pb/^{206}Pb$ | 1σ (%) | $^{208}Pb/^{232}Th$ | 1σ (%) | f208 from 207 (%) | 204-corr | | 204-corr spot ages | | 207-corr | | 207-corr spot ages | |
|---|---|---|---|---|---|---|---|---|---|---|---|---|---|---|---|---|---|---|---|
| | | | | | | | | | | | | $^{208}Pb/^{232}Th$ | 1σ (%) | $^{208}Pb/^{232}Th$ Age (Ma) | 1σ (abs.) | $^{208}Pb/^{232}Th$ | 1σ (%) | $^{208}Pb/^{232}Th$ Age (Ma) | 1σ (abs.) |
| Central Tauern Window | | | | | | | | | | | | | | | | | | | |
| | STEI2@01 | 395 | 15567 | 39 | 1346 | 11 | 0.106 | 2.0 | 0.000873 | 2.12 | 2 | 0.000848 | 2.1 | 17.14 | 0.36 | 0.000859 | 2.1 | 17.36 | 0.37 |
| | STEI2@02 | 403 | 16229 | 40 | 1096 | 10 | 0.113 | 2.0 | 0.000862 | 2.11 | 2 | 0.000833 | 2.1 | 16.82 | 0.35 | 0.000847 | 2.1 | 17.11 | 0.36 |
| | STEI2@03 | 417 | 16643 | 40 | 1022 | 9 | 0.115 | 1.9 | 0.000869 | 2.04 | 2 | 0.000836 | 2.0 | 16.89 | 0.34 | 0.000854 | 2.0 | 17.25 | 0.35 |
| | STEI2@04 | 376 | 17989 | 48 | 1436 | 11 | 0.097 | 2.2 | 0.000854 | 2.15 | 1 | 0.000831 | 2.1 | 16.79 | 0.35 | 0.000844 | 2.1 | 17.05 | 0.37 |
| | STEI2@05 | 348 | 7706 | 22 | 844 | 13 | 0.101 | 2.2 | 0.000860 | 2.50 | 3 | 0.000820 | 2.5 | 16.57 | 0.41 | 0.000837 | 2.5 | 16.92 | 0.42 |
| | STEI2@06 | 288 | 6287 | 22 | 700 | 13 | 0.125 | 2.3 | 0.000892 | 1.90 | 4 | 0.000843 | 1.9 | 17.02 | 0.33 | 0.000857 | 1.9 | 17.32 | 0.33 |
| | STEI2@07 | 257 | 5814 | 23 | 556 | 12 | 0.176 | 2.0 | 0.000915 | 2.06 | 6 | 0.000851 | 2.1 | 17.20 | 0.36 | 0.000858 | 2.1 | 17.34 | 0.36 |
| | STEI2@08 | 387 | 5851 | 15 | 730 | 13 | 0.090 | 2.3 | 0.000874 | 2.49 | 3 | 0.000830 | 2.5 | 16.76 | 0.41 | 0.000848 | 2.5 | 17.13 | 0.43 |
| | STEI2@09 | 443 | 5143 | 12 | 649 | 14 | 0.080 | 2.3 | 0.000859 | 2.51 | 3 | 0.000810 | 2.5 | 16.37 | 0.41 | 0.000832 | 2.5 | 16.82 | 0.43 |
| | STEI2@10 | 295 | 6041 | 20 | 689 | 14 | 0.118 | 2.4 | 0.000875 | 2.18 | 3 | 0.000828 | 2.2 | 16.73 | 0.37 | 0.000844 | 2.2 | 17.06 | 0.37 |
| | STEI2@11 | 370 | 7478 | 20 | 1151 | 15 | 0.088 | 2.4 | 0.000858 | 2.11 | 2 | 0.000829 | 2.1 | 16.76 | 0.35 | 0.000841 | 2.1 | 16.99 | 0.36 |
| | STEI2@12 | 548 | 11690 | 21 | 755 | 10 | 0.103 | 1.8 | 0.000884 | 1.96 | 3 | 0.000838 | 1.9 | 16.94 | 0.33 | 0.000859 | 2.0 | 17.36 | 0.34 |
| | STEI2@13 | 579 | 10095 | 17 | 798 | 11 | 0.101 | 1.8 | 0.000871 | 2.26 | 3 | 0.000829 | 2.2 | 16.75 | 0.37 | 0.000844 | 2.3 | 17.06 | 0.39 |
| | STEI2@14 | 601 | 10283 | 17 | 745 | 10 | 0.099 | 1.8 | 0.000869 | 2.15 | 3 | 0.000824 | 2.1 | 16.65 | 0.35 | 0.000843 | 2.2 | 17.03 | 0.37 |
| | STEI2@15 | 352 | 19439 | 55 | 962 | 9 | 0.138 | 2.0 | 0.000864 | 1.83 | 2 | 0.000829 | 1.8 | 16.75 | 0.30 | 0.000848 | 1.8 | 17.14 | 0.31 |
| | STEI2@16 | 455 | 10595 | 23 | 676 | 10 | 0.127 | 1.8 | 0.000891 | 2.06 | 3 | 0.000840 | 2.0 | 16.96 | 0.34 | 0.000861 | 2.1 | 17.39 | 0.36 |
| | STEI2@17 | 387 | 8068 | 21 | 902 | 13 | 0.091 | 2.2 | 0.000864 | 2.03 | 2 | 0.000827 | 2.0 | 16.71 | 0.34 | 0.000846 | 2.0 | 17.10 | 0.35 |
| | STEI2@18 | 348 | 11391 | 33 | 1180 | 13 | 0.101 | 2.5 | 0.000846 | 2.09 | 1 | 0.000819 | 2.1 | 16.55 | 0.34 | 0.000835 | 2.1 | 16.87 | 0.35 |
| | STEI2@19 | 339 | 12077 | 36 | 1048 | 11 | 0.095 | 2.3 | 0.000876 | 2.20 | 1 | 0.000844 | 2.2 | 17.05 | 0.37 | 0.000864 | 2.2 | 17.45 | 0.39 |
| | STEI2@20 | 323 | 7488 | 23 | 943 | 13 | 0.084 | 2.6 | 0.000871 | 2.04 | 1 | 0.000835 | 2.0 | 16.87 | 0.34 | 0.000858 | 2.0 | 17.33 | 0.35 |
| A | KNOR1@19 | 149 | 12269 | 82 | 466 | 7 | 0.392 | 3.5 | 0.000558 | 2.34 | 4 | 0.000527 | 2.3 | 10.64 | 0.24 | 0.000535 | 2.3 | 10.81 | 0.25 |
| | KNOR1@20 | 181 | 9307 | 52 | 285 | 7 | 0.488 | 3.2 | 0.000587 | 3.28 | 11 | 0.000515 | 3.1 | 10.41 | 0.32 | 0.000522 | 3.3 | 10.55 | 0.35 |
| | KNOR1@21 | 239 | 9337 | 39 | 642 | 13 | 0.400 | 5.1 | 0.000604 | 3.67 | 5 | 0.000574 | 3.6 | 11.60 | 0.42 | 0.000572 | 3.7 | 11.56 | 0.42 |
| | KNOR1@22 | 172 | 8289 | 48 | 512 | 9 | 0.321 | 4.1 | 0.000570 | 2.76 | 4 | 0.000537 | 2.7 | 10.86 | 0.29 | 0.000545 | 2.8 | 11.01 | 0.30 |
| | KNOR1@24 | 194 | 7199 | 37 | 605 | 13 | 0.268 | 5.3 | 0.000549 | 3.18 | 4 | 0.000517 | 3.1 | 10.44 | 0.32 | 0.000529 | 3.2 | 10.68 | 0.34 |
| B | KNOR1@01 | 32 | 7767 | 246 | 189 | 5 | 0.737 | 2.5 | 0.000615 | 2.18 | 18 | 0.000498 | 2.1 | 10.06 | 0.21 | 0.000505 | 2.2 | 10.21 | 0.23 |
| | KNOR1@02 | 35 | 6107 | 175 | 197 | 6 | 0.731 | 2.9 | 0.000637 | 2.60 | 18 | 0.000521 | 2.5 | 10.53 | 0.26 | 0.000524 | 2.6 | 10.59 | 0.28 |
| | KNOR1@03 | 36 | 9885 | 273 | 115 | 4 | 0.784 | 1.8 | 0.000767 | 2.66 | 32 | 0.000518 | 2.3 | 10.48 | 0.24 | 0.000518 | 2.7 | 10.47 | 0.29 |
| | KNOR1@05 | 27 | 9535 | 356 | 102 | 3 | 0.786 | 1.4 | 0.000869 | 2.35 | 36 | 0.000560 | 1.9 | 11.32 | 0.22 | 0.000558 | 2.4 | 11.28 | 0.27 |
| | KNOR1@06 | 33 | 9203 | 277 | 167 | 4 | 0.734 | 2.1 | 0.000661 | 2.18 | 19 | 0.000522 | 2.0 | 10.54 | 0.21 | 0.000533 | 2.2 | 10.77 | 0.24 |
| | KNOR1@07 | 33 | 4983 | 152 | 112 | 5 | 0.726 | 2.1 | 0.000768 | 2.20 | 31 | 0.000522 | 2.2 | 10.56 | 0.23 | 0.000527 | 2.3 | 10.64 | 0.25 |
| | KNOR1@08 | 36 | 3783 | 105 | 136 | 6 | 0.652 | 2.8 | 0.000701 | 2.17 | 24 | 0.000516 | 2.4 | 10.42 | 0.25 | 0.000533 | 2.3 | 10.76 | 0.24 |
| | KNOR1@09 | 39 | 5846 | 149 | 281 | 7 | 0.573 | 3.4 | 0.000577 | 2.30 | 11 | 0.000513 | 2.3 | 10.37 | 0.24 | 0.000514 | 2.3 | 10.38 | 0.24 |
| | KNOR1@04 | 30 | 6902 | 234 | 95 | 3 | 0.759 | 1.6 | 0.000920 | 2.21 | 37 | 0.000555 | 1.9 | 11.21 | 0.22 | 0.000576 | 2.3 | 11.63 | 0.27 |
| C | KNOR1@10 | 48 | 5633 | 118 | 428 | 11 | 0.495 | 5.2 | 0.000542 | 2.37 | 6 | 0.000499 | 2.4 | 10.07 | 0.24 | 0.000508 | 2.4 | 10.27 | 0.24 |
| | KNOR1@11 | 48 | 4611 | 96 | 444 | 12 | 0.478 | 5.6 | 0.000560 | 2.48 | 6 | 0.000525 | 2.6 | 10.61 | 0.27 | 0.000528 | 2.5 | 10.67 | 0.27 |
| | KNOR1@12 | 57 | 4583 | 81 | 399 | 11 | 0.355 | 5.3 | 0.000540 | 2.18 | 5 | 0.000498 | 2.3 | 10.06 | 0.23 | 0.000513 | 2.2 | 10.36 | 0.23 |
| | KNOR1@13 | 54 | 4104 | 77 | 445 | 11 | 0.331 | 5.0 | 0.000541 | 2.29 | 5 | 0.000500 | 2.4 | 10.10 | 0.24 | 0.000513 | 2.3 | 10.37 | 0.24 |
| | KNOR1@14 | 56 | 6093 | 108 | 729 | 13 | 0.285 | 5.6 | 0.000516 | 2.19 | 3 | 0.000495 | 2.2 | 10.00 | 0.22 | 0.000501 | 2.2 | 10.12 | 0.22 |
| | KNOR1@15 | 76 | 6847 | 91 | 639 | 11 | 0.237 | 5.4 | 0.000529 | 2.19 | 2 | 0.000508 | 2.2 | 10.27 | 0.23 | 0.000515 | 2.2 | 10.41 | 0.23 |
| | KNOR1@16 | 65 | 5872 | 91 | 524 | 11 | 0.224 | 5.8 | 0.000529 | 2.17 | 2 | 0.000503 | 2.2 | 10.17 | 0.23 | 0.000517 | 2.2 | 10.45 | 0.23 |
| | KNOR1@18 | 77 | 8867 | 114 | 628 | 10 | 0.141 | 5.7 | 0.000559 | 2.52 | 1 | 0.000544 | 2.6 | 11.00 | 0.28 | 0.000552 | 2.5 | 11.15 | 0.28 |
| | KNOR1@17 | 73 | 6281 | 86 | 585 | 10 | 0.191 | 5.4 | 0.000590 | 2.24 | 2 | 0.000564 | 2.3 | 11.41 | 0.26 | 0.000578 | 2.2 | 11.68 | 0.26 |
| Eastern Tauern Window | | | | | | | | | | | | | | | | | | | |
| A | KAIS6@29 | 12 | 32285 | 2726 | 324 | 2 | 0.816 | 1.1 | 0.001135 | 2.68 | 11 | 0.001014 | 2.4 | 20.48 | 0.49 | 0.001015 | 2.7 | 20.51 | 0.55 |
| | KAIS6@37 | 10 | 35152 | 3587 | 322 | 2 | 0.817 | 1.1 | 0.001192 | 2.71 | 10 | 0.001065 | 2.4 | 21.51 | 0.52 | 0.001072 | 2.7 | 21.66 | 0.59 |
| | KAIS6@38 | 10 | 35481 | 3480 | 428 | 3 | 0.797 | 1.4 | 0.001137 | 2.74 | 8 | 0.001046 | 2.5 | 21.13 | 0.54 | 0.001045 | 2.8 | 21.12 | 0.58 |
| | KAIS6@39 | 10 | 31600 | 3326 | 316 | 3 | 0.820 | 1.3 | 0.001154 | 2.73 | 11 | 0.001022 | 2.4 | 20.65 | 0.50 | 0.001030 | 2.7 | 20.81 | 0.57 |
| | KAIS6@41 | 8 | 32642 | 4280 | 351 | 2 | 0.824 | 1.2 | 0.001173 | 2.74 | 9 | 0.001057 | 2.5 | 21.36 | 0.53 | 0.001063 | 2.8 | 21.48 | 0.59 |
| | KAIS6@42 | 6 | 29873 | 4677 | 292 | 2 | 0.836 | 1.2 | 0.001200 | 2.69 | 11 | 0.001054 | 2.4 | 21.28 | 0.51 | 0.001066 | 2.7 | 21.54 | 0.58 |

**Table 3.** Continued.

| Groups | Analysis ID | U (ppm) | Th (ppm) | Th / U | $^{208}Pb/^{204}Pb$ | 1σ (%) | $^{207}Pb/^{206}Pb$ | 1σ (%) | $^{208}Pb/^{232}Th$ | 1σ (%) | f208 from 207 (%) | 204-corr | | 204-corr spot ages | | 207-corr | | 207-corr spot ages | |
|---|---|---|---|---|---|---|---|---|---|---|---|---|---|---|---|---|---|---|---|
| | | | | | | | | | | | | $^{208}Pb/^{232}Th$ | 1σ (%) | $^{208}Pb/^{232}Th$ Age (Ma) | 1σ (abs.) | $^{208}Pb/^{232}Th$ | 1σ (%) | $^{208}Pb/^{232}Th$ Age (Ma) | 1σ (abs.) |
| Eastern Tauern Window | | | | | | | | | | | | | | | | | | | |
| B | KAIS6@15 | 5 | 21644 | 4568 | 142 | 2 | 0.833 | 0.9 | 0.001399 | 2.69 | 25 | 0.001031 | 2.0 | 20.83 | 0.43 | 0.001045 | 2.8 | 21.12 | 0.59 |
| | KAIS6@16 | 5 | 22052 | 4771 | 161 | 2 | 0.831 | 0.9 | 0.001329 | 2.69 | 23 | 0.001020 | 2.1 | 20.61 | 0.44 | 0.001022 | 2.7 | 20.65 | 0.57 |
| | KAIS6@17 | 5 | 25100 | 4752 | 189 | 2 | 0.825 | 1.0 | 0.001299 | 2.73 | 19 | 0.001046 | 2.2 | 21.12 | 0.47 | 0.001049 | 2.8 | 21.20 | 0.59 |
| | KAIS6@18 | 5 | 25260 | 4905 | 148 | 2 | 0.827 | 0.9 | 0.001392 | 2.81 | 26 | 0.001040 | 2.2 | 21.01 | 0.45 | 0.001025 | 2.9 | 20.71 | 0.61 |
| | KAIS6@19 | 5 | 23495 | 5173 | 148 | 2 | 0.825 | 0.9 | 0.001390 | 2.75 | 24 | 0.001038 | 2.1 | 20.96 | 0.44 | 0.001053 | 2.8 | 21.28 | 0.60 |
| | KAIS6@20 | 5 | 24260 | 5377 | 157 | 2 | 0.829 | 0.9 | 0.001351 | 2.83 | 24 | 0.001032 | 2.2 | 20.85 | 0.46 | 0.001033 | 2.9 | 20.86 | 0.61 |
| | KAIS6@21 | 5 | 25950 | 5040 | 155 | 2 | 0.837 | 0.9 | 0.001320 | 2.73 | 24 | 0.001003 | 2.1 | 20.27 | 0.43 | 0.001007 | 2.8 | 20.35 | 0.57 |
| | KAIS6@22 | 4 | 20175 | 4625 | 134 | 2 | 0.813 | 0.9 | 0.001424 | 2.76 | 27 | 0.001034 | 2.1 | 20.88 | 0.43 | 0.001043 | 2.8 | 21.07 | 0.60 |
| | KAIS6@23 | 3 | 18427 | 5349 | 153 | 2 | 0.828 | 1.0 | 0.001353 | 2.82 | 24 | 0.001028 | 2.2 | 20.76 | 0.46 | 0.001027 | 2.9 | 20.74 | 0.60 |
| | KAIS6@24 | 4 | 17328 | 4822 | 178 | 2 | 0.830 | 1.1 | 0.001313 | 2.69 | 21 | 0.001045 | 2.2 | 21.11 | 0.46 | 0.001041 | 2.7 | 21.02 | 0.58 |
| | KAIS6@25 | 5 | 17901 | 3588 | 154 | 2 | 0.833 | 0.9 | 0.001366 | 2.77 | 24 | 0.001042 | 2.2 | 21.05 | 0.46 | 0.001039 | 2.8 | 20.98 | 0.59 |
| | KAIS6@26 | 4 | 19477 | 5281 | 167 | 2 | 0.820 | 1.0 | 0.001304 | 2.75 | 22 | 0.001020 | 2.2 | 20.60 | 0.46 | 0.001017 | 2.8 | 20.56 | 0.58 |
| | KAIS6@27 | 4 | 19595 | 5290 | 165 | 2 | 0.821 | 1.1 | 0.001325 | 2.72 | 22 | 0.001030 | 2.2 | 20.80 | 0.45 | 0.001036 | 2.8 | 20.93 | 0.58 |
| | KAIS6@28 | 3 | 17683 | 5368 | 162 | 2 | 0.817 | 1.0 | 0.001354 | 2.76 | 23 | 0.001043 | 2.2 | 21.06 | 0.46 | 0.001041 | 2.8 | 21.02 | 0.59 |
| | KAIS6@31 | 3 | 19464 | 6314 | 207 | 2 | 0.826 | 1.2 | 0.001275 | 2.67 | 17 | 0.001049 | 2.2 | 21.19 | 0.48 | 0.001059 | 2.7 | 21.39 | 0.58 |
| | KAIS6@32 | 3 | 17623 | 5729 | 145 | 2 | 0.823 | 1.0 | 0.001352 | 2.75 | 26 | 0.001007 | 2.1 | 20.35 | 0.43 | 0.001003 | 2.8 | 20.26 | 0.57 |
| | KAIS6@33 | 4 | 23433 | 5395 | 191 | 2 | 0.819 | 1.0 | 0.001257 | 2.79 | 18 | 0.001018 | 2.3 | 20.56 | 0.47 | 0.001026 | 2.8 | 20.73 | 0.59 |
| | KAIS6@34 | 3 | 22517 | 6923 | 175 | 2 | 0.836 | 0.9 | 0.001289 | 2.73 | 21 | 0.001016 | 2.2 | 20.52 | 0.45 | 0.001015 | 2.8 | 20.51 | 0.57 |
| | KAIS6@35 | 4 | 23426 | 6129 | 175 | 2 | 0.827 | 0.9 | 0.001299 | 2.72 | 21 | 0.001025 | 2.2 | 20.70 | 0.45 | 0.001031 | 2.8 | 20.82 | 0.58 |
| | KAIS6@36 | 4 | 24762 | 6924 | 169 | 2 | 0.821 | 0.9 | 0.001316 | 2.76 | 21 | 0.001031 | 2.2 | 20.83 | 0.46 | 0.001034 | 2.8 | 20.89 | 0.59 |
| | KAIS6@43 | 4 | 19511 | 4948 | 229 | 2 | 0.828 | 1.2 | 0.001210 | 2.76 | 15 | 0.001024 | 2.4 | 20.68 | 0.49 | 0.001023 | 2.8 | 20.66 | 0.58 |
| | KAIS6@44 | 5 | 20543 | 3995 | 252 | 3 | 0.828 | 1.5 | 0.001177 | 2.72 | 14 | 0.001007 | 2.4 | 20.35 | 0.48 | 0.001009 | 2.8 | 20.39 | 0.56 |
| | KAIS6@45 | 4 | 17366 | 4418 | 225 | 3 | 0.834 | 1.4 | 0.001269 | 2.67 | 15 | 0.001067 | 2.3 | 21.55 | 0.49 | 0.001076 | 2.7 | 21.73 | 0.59 |
| | KAIS6@46 | 4 | 14595 | 3614 | 231 | 3 | 0.813 | 1.5 | 0.001284 | 2.70 | 15 | 0.001083 | 2.3 | 21.88 | 0.51 | 0.001094 | 2.7 | 22.11 | 0.61 |
| C | KAIS6@01 | 2 | 13078 | 6002 | 83 | 2 | 0.844 | 0.8 | 0.001865 | 2.70 | 46 | 0.001011 | 1.7 | 20.43 | 0.34 | 0.001001 | 3.1 | 20.21 | 0.63 |
| | KAIS6@02 | 3 | 14140 | 4835 | 97 | 2 | 0.823 | 0.9 | 0.001682 | 2.76 | 40 | 0.001031 | 1.9 | 20.83 | 0.39 | 0.001012 | 3.0 | 20.44 | 0.62 |
| | KAIS6@05 | 3 | 10157 | 2957 | 96 | 2 | 0.837 | 1.0 | 0.001672 | 2.69 | 38 | 0.001010 | 1.9 | 20.41 | 0.38 | 0.001035 | 3.0 | 20.91 | 0.63 |
| | KAIS6@06 | 4 | 15227 | 3566 | 104 | 2 | 0.828 | 1.0 | 0.001564 | 2.84 | 36 | 0.000995 | 2.0 | 20.11 | 0.40 | 0.000994 | 3.1 | 20.09 | 0.63 |
| | KAIS6@09 | 3 | 10348 | 3946 | 74 | 1 | 0.828 | 0.7 | 0.002146 | 2.71 | 52 | 0.001030 | 1.5 | 20.81 | 0.32 | 0.001037 | 3.7 | 20.94 | 0.77 |
| | KAIS6@10 | 3 | 12624 | 4224 | 90 | 2 | 0.828 | 0.9 | 0.001795 | 2.74 | 42 | 0.001037 | 1.8 | 20.96 | 0.37 | 0.001033 | 3.1 | 20.87 | 0.64 |
| | KAIS6@12 | 3 | 10457 | 3171 | 91 | 2 | 0.822 | 1.0 | 0.001752 | 2.68 | 41 | 0.001020 | 1.8 | 20.61 | 0.37 | 0.001039 | 3.0 | 20.98 | 0.63 |
| *D* | KAIS6@03 | 4 | 15947 | 3922 | 100 | 2 | 0.844 | 1.0 | 0.001524 | 2.91 | 39 | 0.000944 | 2.0 | 19.07 | 0.38 | 0.000924 | 3.2 | 18.67 | 0.59 |
| | KAIS6@04 | 4 | 16156 | 3905 | 91 | 2 | 0.829 | 1.0 | 0.001531 | 3.25 | 40 | 0.000890 | 2.1 | 17.98 | 0.38 | 0.000923 | 3.5 | 18.65 | 0.66 |
| | KAIS6@07 | 6 | 11981 | 2002 | 89 | 4 | 0.843 | 1.6 | 0.001562 | 2.89 | 44 | 0.000887 | 2.3 | 17.93 | 0.40 | 0.000877 | 3.7 | 17.71 | 0.65 |
| | KAIS6@08 | 3 | 10466 | 3145 | 87 | 2 | 0.824 | 0.8 | 0.001711 | 2.68 | 44 | 0.000959 | 1.7 | 19.37 | 0.33 | 0.000956 | 3.1 | 19.31 | 0.59 |
| | KAIS6@11 | 4 | 13094 | 3210 | 89 | 2 | 0.830 | 1.1 | 0.001493 | 2.92 | 42 | 0.000846 | 2.0 | 17.09 | 0.33 | 0.000870 | 3.3 | 17.58 | 0.58 |
| | KAIS6@13 | 4 | 13271 | 3273 | 88 | 2 | 0.842 | 1.0 | 0.001621 | 2.84 | 41 | 0.000917 | 1.9 | 18.52 | 0.35 | 0.000950 | 3.3 | 19.19 | 0.63 |
| | KAIS6@14 | 9 | 13459 | 1568 | 105 | 4 | 0.827 | 1.7 | 0.001323 | 3.57 | 33 | 0.000836 | 2.6 | 16.89 | 0.44 | 0.000881 | 3.8 | 17.79 | 0.68 |
| | KAIS6@30 | 14 | 25376 | 1840 | 225 | 2 | 0.837 | 1.1 | 0.001130 | 2.68 | 16 | 0.000950 | 2.3 | 19.20 | 0.44 | 0.000951 | 2.7 | 19.22 | 0.52 |
| | KAIS6@40 | 10 | 32326 | 3141 | 301 | 3 | 0.800 | 1.4 | 0.001094 | 2.93 | 12 | 0.000962 | 2.6 | 19.44 | 0.51 | 0.000967 | 3.0 | 19.53 | 0.58 |
| | KAIS6@47 | 9 | 31411 | 3692 | 311 | 3 | 0.818 | 1.3 | 0.001069 | 2.68 | 11 | 0.000949 | 2.4 | 19.16 | 0.46 | 0.000955 | 2.7 | 19.28 | 0.52 |
| | *KAIS6@48* | *13* | *18728* | *1403* | *217* | *3* | *0.836* | *1.5* | *0.001218* | *2.67* | *17* | *0.001014* | *2.3* | *20.49* | *0.47* | *0.001014* | *2.7* | *20.48* | *0.56* |
| | *KAIS6@49* | *13* | *18241* | *1449* | *248* | *3* | *0.813* | *1.3* | *0.001252* | *2.69* | *14* | *0.001072* | *2.3* | *21.66* | *0.51* | *0.001083* | *2.7* | *21.87* | *0.59* |
| | SALZ18@01 | 11 | 443 | 40 | 428 | 6 | 0.642 | 2.9 | 0.001001 | 2.30 | 8 | 0.000928 | 2.2 | 18.75 | 0.41 | 0.000921 | 2.31 | 18.61 | 0.43 |
| | SALZ18@02 | 19 | 11907 | 639 | 515 | 6 | 0.546 | 3.0 | 0.000970 | 2.16 | 4 | 0.000914 | 2.1 | 18.46 | 0.39 | 0.000928 | 2.17 | 18.75 | 0.41 |
| | SALZ18@03 | 23 | 12452 | 552 | 1291 | 11 | 0.191 | 7.3 | 0.000859 | 2.25 | 1 | 0.000853 | 2.3 | 17.23 | 0.39 | 0.000854 | 2.25 | 17.25 | 0.39 |
| | SALZ18@04 | 20 | 8334 | 407 | 800 | 10 | 0.246 | 6.5 | 0.000943 | 2.52 | 1 | 0.000909 | 2.5 | 18.36 | 0.46 | 0.000933 | 2.52 | 18.84 | 0.47 |
| | SALZ18@05 | 28 | 6912 | 245 | 1239 | 12 | 0.235 | 6.6 | 0.000911 | 2.20 | 1 | 0.000903 | 2.2 | 18.24 | 0.41 | 0.000902 | 2.20 | 18.22 | 0.40 |
| | SALZ18@06 | 11 | 2256 | 200 | 1200 | 13 | 0.314 | 7.5 | 0.000947 | 2.26 | 1 | 0.000941 | 2.3 | 19.00 | 0.44 | 0.000935 | 2.26 | 18.90 | 0.43 |
| | SALZ18@07 | 23 | 9797 | 429 | 1862 | 19 | 0.208 | 9.6 | 0.000863 | 2.34 | 1 | 0.000858 | 2.4 | 17.33 | 0.41 | 0.000857 | 2.34 | 17.31 | 0.40 |
| | SALZ18@08 | 20 | 4607 | 232 | 980 | 14 | 0.186 | 10.0 | 0.000880 | 2.39 | 1 | 0.000856 | 2.4 | 17.29 | 0.42 | 0.000874 | 2.39 | 17.66 | 0.42 |
| | SALZ18@09 | 18 | 3952 | 224 | 1353 | 18 | 0.180 | 9.3 | 0.000942 | 2.42 | 1 | 0.000934 | 2.5 | 18.87 | 0.47 | 0.000934 | 2.42 | 18.88 | 0.46 |
| | SALZ18@10 | 19 | 3681 | 189 | 894 | 18 | 0.178 | 10.2 | 0.000917 | 2.57 | 1 | 0.000889 | 2.6 | 17.96 | 0.47 | 0.000907 | 2.57 | 18.33 | 0.47 |
| | SALZ18@11 | 13 | 1751 | 134 | 1123 | 15 | 0.312 | 7.3 | 0.000979 | 2.38 | 2 | 0.000962 | 2.4 | 19.44 | 0.47 | 0.000963 | 2.38 | 19.46 | 0.46 |
| | SALZ18@12 | 17 | 4555 | 267 | 731 | 19 | 0.169 | 10.8 | 0.000922 | 2.74 | 1 | 0.000881 | 2.8 | 17.80 | 0.50 | 0.000910 | 2.74 | 18.39 | 0.50 |
| | SALZ18@13 | 17 | 1752 | 106 | 617 | 27 | 0.207 | 11.1 | 0.000887 | 3.43 | 3 | 0.000850 | 3.8 | 17.18 | 0.65 | 0.000860 | 3.43 | 17.37 | 0.60 |
| | SALZ18@14 | 22 | 1037 | 48 | 975 | 11 | 0.270 | 6.1 | 0.000953 | 2.24 | 1 | 0.000938 | 2.3 | 18.95 | 0.43 | 0.000941 | 2.24 | 19.01 | 0.43 |
| | SALZ18@15 | 37 | 9684 | 262 | 1073 | 14 | 0.224 | 7.5 | 0.000792 | 2.37 | 1 | 0.000781 | 2.4 | 15.79 | 0.38 | 0.000783 | 2.37 | 15.81 | 0.37 |

**Table 3.** Continued.

| Groups | Analysis ID | U (ppm) | Th (ppm) | Th / U | $^{208}Pb$ / $^{204}Pb$ | 1σ (%) | $^{207}Pb$ / $^{206}Pb$ | 1σ (%) | $^{208}Pb$ / $^{232}Th$ | 1σ (%) | f208 from 207 (%) | 204-corr | | 204-corr spot ages | | 207-corr | | 207-corr spot ages | |
|---|---|---|---|---|---|---|---|---|---|---|---|---|---|---|---|---|---|---|---|
| | | | | | | | | | | | | $^{208}Pb$ / $^{232}Th$ | 1σ (%) | $^{208}Pb$ / $^{232}Th$ Age (Ma) | 1σ (abs.) | $^{208}Pb$ / $^{232}Th$ | 1σ (%) | $^{208}Pb$ / $^{232}Th$ Age (Ma) | 1σ (abs.) |
| Eastern Tauern Window | | | | | | | | | | | | | | | | | | | |
| A | LOHN4@01 | 14 | 14552 | 1076 | 79 | 1 | 0.826 | 0.7 | 0.001981 | 2.96 | 47 | 0.001031 | 1.7 | 20.84 | 0.35 | 0.001059 | 3.57 | 21.39 | 0.76 |
| | LOHN4@02 | 39 | 25804 | 662 | 272 | 3 | 0.779 | 1.4 | 0.001112 | 3.21 | 13 | 0.000964 | 2.8 | 19.47 | 0.55 | 0.000969 | 3.24 | 19.58 | 0.63 |
| | LOHN4@03 | 11 | 12883 | 1175 | 151 | 2 | 0.805 | 1.2 | 0.001356 | 2.67 | 24 | 0.001026 | 2.1 | 20.73 | 0.44 | 0.001033 | 2.76 | 20.86 | 0.58 |
| | LOHN4@04 | 16 | 16561 | 1017 | 173 | 2 | 0.820 | 1.2 | 0.001332 | 2.87 | 22 | 0.001051 | 2.3 | 21.23 | 0.49 | 0.001045 | 2.96 | 21.12 | 0.63 |
| | LOHN4@07 | 34 | 35456 | 1048 | 338 | 2 | 0.779 | 1.1 | 0.001218 | 2.68 | 10 | 0.001094 | 2.4 | 22.11 | 0.53 | 0.001097 | 2.69 | 22.16 | 0.60 |
| | LOHN4@08 | 31 | 32345 | 1044 | 312 | 2 | 0.782 | 1.0 | 0.001208 | 2.75 | 11 | 0.001074 | 2.5 | 21.70 | 0.53 | 0.001070 | 2.77 | 21.62 | 0.60 |
| | LOHN4@09 | 33 | 34180 | 1040 | 323 | 2 | 0.790 | 1.1 | 0.001224 | 2.70 | 11 | 0.001094 | 2.4 | 22.09 | 0.54 | 0.001092 | 2.71 | 22.07 | 0.60 |
| | LOHN4@10 | 33 | 35690 | 1072 | 349 | 2 | 0.788 | 1.1 | 0.001171 | 2.68 | 10 | 0.001058 | 2.4 | 21.38 | 0.52 | 0.001060 | 2.69 | 21.41 | 0.57 |
| | LOHN4@11 | 34 | 29955 | 888 | 355 | 3 | 0.796 | 1.3 | 0.001085 | 2.67 | 10 | 0.000977 | 2.4 | 19.75 | 0.48 | 0.000977 | 2.68 | 19.74 | 0.53 |
| | LOHN4@12 | 27 | 29155 | 1065 | 366 | 3 | 0.776 | 1.3 | 0.001185 | 2.68 | 9 | 0.001078 | 2.5 | 21.77 | 0.53 | 0.001082 | 2.69 | 21.86 | 0.59 |
| | LOHN4@13 | 26 | 23964 | 935 | 97 | 2 | 0.823 | 0.7 | 0.001750 | 2.99 | 39 | 0.001071 | 1.9 | 21.64 | 0.42 | 0.001066 | 3.32 | 21.54 | 0.72 |
| | LOHN4@14 | 28 | 22365 | 792 | 156 | 2 | 0.806 | 1.0 | 0.001418 | 2.83 | 23 | 0.001087 | 2.2 | 21.97 | 0.49 | 0.001089 | 2.96 | 22.01 | 0.65 |
| | LOHN4@15 | 24 | 20864 | 866 | 523 | 4 | 0.742 | 1.9 | 0.001109 | 2.69 | 6 | 0.001040 | 2.5 | 21.00 | 0.53 | 0.001044 | 2.70 | 21.09 | 0.57 |
| | LOHN4@16 | 30 | 23937 | 797 | 575 | 4 | 0.728 | 2.2 | 0.001062 | 2.75 | 5 | 0.001003 | 2.6 | 20.25 | 0.53 | 0.001006 | 2.76 | 20.33 | 0.56 |
| | LOHN4@19 | 27 | 21599 | 807 | 299 | 3 | 0.788 | 1.3 | 0.001221 | 2.71 | 12 | 0.001075 | 2.4 | 21.71 | 0.52 | 0.001080 | 2.72 | 21.82 | 0.59 |
| | LOHN4@20 | 29 | 23422 | 801 | 350 | 3 | 0.785 | 1.4 | 0.001156 | 2.67 | 10 | 0.001042 | 2.4 | 21.06 | 0.51 | 0.001041 | 2.68 | 21.02 | 0.56 |
| | LOHN4@21 | 16 | 17205 | 1046 | 171 | 2 | 0.798 | 1.0 | 0.001354 | 2.70 | 22 | 0.001064 | 2.2 | 21.49 | 0.47 | 0.001060 | 2.76 | 21.41 | 0.59 |
| | LOHN4@22 | 17 | 16983 | 991 | 165 | 2 | 0.810 | 1.1 | 0.001359 | 2.76 | 22 | 0.001055 | 2.2 | 21.31 | 0.47 | 0.001057 | 2.82 | 21.35 | 0.60 |
| | LOHN4@23 | 16 | 17269 | 1091 | 162 | 2 | 0.819 | 1.0 | 0.001388 | 2.79 | 23 | 0.001074 | 2.2 | 21.70 | 0.48 | 0.001065 | 2.85 | 21.52 | 0.61 |
| | LOHN4@24 | 20 | 21768 | 1108 | 176 | 2 | 0.810 | 1.1 | 0.001258 | 2.87 | 22 | 0.000990 | 2.3 | 20.00 | 0.46 | 0.000985 | 2.93 | 19.90 | 0.58 |
| | LOHN4@25 | 18 | 15361 | 875 | 174 | 3 | 0.823 | 1.2 | 0.001232 | 2.68 | 21 | 0.000969 | 2.2 | 19.58 | 0.43 | 0.000979 | 2.74 | 19.77 | 0.54 |
| | LOHN4@26 | 15 | 17857 | 1172 | 172 | 2 | 0.806 | 1.1 | 0.001276 | 2.68 | 21 | 0.001001 | 2.2 | 20.21 | 0.44 | 0.001012 | 2.73 | 20.44 | 0.56 |
| | LOHN4@27 | 27 | 26405 | 974 | 184 | 2 | 0.819 | 0.9 | 0.001317 | 2.72 | 19 | 0.001056 | 2.2 | 21.34 | 0.47 | 0.001064 | 2.76 | 21.50 | 0.59 |
| | LOHN4@28 | 28 | 27181 | 955 | 190 | 2 | 0.816 | 0.9 | 0.001324 | 2.80 | 20 | 0.001068 | 2.3 | 21.58 | 0.49 | 0.001066 | 2.84 | 21.53 | 0.61 |
| | LOHN4@29 | 27 | 25484 | 955 | 191 | 2 | 0.809 | 1.0 | 0.001304 | 2.85 | 20 | 0.001051 | 2.3 | 21.22 | 0.50 | 0.001048 | 2.90 | 21.18 | 0.61 |
| | LOHN4@30 | 27 | 25099 | 915 | 190 | 2 | 0.798 | 0.9 | 0.001322 | 2.71 | 19 | 0.001067 | 2.2 | 21.55 | 0.48 | 0.001068 | 2.75 | 21.58 | 0.59 |
| | LOHN4@31 | 30 | 25226 | 855 | 433 | 3 | 0.777 | 1.6 | 0.001235 | 2.67 | 8 | 0.001139 | 2.5 | 23.00 | 0.57 | 0.001134 | 2.68 | 22.92 | 0.61 |
| | LOHN4@32 | 36 | 21812 | 606 | 287 | 4 | 0.797 | 1.7 | 0.001212 | 2.70 | 13 | 0.001061 | 2.4 | 21.43 | 0.52 | 0.001053 | 2.73 | 21.27 | 0.58 |
| | LOHN4@33 | 27 | 23182 | 856 | 199 | 2 | 0.805 | 1.0 | 0.001233 | 2.67 | 18 | 0.001002 | 2.2 | 20.24 | 0.45 | 0.001011 | 2.71 | 20.42 | 0.55 |
| | LOHN4@34 | 26 | 24807 | 948 | 188 | 2 | 0.812 | 1.0 | 0.001293 | 2.71 | 19 | 0.001043 | 2.2 | 21.06 | 0.47 | 0.001044 | 2.75 | 21.09 | 0.58 |
| | LOHN4@35 | 25 | 23076 | 925 | 174 | 2 | 0.812 | 0.9 | 0.001327 | 3.07 | 21 | 0.001045 | 2.5 | 21.11 | 0.52 | 0.001052 | 3.14 | 21.26 | 0.67 |
| | LOHN4@36 | 26 | 25326 | 972 | 190 | 2 | 0.786 | 0.9 | 0.001308 | 2.73 | 19 | 0.001052 | 2.2 | 21.25 | 0.47 | 0.001061 | 2.77 | 21.43 | 0.59 |
| | LOHN4@37 | 27 | 26268 | 980 | 210 | 2 | 0.802 | 1.0 | 0.001282 | 2.78 | 17 | 0.001062 | 2.3 | 21.45 | 0.50 | 0.001061 | 2.81 | 21.43 | 0.60 |
| | LOHN4@38 | 27 | 27571 | 1016 | 218 | 2 | 0.812 | 1.0 | 0.001239 | 2.72 | 16 | 0.001033 | 2.3 | 20.87 | 0.48 | 0.001040 | 2.75 | 21.02 | 0.58 |
| | LOHN4@39 | 26 | 25481 | 988 | 207 | 2 | 0.806 | 0.9 | 0.001272 | 2.69 | 18 | 0.001047 | 2.2 | 21.16 | 0.48 | 0.001044 | 2.72 | 21.08 | 0.57 |
| | LOHN4@40 | 26 | 26144 | 1007 | 211 | 2 | 0.814 | 1.0 | 0.001245 | 2.78 | 17 | 0.001029 | 2.3 | 20.78 | 0.48 | 0.001032 | 2.81 | 20.85 | 0.59 |
| | LOHN4@41 | 19 | 24124 | 1248 | 221 | 2 | 0.800 | 1.0 | 0.001271 | 2.72 | 17 | 0.001061 | 2.3 | 21.44 | 0.49 | 0.001057 | 2.75 | 21.35 | 0.59 |
| | LOHN4@42 | 19 | 23602 | 1235 | 226 | 2 | 0.816 | 1.1 | 0.001279 | 2.74 | 16 | 0.001078 | 2.3 | 21.78 | 0.51 | 0.001076 | 2.77 | 21.73 | 0.60 |
| | LOHN4@43 | 21 | 23764 | 1157 | 236 | 2 | 0.802 | 1.1 | 0.001247 | 2.70 | 15 | 0.001057 | 2.3 | 21.36 | 0.49 | 0.001059 | 2.72 | 21.40 | 0.58 |
| | LOHN4@44 | 20 | 23194 | 1138 | 231 | 2 | 0.803 | 1.1 | 0.001254 | 2.72 | 15 | 0.001055 | 2.3 | 21.32 | 0.49 | 0.001067 | 2.74 | 21.56 | 0.59 |
| | LOHN4@45 | 20 | 23831 | 1188 | 232 | 2 | 0.787 | 1.0 | 0.001255 | 2.70 | 15 | 0.001058 | 2.3 | 21.37 | 0.49 | 0.001065 | 2.72 | 21.51 | 0.58 |
| | LOHN4@46 | 20 | 20913 | 1027 | 204 | 2 | 0.813 | 1.0 | 0.001277 | 2.67 | 17 | 0.001047 | 2.2 | 21.16 | 0.47 | 0.001058 | 2.70 | 21.38 | 0.58 |
| | LOHN4@48 | 22 | 23727 | 1093 | 262 | 2 | 0.808 | 1.1 | 0.001210 | 2.78 | 14 | 0.001045 | 2.4 | 21.12 | 0.51 | 0.001046 | 2.80 | 21.13 | 0.59 |
| | LOHN4@49 | 22 | 23546 | 1065 | 259 | 2 | 0.789 | 1.1 | 0.001179 | 2.73 | 13 | 0.001018 | 2.4 | 20.56 | 0.49 | 0.001022 | 2.75 | 20.65 | 0.57 |
| | LOHN4@50 | 21 | 22193 | 1049 | 260 | 2 | 0.806 | 1.2 | 0.001208 | 2.70 | 13 | 0.001045 | 2.4 | 21.12 | 0.50 | 0.001047 | 2.72 | 21.15 | 0.57 |
| | LOHN4@51 | 20 | 22103 | 1121 | 259 | 2 | 0.800 | 1.2 | 0.001179 | 2.67 | 14 | 0.001014 | 2.3 | 20.48 | 0.48 | 0.001011 | 2.69 | 20.43 | 0.55 |
| | LOHN4@52 | 20 | 20091 | 1023 | 242 | 2 | 0.785 | 1.2 | 0.001146 | 2.68 | 14 | 0.000973 | 2.3 | 19.66 | 0.45 | 0.000987 | 2.70 | 19.93 | 0.54 |
| | LOHN4@53 | 10 | 15092 | 1539 | 136 | 2 | 0.818 | 1.0 | 0.001422 | 2.69 | 28 | 0.001029 | 2.0 | 20.80 | 0.42 | 0.001030 | 2.79 | 20.80 | 0.58 |
| | LOHN4@54 | 10 | 13028 | 1330 | 137 | 2 | 0.812 | 1.1 | 0.001350 | 2.66 | 26 | 0.000979 | 2.0 | 19.78 | 0.40 | 0.000993 | 2.78 | 20.07 | 0.56 |
| | LOHN4@55 | 10 | 14821 | 1515 | 137 | 2 | 0.806 | 1.0 | 0.001355 | 2.67 | 27 | 0.000982 | 2.0 | 19.83 | 0.40 | 0.000983 | 2.78 | 19.85 | 0.55 |
| B | LOHN4@05 | 19 | 14990 | 787 | 171 | 4 | 0.821 | 1.6 | 0.001129 | 3.06 | 22 | 0.000882 | 2.5 | 17.83 | 0.45 | 0.000875 | 3.15 | 17.68 | 0.56 |
| | LOHN4@06 | 31 | 9191 | 298 | 146 | 5 | 0.794 | 2.3 | 0.001237 | 3.80 | 26 | 0.000913 | 3.1 | 18.45 | 0.58 | 0.000912 | 3.95 | 18.42 | 0.73 |
| | LOHN4@17 | 32 | 23011 | 717 | 714 | 6 | 0.732 | 2.8 | 0.000980 | 3.29 | 5 | 0.000936 | 3.2 | 18.91 | 0.60 | 0.000933 | 3.29 | 18.85 | 0.62 |
| | LOHN4@18 | 39 | 23334 | 591 | 461 | 5 | 0.760 | 2.3 | 0.001003 | 3.06 | 8 | 0.000927 | 2.9 | 18.73 | 0.54 | 0.000923 | 3.07 | 18.66 | 0.57 |
| | LOHN4@47 | 23 | 19054 | 816 | 222 | 3 | 0.808 | 1.2 | 0.001120 | 2.66 | 15 | 0.000933 | 2.3 | 18.85 | 0.43 | 0.000946 | 2.70 | 19.12 | 0.52 |
| | LOHN4@56 | 9 | 11815 | 1254 | 129 | 2 | 0.833 | 1.2 | 0.001272 | 2.78 | 28 | 0.000895 | 2.1 | 18.07 | 0.38 | 0.000913 | 2.90 | 18.45 | 0.53 |
| | LOHN4@57 | 13 | 11550 | 862 | 133 | 3 | 0.826 | 1.5 | 0.001194 | 3.44 | 28 | 0.000847 | 2.6 | 17.12 | 0.45 | 0.000855 | 3.58 | 17.28 | 0.62 |

**Table 3.** Continued.

| Groups | Analysis ID | U (ppm) | Th (ppm) | Th / U | $^{208}Pb/^{204}Pb$ | 1σ (%) | $^{207}Pb/^{206}Pb$ | 1σ (%) | $^{208}Pb/^{232}Th$ | 1σ (%) | f208 from 207 (%) | 204-corr $^{208}Pb/^{232}Th$ | 204-corr 1σ (%) | 204-corr spot ages $^{208}Pb/^{232}Th$ Age (Ma) | 204-corr spot ages 1σ (abs.) | 207-corr $^{208}Pb/^{232}Th$ | 207-corr 1σ (%) | 207-corr spot ages $^{208}Pb/^{232}Th$ Age (Ma) | 207-corr spot ages 1σ (abs.) |
|---|---|---|---|---|---|---|---|---|---|---|---|---|---|---|---|---|---|---|---|
| Eastern Tauern Window | | | | | | | | | | | | | | | | | | | |
| | ORT1@01 | 367 | 5825 | 16 | 1263 | 17 | 0.084 | 2.3 | 0.000945 | 2.48 | 2 | 0.000912 | 2.5 | 18.43 | 0.46 | 0.000922 | 2.5 | 18.63 | 0.47 |
| | ORT1@02 | 316 | 4437 | 14 | 711 | 23 | 0.087 | 2.4 | 0.000956 | 2.43 | 3 | 0.000905 | 2.4 | 18.27 | 0.44 | 0.000930 | 2.5 | 18.80 | 0.46 |
| | ORT1@03 | 277 | 4950 | 18 | 1166 | 16 | 0.097 | 2.5 | 0.000936 | 2.26 | 3 | 0.000896 | 2.3 | 18.10 | 0.41 | 0.000911 | 2.3 | 18.41 | 0.42 |
| | ORT1@04 | 356 | 4831 | 14 | 926 | 16 | 0.088 | 2.4 | 0.000905 | 2.92 | 3 | 0.000861 | 2.9 | 17.40 | 0.50 | 0.000877 | 3.0 | 17.73 | 0.53 |
| | ORT1@05 | 161 | 5336 | 33 | 930 | 18 | 0.139 | 2.6 | 0.000970 | 2.17 | 3 | 0.000924 | 2.2 | 18.67 | 0.41 | 0.000941 | 2.2 | 19.01 | 0.42 |
| | ORT1@06 | 222 | 3688 | 17 | 382 | 16 | 0.166 | 2.1 | 0.001012 | 2.99 | 7 | 0.000897 | 3.0 | 18.12 | 0.54 | 0.000938 | 3.2 | 18.95 | 0.61 |
| | ORT1@07 | 219 | 5005 | 23 | 277 | 13 | 0.272 | 1.6 | 0.001039 | 2.23 | 13 | 0.000893 | 2.3 | 18.05 | 0.41 | 0.000902 | 2.4 | 18.21 | 0.43 |
| | ORT1@08 | 189 | 5091 | 27 | 422 | 18 | 0.220 | 2.0 | 0.000979 | 2.96 | 8 | 0.000896 | 2.9 | 18.09 | 0.52 | 0.000901 | 3.1 | 18.21 | 0.56 |
| | ORT1@09 | 262 | 6320 | 24 | 591 | 17 | 0.139 | 2.3 | 0.000880 | 3.78 | 4 | 0.000824 | 3.6 | 16.65 | 0.60 | 0.000841 | 3.8 | 16.98 | 0.65 |
| | ORT1@10 | 199 | 7415 | 37 | 214 | 11 | 0.411 | 1.2 | 0.001086 | 2.24 | 16 | 0.000892 | 2.1 | 18.01 | 0.38 | 0.000912 | 2.4 | 18.43 | 0.44 |
| | ORT1@11 | 101 | 3205 | 32 | 655 | 17 | 0.172 | 3.0 | 0.000981 | 2.61 | 4 | 0.000926 | 2.7 | 18.71 | 0.50 | 0.000941 | 2.7 | 19.01 | 0.51 |
| | ORT1@12 | 106 | 3602 | 34 | 661 | 28 | 0.191 | 2.9 | 0.000933 | 3.58 | 4 | 0.000863 | 3.5 | 17.44 | 0.60 | 0.000895 | 3.6 | 18.08 | 0.66 |
| | ORT1@13 | 95 | 4969 | 52 | 607 | 18 | 0.195 | 2.9 | 0.000910 | 2.82 | 3 | 0.000855 | 2.8 | 17.28 | 0.48 | 0.000883 | 2.9 | 17.83 | 0.51 |
| | ORT1@14 | 96 | 3780 | 40 | 628 | 13 | 0.183 | 2.9 | 0.000960 | 2.17 | 4 | 0.000884 | 2.3 | 17.86 | 0.40 | 0.000923 | 2.2 | 18.65 | 0.42 |
| | *ORT1@15* | *105* | *4304* | *41* | *445* | *21* | *0.370* | *1.9* | *0.001022* | *4.60* | *12* | *0.000894* | *4.2* | *18.06* | *0.76* | *0.000903* | *5.7* | *18.24* | *1.04* |
| | EUKL2@01 | 9 | 296 | 32 | 160 | 3 | 0.803 | 1.2 | 0.001359 | 2.12 | 22 | 0.001043 | 1.7 | 21.07 | 0.37 | 0.001063 | 2.21 | 21.47 | 0.47 |
| | EUKL2@02 | 14 | 301 | 22 | 209 | 3 | 0.803 | 1.2 | 0.001317 | 2.51 | 18 | 0.001089 | 2.1 | 22.00 | 0.47 | 0.001080 | 2.56 | 21.81 | 0.56 |
| | EUKL2@03 | 13 | 21097 | 1580 | 205 | 2 | 0.824 | 1.2 | 0.001303 | 2.25 | 17 | 0.001072 | 1.9 | 21.65 | 0.41 | 0.001078 | 2.30 | 21.77 | 0.50 |
| | EUKL2@04 | 14 | 18352 | 1313 | 231 | 3 | 0.812 | 1.5 | 0.001253 | 2.08 | 16 | 0.001059 | 1.8 | 21.39 | 0.39 | 0.001048 | 2.13 | 21.16 | 0.45 |
| | EUKL2@05 | 33 | 52673 | 1620 | 345 | 3 | 0.782 | 1.3 | 0.001194 | 2.17 | 10 | 0.001076 | 2.0 | 21.74 | 0.43 | 0.001079 | 2.18 | 21.79 | 0.48 |
| | EUKL2@06 | 19 | 25562 | 1351 | 218 | 2 | 0.795 | 1.2 | 0.001315 | 2.10 | 16 | 0.001097 | 1.8 | 22.17 | 0.40 | 0.001102 | 2.14 | 22.26 | 0.48 |
| | EUKL2@07 | 19 | 16767 | 868 | 234 | 3 | 0.800 | 1.2 | 0.001282 | 2.10 | 15 | 0.001085 | 1.8 | 21.91 | 0.40 | 0.001085 | 2.14 | 21.92 | 0.47 |
| A | HOAR1@27 | 148 | 1591 | 11 | 235 | 13 | 0.195 | 2.2 | 0.001164 | 1.5 | 14 | 0.000973 | 2.4 | 19.65 | 0.48 | 0.001003 | 1.6 | 20.26 | 0.32 |
| | HOAR1@28 | 100 | 1383 | 14 | 149 | 11 | 0.248 | 2.2 | 0.001269 | 1.2 | 19 | 0.000940 | 2.9 | 19.00 | 0.55 | 0.001031 | 1.3 | 20.84 | 0.28 |
| | HOAR1@29 | 95 | 19676 | 208 | 1211 | 8 | 0.201 | 2.5 | 0.001023 | 0.8 | 1 | 0.000990 | 0.9 | 20.00 | 0.17 | 0.001013 | 0.8 | 20.47 | 0.17 |
| | HOAR1@30 | 80 | 650 | 8 | 214 | 19 | 0.170 | 3.3 | 0.001153 | 3.6 | 15 | 0.000946 | 4.6 | 19.10 | 0.88 | 0.000978 | 3.7 | 19.76 | 0.74 |
| | HOAR1@31 | 124 | 2725 | 22 | 497 | 14 | 0.169 | 2.6 | 0.001070 | 0.9 | 6 | 0.000987 | 1.4 | 19.94 | 0.28 | 0.001007 | 0.9 | 20.35 | 0.19 |
| | HOAR1@32 | 316 | 1076 | 3 | 160 | 12 | 0.132 | 2.0 | 0.001240 | 3.4 | 21 | 0.000950 | 4.0 | 19.20 | 0.76 | 0.000985 | 3.5 | 19.91 | 0.70 |
| B | HOAR1@01 | 50 | 926 | 18 | 322 | 20 | 0.244 | 3.7 | 0.001121 | 4.3 | 9 | 0.000999 | 4.6 | 20.18 | 0.92 | 0.001017 | 4.4 | 20.55 | 0.91 |
| | HOAR1@02 | 51 | 782 | 15 | 200 | 18 | 0.296 | 3.5 | 0.001128 | 3.5 | 15 | 0.000911 | 4.5 | 18.40 | 0.83 | 0.000954 | 4.5 | 19.27 | 0.87 |
| | HOAR1@03 | 48 | 969 | 20 | 250 | 17 | 0.205 | 3.5 | 0.001088 | 4.7 | 8 | 0.000920 | 4.8 | 18.59 | 0.89 | 0.000997 | 5.0 | 20.13 | 1.00 |
| | HOAR1@04 | 71 | 1075 | 15 | 259 | 18 | 0.182 | 3.5 | 0.001075 | 4.3 | 9 | 0.000926 | 4.6 | 18.70 | 0.85 | 0.000982 | 4.5 | 19.84 | 0.89 |
| | HOAR1@05 | 79 | 643 | 8 | 233 | 21 | 0.197 | 3.4 | 0.001118 | 4.2 | 16 | 0.000932 | 4.9 | 18.84 | 0.92 | 0.000940 | 5.0 | 18.98 | 0.94 |
| | HOAR1@06 | 118 | 1676 | 14 | 330 | 15 | 0.148 | 2.9 | 0.001046 | 2.8 | 7 | 0.000924 | 3.1 | 18.66 | 0.57 | 0.000977 | 3.0 | 19.73 | 0.59 |
| | HOAR1@07 | 106 | 1764 | 17 | 448 | 17 | 0.162 | 2.9 | 0.001065 | 2.6 | 7 | 0.000973 | 2.8 | 19.66 | 0.55 | 0.000993 | 2.8 | 20.07 | 0.56 |
| | HOAR1@08 | 67 | 1358 | 20 | 339 | 18 | 0.237 | 3.2 | 0.001049 | 2.8 | 11 | 0.000938 | 3.3 | 18.94 | 0.62 | 0.000938 | 3.0 | 18.95 | 0.57 |
| | HOAR1@09 | 62 | 1579 | 25 | 364 | 16 | 0.191 | 3.3 | 0.001110 | 3.0 | 5 | 0.000992 | 3.1 | 20.04 | 0.63 | 0.001050 | 3.2 | 21.20 | 0.67 |
| | HOAR1@10 | 266 | 1995 | 8 | 433 | 15 | 0.097 | 2.4 | 0.001076 | 2.4 | 5 | 0.000980 | 2.6 | 19.79 | 0.52 | 0.001019 | 2.6 | 20.59 | 0.54 |
| | HOAR1@11 | 56 | 6609 | 117 | 714 | 11 | 0.242 | 2.7 | 0.001032 | 2.2 | 3 | 0.000976 | 2.2 | 19.71 | 0.43 | 0.001005 | 2.2 | 20.31 | 0.45 |
| | HOAR1@12 | 104 | 2748 | 26 | 263 | 10 | 0.359 | 1.8 | 0.001163 | 2.3 | 15 | 0.000992 | 2.4 | 20.04 | 0.49 | 0.000988 | 2.4 | 19.96 | 0.48 |
| | HOAR1@13 | 103 | 3259 | 32 | 679 | 15 | 0.171 | 2.7 | 0.000998 | 3.0 | 4 | 0.000941 | 3.0 | 19.01 | 0.56 | 0.000959 | 3.0 | 19.37 | 0.59 |
| | HOAR1@14 | 107 | 1940 | 18 | 272 | 12 | 0.213 | 2.3 | 0.001115 | 3.9 | 10 | 0.000957 | 3.7 | 19.33 | 0.72 | 0.001005 | 4.4 | 20.30 | 0.88 |
| | HOAR1@16 | 145 | 2711 | 19 | 632 | 16 | 0.139 | 2.6 | 0.001076 | 2.5 | 4 | 0.001010 | 2.5 | 20.41 | 0.51 | 0.001029 | 2.5 | 20.78 | 0.53 |
| | HOAR1@17 | 72 | 1305 | 18 | 263 | 15 | 0.211 | 3.1 | 0.001059 | 3.7 | 8 | 0.000904 | 3.9 | 18.26 | 0.71 | 0.000969 | 3.9 | 19.58 | 0.77 |
| | HOAR1@18 | 74 | 1381 | 19 | 292 | 15 | 0.196 | 3.1 | 0.001088 | 4.2 | 8 | 0.000944 | 4.2 | 19.07 | 0.79 | 0.000998 | 4.4 | 20.16 | 0.89 |
| | HOAR1@19 | 60 | 1129 | 19 | 389 | 19 | 0.240 | 3.0 | 0.001129 | 3.7 | 10 | 0.001026 | 3.9 | 20.73 | 0.81 | 0.001019 | 4.0 | 20.58 | 0.82 |
| | HOAR1@20 | 60 | 1818 | 30 | 499 | 17 | 0.206 | 3.2 | 0.001035 | 2.6 | 5 | 0.000955 | 2.7 | 19.29 | 0.53 | 0.000978 | 2.8 | 19.76 | 0.55 |
| | HOAR1@21 | 45 | 1000 | 22 | 183 | 14 | 0.309 | 3.0 | 0.001130 | 3.8 | 15 | 0.000891 | 4.2 | 18.01 | 0.76 | 0.000964 | 4.2 | 19.47 | 0.82 |
| | HOAR1@22 | 49 | 1540 | 31 | 194 | 12 | 0.305 | 2.8 | 0.001127 | 2.5 | 9 | 0.000909 | 3.1 | 18.37 | 0.57 | 0.001025 | 2.9 | 20.70 | 0.59 |
| | HOAR1@23 | 126 | 1838 | 15 | 824 | 24 | 0.119 | 3.4 | 0.001015 | 3.2 | 5 | 0.000968 | 3.2 | 19.55 | 0.63 | 0.000966 | 3.3 | 19.52 | 0.64 |
| | HOAR1@24 | 85 | 1927 | 23 | 511 | 18 | 0.147 | 3.3 | 0.001026 | 2.6 | 5 | 0.000954 | 2.8 | 19.27 | 0.53 | 0.000974 | 2.8 | 19.67 | 0.54 |
| | HOAR1@25 | 53 | 1330 | 25 | 384 | 19 | 0.230 | 3.5 | 0.001022 | 2.9 | 8 | 0.000919 | 3.2 | 18.57 | 0.60 | 0.000944 | 3.0 | 19.08 | 0.58 |
| | HOAR1@26 | 60 | 1206 | 20 | 343 | 18 | 0.197 | 3.5 | 0.001023 | 3.1 | 8 | 0.000908 | 3.5 | 18.34 | 0.63 | 0.000940 | 3.3 | 18.99 | 0.63 |
| | *HOAR1@15* | *111* | *2877* | *26* | *112* | *6* | *0.516* | *1.2* | *0.001353* | *5.1* | *29* | *0.000885* | *3.9* | *17.88* | *0.70* | *0.000964* | *7.9* | *19.47* | *1.53* |

**Table 3.** Continued.

| Groups | Analysis ID | U (ppm) | Th (ppm) | Th / U | $^{208}Pb$ / $^{204}Pb$ | 1σ (%) | $^{207}Pb$ / $^{206}Pb$ | 1σ (%) | $^{208}Pb$ / $^{232}Th$ | 1σ (%) | f208 from 207 (%) | 204-corr | | 204-corr spot ages | | 207-corr | | 207-corr spot ages | |
|---|---|---|---|---|---|---|---|---|---|---|---|---|---|---|---|---|---|---|---|
| | | | | | | | | | | | | $^{208}Pb$ / $^{232}Th$ | 1σ (%) | $^{208}Pb$ / $^{232}Th$ Age (Ma) | 1σ (abs.) | $^{208}Pb$ / $^{232}Th$ | 1σ (%) | $^{208}Pb$ / $^{232}Th$ Age (Ma) | 1σ (abs.) |
| Eastern Tauern Window | | | | | | | | | | | | | | | | | | | |
| A | MOKR1@07 | 307 | 3840 | 13 | 172 | 11 | 0.228 | 2.1 | 0.001121 | 3.2 | 18 | 0.000876 | 3.6 | 17.69 | 0.64 | 0.000915 | 3.3 | 18.48 | 0.61 |
| | MOKR1@08 | 393 | 5762 | 15 | 259 | 15 | 0.228 | 2.8 | 0.000997 | 2.7 | 13 | 0.000848 | 3.2 | 17.13 | 0.55 | 0.000869 | 2.8 | 17.55 | 0.48 |
| | MOKR1@09 | 916 | 5949 | 6 | 260 | 14 | 0.128 | 2.3 | 0.000993 | 2.6 | 12 | 0.000845 | 3.1 | 17.08 | 0.52 | 0.000879 | 2.7 | 17.75 | 0.48 |
| | MOKR1@10 | 814 | 2999 | 4 | 166 | 13 | 0.134 | 2.0 | 0.001143 | 3.7 | 22 | 0.000878 | 4.1 | 17.74 | 0.73 | 0.000890 | 3.8 | 17.99 | 0.68 |
| | MOKR1@11 | 1852 | 2971 | 2 | 148 | 21 | 0.138 | 3.2 | 0.001168 | 2.9 | 26 | 0.000976 | 6.4 | 19.71 | 1.25 | 0.000859 | 3.3 | 17.36 | 0.57 |
| | MOKR1@12 | 702 | 7328 | 10 | 245 | 16 | 0.224 | 3.1 | 0.001029 | 2.6 | 13 | 0.000867 | 3.4 | 17.51 | 0.59 | 0.000899 | 2.6 | 18.15 | 0.47 |
| | MOKR1@20 | 442 | 2417 | 5 | 255 | 47 | 0.062 | 10.0 | 0.000754 | 1.0 | 5 | 0.000639 | 7.2 | 12.92 | 0.94 | 0.000714 | 1.4 | 14.42 | 0.21 |
| | MOKR1@21 | 473 | 5279 | 11 | 1029 | 55 | 0.063 | 10.2 | 0.001134 | 1.0 | 1 | 0.001091 | 2.3 | 22.05 | 0.50 | 0.001124 | 1.1 | 22.70 | 0.24 |
| | MOKR1@22 | 410 | 5545 | 14 | 2865 | 95 | 0.070 | 11.4 | 0.001130 | 1.6 | 1 | 0.001115 | 2.1 | 22.52 | 0.46 | 0.001119 | 1.7 | 22.61 | 0.37 |
| | MOKR1@23 | 341 | 2318 | 7 | 483 | 47 | 0.104 | 6.6 | 0.001093 | 1.3 | 8 | 0.001049 | 4.4 | 21.18 | 0.94 | 0.001011 | 1.6 | 20.43 | 0.32 |
| | MOKR1@24 | 507 | 7589 | 15 | 3668 | 67 | 0.057 | 6.1 | 0.001049 | 1.5 | 1 | 0.001038 | 1.7 | 20.97 | 0.35 | 0.001042 | 1.5 | 21.06 | 0.32 |
| | MOKR1@25 | 336 | 4029 | 12 | 1546 | 67 | 0.087 | 7.7 | 0.001041 | 1.5 | 3 | 0.001015 | 2.2 | 20.51 | 0.46 | 0.001011 | 1.6 | 20.43 | 0.32 |
| | MOKR1@26 | 220 | 4084 | 19 | 646 | 39 | 0.101 | 6.7 | 0.001072 | 1.3 | 4 | 0.001008 | 2.6 | 20.37 | 0.53 | 0.001034 | 1.3 | 20.89 | 0.28 |
| | MOKR1@27 | 295 | 3072 | 10 | 626 | 55 | 0.108 | 8.3 | 0.001021 | 1.3 | 5 | 0.000958 | 3.6 | 19.35 | 0.69 | 0.000969 | 1.4 | 19.58 | 0.28 |
| | MOKR1@28 | 395 | 5188 | 13 | 1611 | 67 | 0.067 | 9.2 | 0.001011 | 1.1 | 1 | 0.000987 | 1.9 | 19.93 | 0.39 | 0.000997 | 1.2 | 20.15 | 0.23 |
| | MOKR1@29 | 469 | 3095 | 7 | 846 | 55 | 0.066 | 6.5 | 0.001059 | 1.0 | 3 | 0.001011 | 2.7 | 20.42 | 0.55 | 0.001025 | 1.2 | 20.72 | 0.25 |
| | MOKR1@30 | 688 | 4284 | 6 | 802 | 55 | 0.062 | 7.1 | 0.000922 | 1.2 | 3 | 0.000878 | 2.9 | 17.74 | 0.51 | 0.000893 | 1.4 | 18.03 | 0.25 |
| | MOKR1@31 | 683 | 4946 | 7 | 2982 | 95 | 0.056 | 7.6 | 0.001030 | 1.0 | 1 | 0.001017 | 1.6 | 20.54 | 0.33 | 0.001015 | 1.1 | 20.51 | 0.23 |
| B | MOKR1@01 | 132 | 23439 | 178 | 573 | 9 | 0.324 | 2.3 | 0.000991 | 2.6 | 3 | 0.000924 | 2.5 | 18.68 | 0.46 | 0.000959 | 2.6 | 19.37 | 0.50 |
| | MOKR1@02 | 167 | 21412 | 128 | 789 | 12 | 0.283 | 2.7 | 0.001001 | 2.6 | 3 | 0.000952 | 2.5 | 19.23 | 0.49 | 0.000970 | 2.6 | 19.60 | 0.51 |
| | MOKR1@03 | 149 | 20039 | 134 | 694 | 12 | 0.307 | 2.7 | 0.001011 | 2.6 | 3 | 0.000955 | 2.6 | 19.29 | 0.49 | 0.000977 | 2.6 | 19.73 | 0.52 |
| | MOKR1@04 | 162 | 15315 | 95 | 570 | 12 | 0.296 | 2.6 | 0.001007 | 2.7 | 5 | 0.000943 | 2.6 | 19.05 | 0.50 | 0.000960 | 2.7 | 19.40 | 0.51 |
| | MOKR1@05 | 182 | 11017 | 61 | 391 | 12 | 0.299 | 2.6 | 0.000978 | 2.6 | 7 | 0.000882 | 2.6 | 17.81 | 0.47 | 0.000913 | 2.6 | 18.45 | 0.48 |
| | MOKR1@06 | 239 | 10746 | 45 | 355 | 12 | 0.242 | 2.6 | 0.000993 | 2.6 | 6 | 0.000885 | 2.6 | 17.88 | 0.47 | 0.000932 | 2.6 | 18.83 | 0.48 |
| | MOKR1@13 | 127 | 16222 | 128 | 541 | 10 | 0.343 | 2.3 | 0.001014 | 2.6 | 5 | 0.000942 | 2.5 | 19.03 | 0.47 | 0.000967 | 2.6 | 19.53 | 0.50 |
| | MOKR1@14 | 363 | 17133 | 47 | 608 | 12 | 0.200 | 2.4 | 0.000949 | 2.6 | 4 | 0.000889 | 2.5 | 17.95 | 0.45 | 0.000908 | 2.6 | 18.35 | 0.47 |
| | MOKR1@15 | 446 | 16751 | 38 | 468 | 11 | 0.191 | 2.5 | 0.000948 | 2.6 | 4 | 0.000869 | 2.5 | 17.57 | 0.45 | 0.000906 | 2.6 | 18.30 | 0.47 |
| | MOKR1@16 | 517 | 16572 | 32 | 462 | 12 | 0.190 | 2.6 | 0.000943 | 2.6 | 5 | 0.000864 | 2.6 | 17.46 | 0.45 | 0.000899 | 2.6 | 18.16 | 0.47 |
| | MOKR1@17 | 141 | 16023 | 113 | 717 | 13 | 0.323 | 2.6 | 0.001031 | 2.6 | 4 | 0.000975 | 2.6 | 19.70 | 0.50 | 0.000986 | 2.6 | 19.92 | 0.52 |
| | MOKR1@18 | 303 | 8214 | 27 | 380 | 18 | 0.303 | 3.2 | 0.000949 | 2.7 | 10 | 0.000859 | 3.0 | 17.35 | 0.53 | 0.000851 | 2.7 | 17.19 | 0.46 |
| | *MOKR1@19* | *263* | *4051* | *15* | / | *0* | *0.072* | *7.2* | *0.001023* | *1.1* | *2* | *0.001023* | / | *20.67* | / | *0.001002* | *1.1* | *20.24* | *0.23* |
| A | SAND1@01 | 259 | 3167 | 12 | 125 | 17 | 0.337 | 3.8 | 0.001114 | 4.0 | 21 | 0.000770 | 5.9 | 15.56 | 0.92 | 0.000877 | 4.1 | 17.72 | 0.73 |
| | SAND1@02 | 252 | 3570 | 14 | 175 | 21 | 0.430 | 3.9 | 0.001104 | 3.1 | 24 | 0.000860 | 5.2 | 17.38 | 0.90 | 0.000843 | 3.3 | 17.03 | 0.56 |
| | SAND1@04 | 323 | 5540 | 17 | 184 | 19 | 0.441 | 4.0 | 0.001150 | 2.6 | 17 | 0.000908 | 4.4 | 18.35 | 0.80 | 0.000958 | 2.7 | 19.34 | 0.51 |
| | SAND1@05 | 580 | 5757 | 10 | 203 | 19 | 0.331 | 3.8 | 0.001106 | 2.8 | 15 | 0.000896 | 4.2 | 18.10 | 0.76 | 0.000938 | 2.9 | 18.96 | 0.54 |
| | SAND1@06 | 601 | 5846 | 10 | 216 | 20 | 0.328 | 4.0 | 0.001123 | 2.7 | 15 | 0.000923 | 4.2 | 18.64 | 0.77 | 0.000959 | 2.8 | 19.38 | 0.54 |
| | SAND1@07 | 272 | 5768 | 21 | 212 | 12 | 0.274 | 2.6 | 0.001006 | 2.6 | 12 | 0.000829 | 3.1 | 16.74 | 0.52 | 0.000883 | 2.6 | 17.85 | 0.47 |
| | SAND1@08 | 251 | 6655 | 27 | 332 | 15 | 0.277 | 2.9 | 0.000972 | 2.6 | 10 | 0.000859 | 2.9 | 17.35 | 0.50 | 0.000879 | 2.6 | 17.76 | 0.46 |
| | SAND1@21 | 181 | 7714 | 43 | 2354 | 55 | 0.087 | 8.6 | 0.001049 | 1.3 | 1 | 0.001032 | 1.6 | 20.85 | 0.33 | 0.001039 | 1.3 | 20.99 | 0.28 |
| | SAND1@22 | 285 | 6564 | 23 | 1186 | 55 | 0.096 | 10.8 | 0.001045 | 1.4 | 1 | 0.001011 | 2.3 | 20.43 | 0.46 | 0.001030 | 1.4 | 20.80 | 0.30 |
| | SAND1@24 | 289 | 6472 | 22 | 1758 | 67 | 0.098 | 10.4 | 0.001054 | 1.2 | 2 | 0.001031 | 1.9 | 20.82 | 0.39 | 0.001036 | 1.2 | 20.93 | 0.26 |
| | SAND1@25 | 302 | 7743 | 26 | 2074 | 67 | 0.107 | 10.3 | 0.001107 | 1.1 | 1 | 0.001086 | 1.6 | 21.94 | 0.36 | 0.001090 | 1.1 | 22.03 | 0.25 |
| | SAND1@26 | 302 | 7711 | 26 | 1385 | 55 | 0.140 | 8.6 | 0.001117 | 1.4 | 3 | 0.001086 | 2.1 | 21.94 | 0.45 | 0.001089 | 1.4 | 22.01 | 0.32 |
| | SAND1@28 | 468 | 728 | 2 | 513 | 95 | 0.066 | 8.6 | 0.001116 | 1.4 | 10 | 0.001032 | 7.3 | 20.85 | 1.51 | 0.001004 | 3.4 | 20.28 | 0.68 |

**Table 3.** Continued.

| Groups | Analysis ID | U (ppm) | Th (ppm) | Th / U | $^{208}Pb/^{204}Pb$ | 1σ (%) | $^{207}Pb/^{206}Pb$ | 1σ (%) | $^{208}Pb/^{232}Th$ | 1σ (%) | f208 from 207 (%) | 204-corr | | 204-corr spot ages | | 207-corr | | 207-corr spot ages | |
|---|---|---|---|---|---|---|---|---|---|---|---|---|---|---|---|---|---|---|---|
| | | | | | | | | | | | | $^{208}Pb/^{232}Th$ | 1σ (%) | $^{208}Pb/^{232}Th$ Age (Ma) | 1σ (abs.) | $^{208}Pb/^{232}Th$ | 1σ (%) | $^{208}Pb/^{232}Th$ Age (Ma) | 1σ (abs.) |
| Eastern Tauern Window | | | | | | | | | | | | | | | | | | | |
| B | SAND1@09 | 483 | 2027 | 4 | 137 | 14 | 0.176 | 2.2 | 0.001145 | 4.2 | 28 | 0.000822 | 4.9 | 16.61 | 0.81 | 0.000820 | 4.4 | 16.56 | 0.72 |
| | SAND1@10 | 646 | 2420 | 4 | 109 | 14 | 0.176 | 2.7 | 0.001136 | 3.3 | 26 | 0.000732 | 5.5 | 14.80 | 0.81 | 0.000842 | 3.5 | 17.01 | 0.60 |
| | SAND1@12 | 729 | 3802 | 5 | 203 | 16 | 0.150 | 2.8 | 0.001027 | 2.6 | 16 | 0.000831 | 3.8 | 16.79 | 0.63 | 0.000858 | 2.7 | 17.34 | 0.47 |
| | SAND1@13 | 628 | 2842 | 5 | 170 | 14 | 0.136 | 2.3 | 0.001072 | 3.0 | 19 | 0.000839 | 3.9 | 16.95 | 0.67 | 0.000873 | 3.0 | 17.63 | 0.54 |
| | SAND1@14 | 966 | 3518 | 4 | 124 | 16 | 0.194 | 3.1 | 0.001118 | 2.6 | 23 | 0.000771 | 5.2 | 15.57 | 0.81 | 0.000862 | 2.8 | 17.41 | 0.48 |
| | SAND1@18 | 278 | 1247 | 4 | 67 | 14 | 0.309 | 2.9 | 0.001372 | 5.0 | 43 | 0.000578 | 8.4 | 11.67 | 0.97 | 0.000783 | 5.5 | 15.81 | 0.88 |
| | SAND1@19 | 277 | 811 | 3 | 70 | 16 | 0.321 | 3.0 | 0.001620 | 5.1 | 55 | 0.000731 | 9.2 | 14.77 | 1.36 | 0.000725 | 6.5 | 14.66 | 0.96 |
| | *SAND1@11* | *659* | *2325* | 4 | *92* | *16* | *0.217* | *3.1* | *0.001572* | *8.4* | *35* | *0.000909* | *8.5* | *18.36* | *1.56* | *0.001021* | *8.6* | *20.62* | *1.78* |
| | *SAND1@15* | *189* | *964* | 5 | *49* | *11* | *0.307* | *2.4* | *0.001476* | *6.1* | *49* | *0.000322* | *8.3* | *6.51* | *0.54* | *0.000751* | *6.7* | *15.17* | *1.01* |
| | *SAND1@16* | *228* | *601* | 3 | *59* | *15* | *0.307* | *2.8* | *0.001752* | *6.7* | *62* | *0.000612* | *10.1* | *12.36* | *1.25* | *0.000664* | *8.7* | *13.41* | *1.17* |
| | *SAND1@17* | *202* | *401* | 2 | *46* | *15* | *0.312* | *2.9* | *0.002061* | *8.4* | *73* | *0.000324* | *12.4* | *6.56* | *0.81* | *0.000559* | *13.0* | *11.30* | *1.47* |
| | *SAND1@20* | *233* | *376* | 2 | *54* | *17* | *0.305* | *3.0* | *0.002238* | *7.9* | *74* | *0.000741* | *12.4* | *14.98* | *1.86* | *0.000578* | *13.8* | *11.68* | *1.61* |
| | *SAND1@29* | *493* | *448* | *1* | *112* | *67* | *0.056* | *11.1* | *0.001114* | *2.4* | *9* | *0.000729* | *23.3* | *14.72* | *3.43* | *0.001014* | *6.8* | *20.49* | *1.39* |
| | *SAND1@30* | *640* | *398* | *1* | *186* | *95* | *0.060* | *11.3* | *0.001180* | *3.8* | *14* | *0.000935* | *20.0* | *18.88* | *3.78* | *0.001019* | *9.3* | *20.59* | *1.91* |
| | *SAND1@31* | *636* | *404* | *1* | *95* | *67* | *0.061* | *10.6* | *0.001085* | *3.4* | *21* | *0.001505* | *38.9* | *30.39* | *11.80* | *0.000856* | *10.2* | *17.30* | *1.76* |
| | *SAND1@23* | *299* | *5895* | *20* | */* | *0* | *0.112* | *10.5* | *0.000878* | *1.2* | *3* | *0.000878* | */* | *17.73* | */* | *0.000855* | *1.2* | *17.27* | *0.21* |
| | *SAND1@27* | *284* | *679* | *2* | */* | *0* | *0.069* | *7.7* | *0.001130* | *1.0* | *9* | *0.001130* | */* | *22.84* | */* | *0.001027* | *2.8* | *20.74* | *0.58* |
| | *SAND1@32* | *573* | *501* | *1* | *33* | *96* | *0.017* | *17.8* | *0.000118* | *15.8* | *89* | */* | */* | *−0.43* | *−0.49* | *0.000013* | *251* | *0.26* | *0.66* |
| | *SAND1@33* | *919* | *304* | *0* | */* | *0* | *0.035* | *18.9* | *0.000222* | *13.7* | *184* | *0.000222* | */* | *4.49* | */* | */* | *−76* | *−3.76* | *2.86* |
| | *SAND1@35* | *1160* | *691* | *1* | */* | *0* | *0.057* | *12.0* | *0.001323* | *2.2* | *8* | *0.001323* | */* | *26.73* | */* | *0.001215* | *5.7* | *24.54* | *1.39* |
| | *SAND1@36* | *935* | *512* | *1* | */* | *0* | *0.067* | *11.3* | *0.001293* | *1.9* | *20* | *0.001293* | */* | *26.11* | */* | *0.001037* | *8.8* | *20.95* | *1.84* |
| A | REIS1@27 | 166 | 541 | 3 | 188 | 25 | 0.088 | 4.1 | 0.000926 | 2.32 | 13 | 0.000762 | 5.7 | 15.39 | 0.88 | 0.000806 | 2.7 | 16.28 | 0.44 |
| | REIS1@28 | 288 | 1516 | 5 | 601 | 30 | 0.077 | 3.8 | 0.000836 | 2.25 | 6 | 0.000783 | 2.8 | 15.81 | 0.45 | 0.000788 | 2.3 | 15.93 | 0.37 |
| | REIS1@29 | 185 | 697 | 4 | 530 | 42 | 0.093 | 4.6 | 0.000853 | 2.24 | 11 | 0.000791 | 3.7 | 15.99 | 0.59 | 0.000760 | 2.5 | 15.36 | 0.39 |
| | REIS1@31 | 141 | 763 | 5 | 226 | 42 | 0.121 | 3.8 | 0.000977 | 2.60 | 20 | 0.000810 | 7.6 | 16.37 | 1.24 | 0.000779 | 4.2 | 15.74 | 0.66 |
| | REIS1@32 | 306 | 2964 | 10 | 260 | 26 | 0.059 | 3.6 | 0.000893 | 2.48 | 15 | 0.000760 | 4.4 | 15.36 | 0.68 | 0.000759 | 2.8 | 15.33 | 0.42 |
| | REIS1@33 | 762 | 737 | 1 | 874 | 24 | 0.050 | 2.7 | 0.000877 | 2.56 | 2 | 0.000839 | 2.7 | 16.94 | 0.45 | 0.000863 | 2.6 | 17.44 | 0.45 |
| | REIS1@35 | 195 | 618 | 3 | 290 | 32 | 0.083 | 4.3 | 0.000966 | 2.95 | 10 | 0.000865 | 5.2 | 17.48 | 0.90 | 0.000865 | 3.2 | 17.48 | 0.56 |
| | REIS1@36 | 153 | 668 | 4 | 222 | 27 | 0.125 | 4.0 | 0.000963 | 2.87 | 18 | 0.000796 | 5.3 | 16.08 | 0.86 | 0.000794 | 3.2 | 16.05 | 0.52 |
| | REIS1@23 | 236 | 324 | 1 | 326 | 47 | 0.053 | 5.0 | 0.000821 | 2.56 | 8 | 0.000771 | 6.7 | 15.57 | 1.04 | 0.000756 | 3.8 | 15.27 | 0.58 |
| | REIS1@17 | 437 | 738 | 2 | 515 | 33 | 0.055 | 2.9 | 0.000903 | 2.26 | 7 | 0.000852 | 3.4 | 17.21 | 0.59 | 0.000842 | 2.7 | 17.01 | 0.45 |
| | REIS1@19 | 384 | 454 | 1 | 318 | 33 | 0.062 | 3.2 | 0.000932 | 2.69 | 15 | 0.000819 | 4.7 | 16.54 | 0.78 | 0.000793 | 3.8 | 16.03 | 0.61 |
| | REIS1@20 | 353 | 562 | 2 | 1500 | 67 | 0.062 | 3.3 | 0.000894 | 2.24 | 11 | 0.000870 | 2.8 | 17.59 | 0.49 | 0.000798 | 2.9 | 16.13 | 0.46 |
| | REIS1@21 | 288 | 433 | 2 | 336 | 36 | 0.060 | 3.4 | 0.000981 | 2.54 | 10 | 0.000868 | 4.7 | 17.54 | 0.82 | 0.000881 | 3.6 | 17.81 | 0.63 |
| B | REIS1@18 | 328 | 486 | 1 | 467 | 42 | 0.061 | 3.3 | 0.000802 | 2.96 | 18 | 0.000736 | 4.4 | 14.87 | 0.66 | 0.000657 | 4.1 | 13.27 | 0.55 |
| | REIS1@24 | 218 | 398 | 2 | 689 | 67 | 0.064 | 4.9 | 0.000791 | 3.13 | 14 | 0.000747 | 4.8 | 15.08 | 0.72 | 0.000679 | 4.1 | 13.71 | 0.56 |
| | REIS1@25 | 189 | 225 | 1 | 321 | 55 | 0.061 | 5.0 | 0.000851 | 3.74 | 17 | 0.000748 | 7.4 | 15.12 | 1.11 | 0.000705 | 6.1 | 14.25 | 0.87 |
| | REIS1@30 | 297 | 441 | 1 | 778 | 47 | 0.083 | 5.2 | 0.000749 | 3.54 | 10 | 0.000712 | 4.1 | 14.38 | 0.59 | 0.000676 | 4.6 | 13.66 | 0.63 |
| | REIS1@34 | 560 | 505 | 1 | 437 | 47 | 0.044 | 3.3 | 0.000773 | 3.93 | 14 | 0.000738 | 6.0 | 14.90 | 0.89 | 0.000666 | 6.2 | 13.45 | 0.84 |
| | *REIS1@22* | *881* | *386* | 0 | 229 | *32* | *0.051* | *2.3* | *0.000979* | *2.77* | *25* | *0.000814* | *5.8* | *16.45* | *0.95* | *0.000736* | *34.6* | *14.88* | *5.15* |
| | *REIS1@26* | *201* | *197* | 1 | 199 | *47* | *0.075* | *4.5* | *0.000867* | *3.41* | *41* | *0.000781* | *10.7* | *15.79* | *1.69* | *0.000508* | *11.6* | *10.26* | *1.19* |

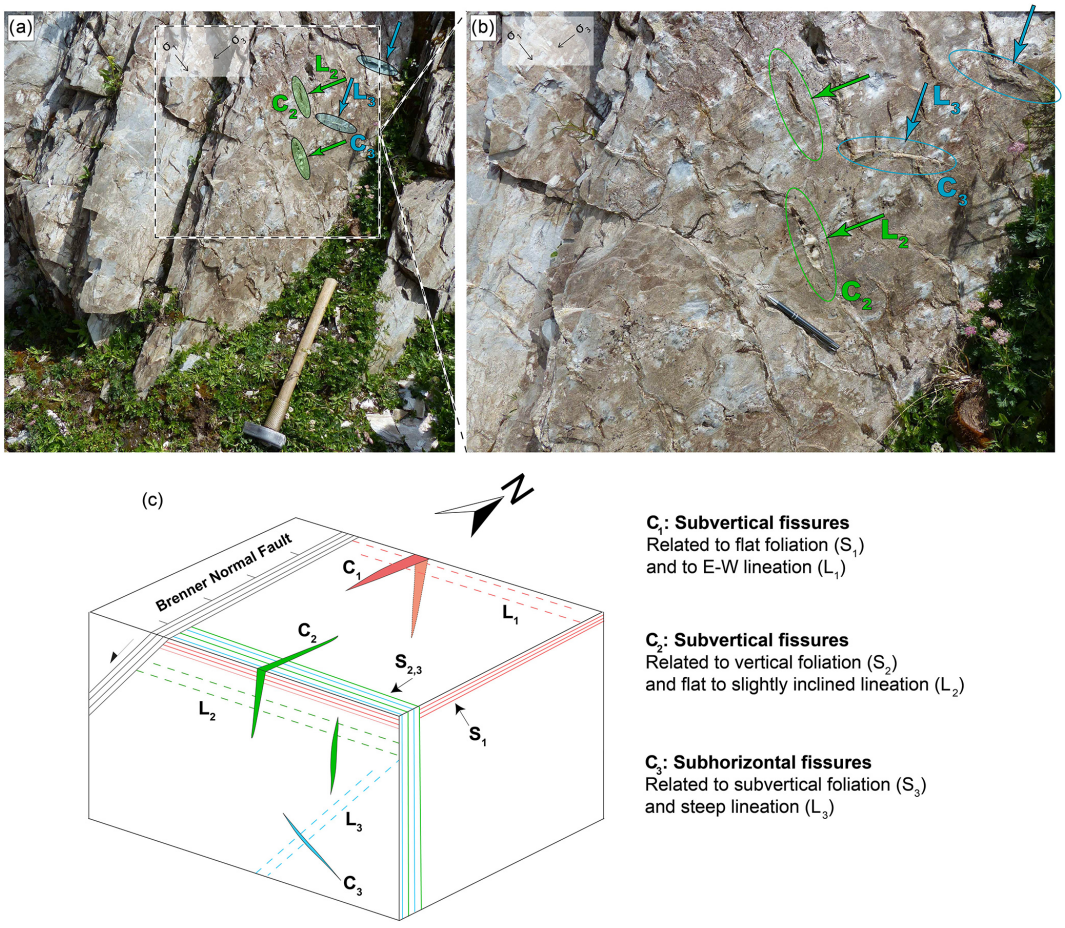


**Figure 2. (a)** Two generations of late fissures visible in a road outcrop located between monazite locality (46°59.436′ N, 011°39.240′ E) and Pfitscherjoch. Steeply oriented fissures ($C_2$: ∼ 090/65) are older and deformed (green ellipses), and seem related to a flatter lineation ($L_2$: ∼ 250/30, green arrows) visible on some of the foliation planes. Younger and flatter oriented fissures ($C_3$: ∼ 085/30) are straight (blue ellipses) and seem related to a steeper lineation ($L_3$: 270/70, blue arrows). These observations indicate that a fissure can be deformed during its existence. The length of the hammer handle is 60 cm. **(b)** Enlargement of panel **(a)**. **(c)** Schematic illustration of the three fissure generations observed in this study ($C_1$, $C_2$ and $C_3$), together with respective orientation, foliation ($S_1$, $S_2$ and $S_3$) and lineation ($L_1$, $L_2$ and $L_3$). The first fissure generation ($C_1$) is related to E–W extension, the second fissure generation ($C_2$) is linked to strike-slip movements and the third fissure generation ($C_3$) is related to the oblique-slip movements.

lated to flat foliation ($S_1$) and E–W-stretching lineation ($L_1$); these are oriented perpendicular to the main fold axes (and lineation) of the TW and are associated with E–W extension (e.g. Gnos et al., 2015; Rosenberg et al., 2018; Schneider et al., 2013). (ii) Younger subvertical fissures ($C_2$, Fig. 2c) are associated with subvertical E–W-oriented foliation ($S_2$) and flat to inclined lineation ($L_2$), and are oriented perpendicular to strike-slip faults (mainly in the western part of the TW; Fig. 2c). At Pfitscherjoch, the shape of $C_2$ fissures, indicating overprinting by sinistral sense of shear, is in agreement with the larger-scale sinistral shearing of the GSZ shear zone. (iii) A third generation of fissures ($C_3$, Fig. 2c) is locally observed, for example, in the Pfitscherjoch locality (Fig. 2a and b) and is at a high angle with $C_1$ and $C_2$ fissures. This third fissure generation observed in the Pfitscherjoch locality is associated with a subvertical E–W-striking foliation ($S_3$). Stretching lineation related to the BNF activity is subparallel to $C_3$ lineation; however, its foliation is striking N–S (Fig. 2c). We suggest that $C_3$ fissures are related to oblique-slip movements, in line with the observed E–W-striking foliation and not the BNF activity.

### 4.2 Monazite dating and composition

The monazite grains selected for in situ Th-Pb dating are millimetre sized and, when BSE zoning is visible, they show two distinct textures: regular and patchy (Figs. 3, 4 and 5; Table 4). The term "regular" refers to crystals showing growth zonation, whereas a patchy texture is interpreted as a replacement by secondary dissolution–reprecipitation processes (e.g. Ayers et al., 1999; Bergemann et al., 2018, 2019,

**Table 4.** Summary of weighted mean ages of monazite growth domains and spot age ranges of each grain from the TW.

| Sample domain | ID no. | Figure | Table | Zoning of the grains | Weighted mean domain $^{208}Pb$ / $^{232}Th$ ages (Ma, $\pm1\sigma$) | MSWD | Number of analyses | Spot $^{208}Pb$ / $^{232}Th$ age range of entire grain (Ma, $\pm1\sigma$) | Reference |
|---|---|---|---|---|---|---|---|---|---|
| Western Tauern Window | | | | | | | | | |
| INNB1 | 1 | 3a | 3 | Regular | – | – | – | 11.5 ± 0.2–10.4 ± 0.2 | This study |
| ZEI1 – A | 2 | 3b | 3 | Regular | 10.0 ± 0.2 | 1.8 | 20 | 10.8 ± 0.3–7.2 ± 0.2 | This study |
| SCHR1 – A | 3 | 3c | 3 | Regular | 20.9 ± 0.6 | 1.7 | 6 | 21.9 ± 0.5–19.3 ± 0.5 | This study |
| SCHR1 – B | | | | | 20.3 ± 0.2 | 0.98 | 16 | | |
| SCHR1 – C | | | | | 19.7 ± 0.4 | 1.00 | 6 | | |
| MAYR4 | 3 | 3d | 3 | Regular | – | – | – | 11.8 ± 0.2–8.9 ± 0.2 | This study |
| PFIT1 – A | 5 | 3e | 3 | Patchy core | 17.3 ± 0.3 | 1.2 | 9 | 17.8 ± 0.4–12.9 ± 0.3 | This study |
| PFIT1 – B | | | | | 13.2 ± 0.3 | 0.38 | 5 | | |
| BURG2 | 6 | 3f | 3 | Regular | – | – | – | 17.1 ± 0.4–12.1 ± 0.3 | This study |
| PLAN1 – A | 7 | 3g | 3 | Patchy core | 11.9 ± 0.2 | 2.2 | 37 | 12.6 ± 0.3–7.8 ± 0.2 | This study |
| Central Tauern Window | | | | | | | | | |
| SCHEI1 – A | 8 | 4a | 3 | Regular | 18.3 ± 1.1 | 2.0 | 4 | 18.9 ± 0.5–15.9 ± 0.4 | This study |
| SCHEI1 – B | | | | | 17.4 ± 0.4 | 1.5 | 5 | | |
| SCHEI1 – C | | | | | 16.6 ± 0.2 | 1.9 | 23 | | |
| HOPF2 – B | 9 | 4b | 3 | Regular | 12.2 ± 0.4 | 2.6 | 8 | 13.7 ± 0.4–11.0 ± 0.3 | This study |
| HOPF2 – C | | | | | 12.2 ± 0.5 | 2.9 | 6 | | |
| GART1 – A | 10 | 4c | 3 | Regular | 16.3 ± 0.2 | 0.69 | 10 | 16.9 ± 0.3–14.5 ± 0.4 | This study |
| NOWA3 – B | 11 | 4d | 3 | Regular | 15.8 ± 0.5 | 0.27 | 5 | 17.0 ± 0.2–13.8 ± 0.8 | This study |
| NOWA3 – C | | | | | 14.9 ± 1.1 | 2.4 | 5 | | |
| GART3 – B | 12 | 4e | 3 | Regular | 15.0 ± 0.5 | 2.3 | 11 | 16.1 ± 0.4–12.0 ± 0.4 | This study |
| STEI2 | 13 | 4f | 3 | Regular/patchy tail | 17.2 ± 0.2 | 0.24 | 20 | 17.5 ± 0.4–16.8 ± 0.4 | This study |
| KNOR1 – A | 14 | 4g | 3 | Regular | 10.8 ± 0.3 | 1.02 | 5 | 11.6 ± 0.4–10.8 ± 0.3 | This study |
| KNOR1 – B | | | | | 10.6 ± 0.3 | 1.6 | 8 | | |
| KNOR1 – C | | | | | 10.4 ± 0.2 | 1.4 | 8 | | |
| Eastern Tauern Window | | | | | | | | | |
| KAIS6 – A | 15 | 5a | 3 | Patchy border | 21.2 ± 0.5 | 0.64 | 6 | 22.1 ± 0.6–17.6 ± 0.6 | This study |
| KAIS6 – B | | | | | 20.9 ± 0.2 | 0.53 | 24 | | |
| KAIS6 – C | | | | | 20.6 ± 0.5 | 0.34 | 7 | | |
| KAIS6 – D | | | | | 18.8 ± 0.5 | 1.5 | 10 | | |
| SALZ18 – A | 16a | 5b | 3 | Regular | 18.3 ± 0.4 | 2.6 | 14 | 19.5 ± 0.5–15.8 ± 0.4 | This study |
| T3 | 16b | | – | Regular | 18.1 ± 0.4 | 0.51 | 4 | 18.5 ± 0.4–14.8 ± 0.4 | Gnos et al. (2015) |
| | | | | | 17.2 ± 0.5 | 3.4 | 10 | | |
| | | | | | 16.0 ± 0.3 | 0.51 | 8 | | |
| | | | | | 15.5 ± 0.2 | 0.74 | 24 | | |
| LOHN4 – A | 17 | 5c | 3 | Patchy core | 21.1 ± 0.2 | 1.4 | 50 | 22.9 ± 0.6–17.3 ± 0.6 | This study |
| LOHN4 – B | | | | | 18.4 ± 0.6 | 1.3 | 7 | | |
| ORT1 | 18 | 5d | 3 | Regular | 18.4 ± 0.3 | 1.07 | 13 | 19.0 ± 0.6–17.0 ± 0.7 | This study |
| EUKL2 | 19a | 5e | 3 | Regular | 21.7 ± 0.4 | 0.56 | 7 | 22.3 ± 0.5–21.2 ± 0.5 | This study |
| T2 | 19b | | – | Patchy | 15.1 ± 0.5 | 0.26 | 4 | 15.4 ± 0.4–15.0 ± 0.7 | Gnos et al. (2015) |
| HOAR1 – A | 20 | 5f | 3 | Patchy | 20.4 ± 0.2 | 0.80 | 6 | 21.2 ± 0.7–19.0 ± 0.9 | This study |
| HOAR1 – B | | | | | 19.9 ± 0.3 | 0.95 | 25 | | |
| T1 | 21 | | – | Regular | 19.0 ± 0.5 | 0.51 | 5 | 19.2 ± 0.5–14.3 ± 0.5 | Gnos et al. (2015) |
| | | | | | 17.6 ± 0.6 | 1.6 | 8 | | |
| | | | | | 16.3 ± 0.6 | 3.0 | 12 | | |
| | | | | | 15.0 ± 0.5 | 1.7 | 8 | | |
| T4 | 22 | | – | Patchy | 15.6 ± 0.7 | 9.1 | 21 | 18.3 ± 1.1–13.1 ± 0.8 | Gnos et al. (2015) |
| MOKR1 – B | 23 | 5g | 3 | Regular | 18.8 ± 0.5 | 2.9 | 12 | 22.6 ± 0.4–14.4 ± 0.2 | This study |
| SAND1 – B | 24 | 5h | 3 | Regular | 17.0 ± 0.8 | 1.8 | 7 | 22.0 ± 0.3–14.7 ± 1.0 | This study |
| REIS1 – A | 25 | 5i | 3 | Regular | 16.2 ± 0.5 | 2.9 | 13 | 17.8 ± 0.6–13.5 ± 0.8 | This study |
| REIS1 – B | | | | | 13.6 ± 0.6 | 0.25 | 5 | | |

2020; Gnos et al., 2015). Thorium and uranium (U) contents of the dated fissure monazites display a large variability, ranging from ∼ 200 to 63 000 ppm Th and ∼ 2 to 2000 ppm U, with variations in Th/U ratio from 1 up to ∼ 7000 (Figs. 3, 4 and 5; Table 3). $^{232}$Th-$^{208}$Pb ages presented on the right-hand panel of Figs. 3, 4 and 5 are arranged according to the order established in Table 3. A detailed description of each monazite grain is provided in the Supplement. Average ages are reported for groups of dates on texturally and/or chemically similar domains. In order to ensure that a group of dates from a domain is internally consistent, rare outliers have been excluded to bring the mean square weighted deviation (MSWD) within acceptable values (MSWD < 3; Spencer et al., 2016). In a few cases, the dates for specific monazite domains have a scatter above analytical uncertainty (e.g. grains 6, 9 and 24), which probably reflects the complex formation process of fissure monazite.

The investigated grains from the western part of the western TW subdome come from the Venediger Duplex, with the exception of sample 6, which comes from the Glockner nappe system (Fig. 1; Table 1). Samples 2, 4 and 6 were collected near the major Brenner normal fault, which delimits the TW to the west, and samples 1, 3, 5 and 7 were collected in the vicinity of sinistral strike-slip faults (Fig. 1). Average growth domain ages range from $20.9 \pm 0.6$ to $10.0 \pm 0.2$ Ma (samples 3 and 2), with the youngest ages recorded in the western TW (Figs. 1, 3 and 6a; Tables 3 and 4).

The central part of the TW displays growth domain ages between $18.3 \pm 1.1$ and $10.4 \pm 0.2$ (samples 8 and 14; Figs. 1 and 4; Tables 3 and 4), but the majority of the dated crystals in this area record ages around 17 Ma (Fig. 6b). Samples 8, 9 and 10 were collected between the eastern and western termination of the ASZ and the SEMP fault (Fig. 1). Another three samples (11, 12 and 13; Table 1) were collected in the northern prolongation of the AhSZ, and a seventh monazite (grain 14) was sampled near the southern border of the eastern part of the western subdome (Fig. 1).

The oldest ages are principally recorded in the eastern part of the TW at around 21 Ma (Fig. 6c). Average ages of growth domains range from $21.7 \pm 0.4$ to $13.6 \pm 0.6$ Ma (samples 19a and 25; Figs. 1, 4 and 6c; Tables 3 and 4). The samples were mainly collected at the western border of the eastern subdome, in the Venediger Duplex or near the boundary with the Glockner–Modereck nappe systems (Fig. 1). Sample 25 was taken at some distance from the other samples, near the southeastern border of the eastern subdome (Fig. 1).

## 5 Discussion

### 5.1 Fissure monazite ages

The oldest monazite ages of $21.7 \pm 0.4$ to $19.9 \pm 0.3$ Ma (found in samples 19a and 20; Figs. 1, 6c and 7a and d) are common in the eastern TW but can also be found in the western area (Fig. 7a, c and d, red symbols). This in line with regional fault activity recorded at ∼ 21 Ma based on Pleuger et al. (2012) (Fig. 8a) which corresponds to the main indentation phase (Favaro et al., 2017). We interpret these as a first monazite crystallization event during E–W extension in association with the dome formation (N–S shortening) when the existing clefts reached $P$–$T$ conditions at which fissure monazite starts to grow (phase 1, red symbols in Fig. 7). When comparing an assumed fissure formation temperature of 450 °C (typically obtained in quartz fluid inclusion studies on early alpine fissures (e.g. Mullis, 1996) with thermochronological data of the eastern TW (compiled in Wölfler et al., 2012), the onset of fissure formation, predating primary monazite crystallization, is estimated at around 25 Ma. Based on a comparison with thermochronological data, monazite crystallization recorded between 19 and 15 Ma was estimated to have occurred at ∼ 200–300 °C in the eastern TW (Gnos et al., 2015). New monazite ages from this study in the eastern TW are up to ∼ 22 Ma (sample 19 in Fig. 1), suggesting that early monazite crystallization in the area may have occurred at higher temperatures of 350–400 °C.

While early fissure formation is related to E–W extension (leading to flat foliation and E–W mineral lineations; Fig. 2c), we suggest that monazite formation also occurred along the sinistral strike-slip to oblique-slip movements (vertical foliation and flat to inclined lineation; Fig. 2), particularly developed in the central and western parts of the TW (e.g. Rosenberg et al., 2018; Schneider et al., 2013). These shear zones developed as a result of bending of the E–W-oriented upright folds around a vertical axis (leading edge of the Dolomite indenter) (Fig. 1). This occurred when N–S shortening could no longer be accommodated by folding and doming within the TW. Associated with these movements is the formation of a younger generation of fissures (see Pfitscherjoch example above), the peak activity of which is recorded at ∼ 17 Ma (phase 2, green symbols in Fig. 7). This fissure generation is associated with a steep foliation and a flat lineation (Fig. 2) but subparallel in orientation to the earlier fissure formation. The monazite ages at ∼ 17 Ma found in the western and central TW (Figs. 1, 6 and 7; samples 5, 8, 13; Table 4) are associated with sinistral fault zones, as in the Pfitscherjoch region or near the eastern termination of the ASZ and AhSZ faults (see above). Unfortunately, we do not have structural information on the westernmost and easternmost analysed samples (6 and 25; Figs. 1, 6 and 7), but they can be speculated to also have formed in association with a strike-slip shear zone or the BNF and KNF in the case of samples 6 and 25, respectively. At larger scale, these movements seem to have been associated with the development of the sinistral Giudicarie fault (GF, located at the southwestern corner of the TW), offsetting the Periadriatic fault (PF; Fig. 8b, e.g. Pleuger et al., 2012). Ages of ∼ 17 Ma are also recorded in the eastern part of the TW,

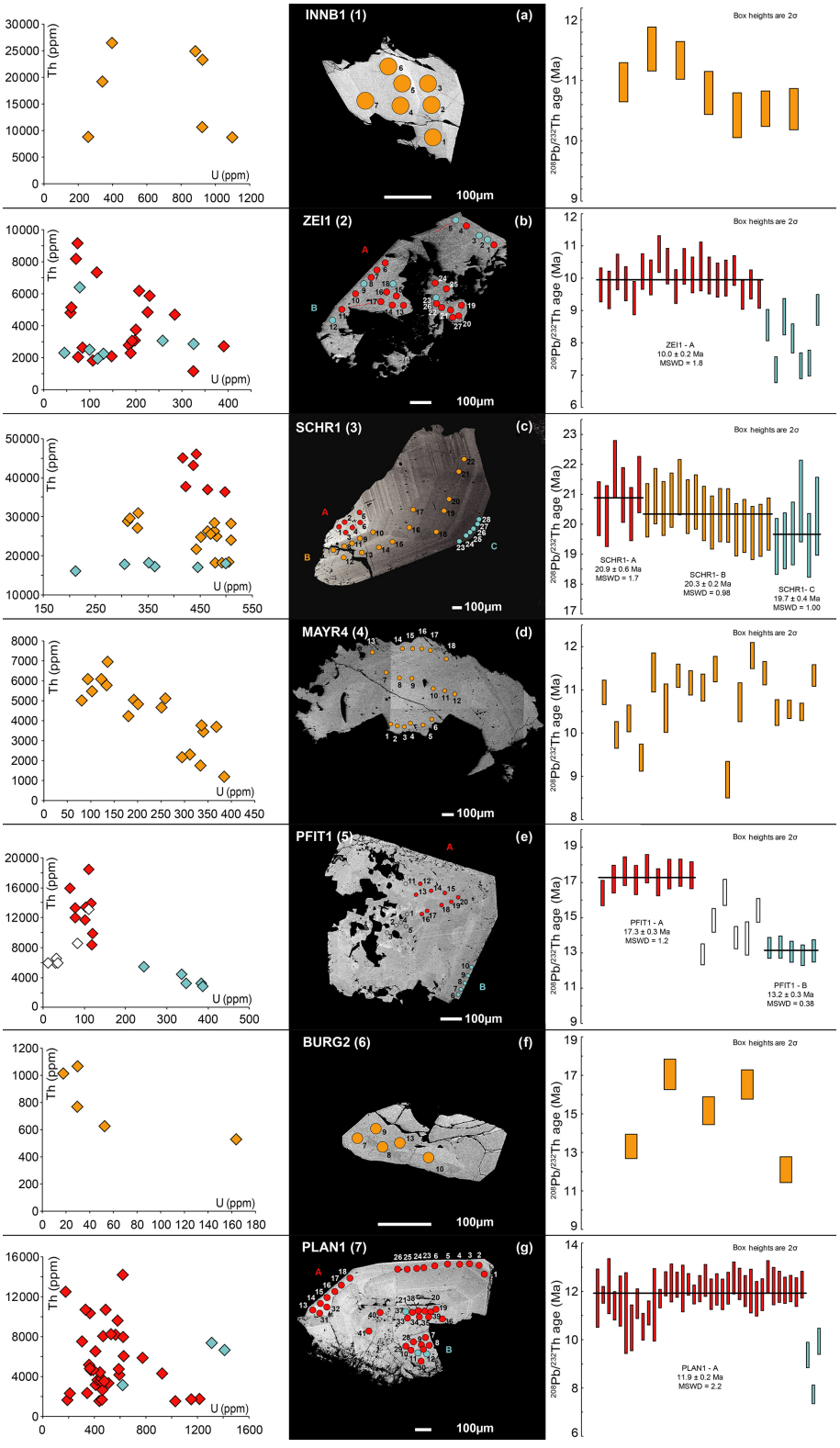


**Figure 3.** Chemical, textural and geochronological information of monazite grains from the western TW. On BSE images, colour-filled circles correspond to ion probe spot locations. Note that the square-shape shading in grain 4 is due to an artefact of composing BSE images with diverse contrast.

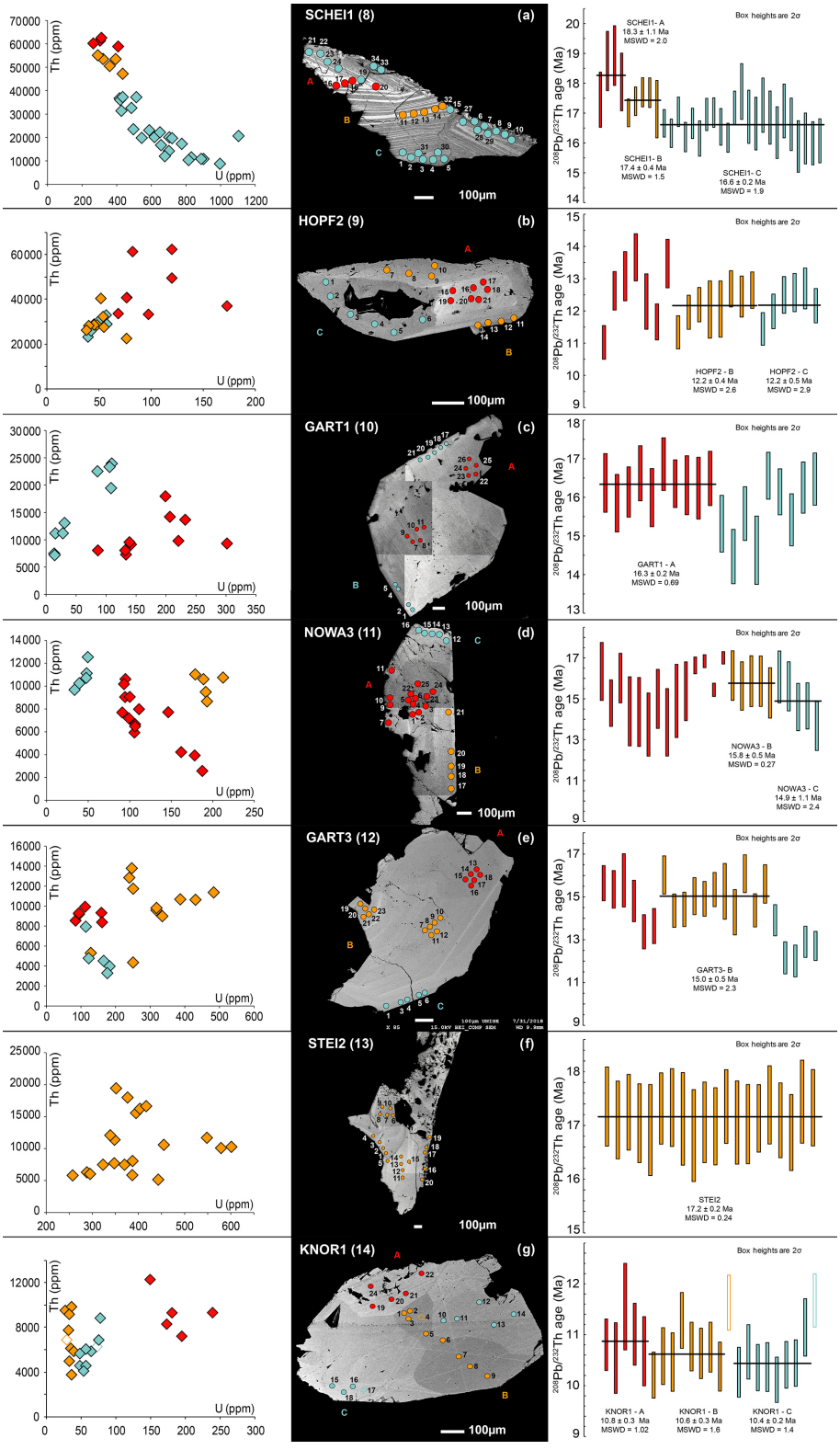


**Figure 4.** Chemical, textural and geochronological information of monazite grains from the central TW. On BSE images, colour-filled circles correspond to ion probe spot locations. Note that the square-shape shading in grains 10 and 11 is due to an artefact of composing BSE images with diverse contrast.

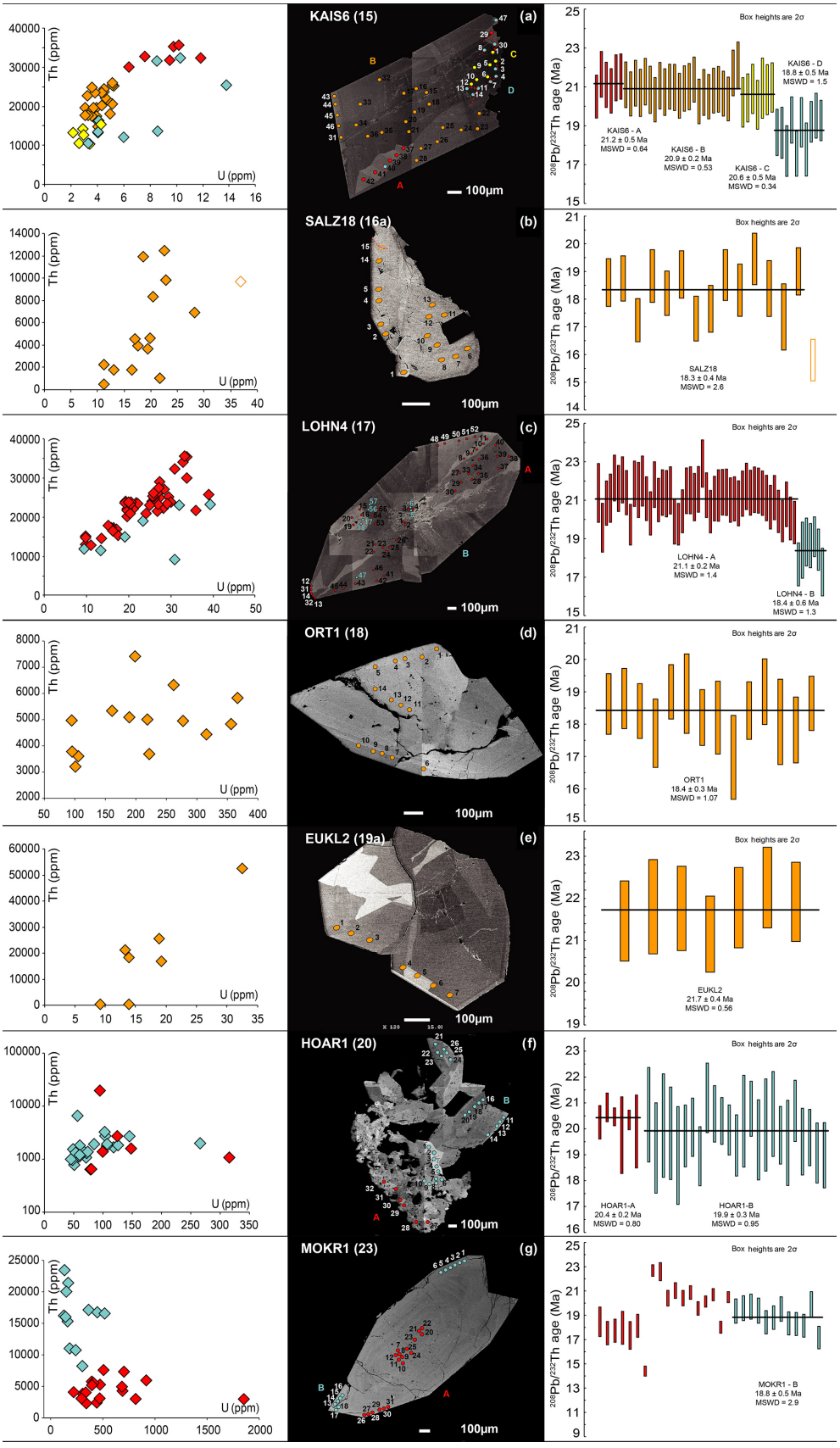
KAIS6 (15)
(a)
100µm
KAIS6 - A
21.2 ± 0.5 Ma
MSWD = 0.64
KAIS6 - B
20.9 ± 0.2 Ma
MSWD = 0.53
KAIS6 - C
20.6 ± 0.5 Ma
MSWD = 0.34
KAIS6 - D
18.8 ± 0.5 Ma
MSWD = 1.5
SALZ18 (16a)
(b)
100µm
SALZ18
18.3 ± 0.4 Ma
MSWD = 2.6
LOHN4 (17)
(c)
100µm
LOHN4 - A
21.1 ± 0.2 Ma
MSWD = 1.4
LOHN4 - B
18.4 ± 0.6 Ma
MSWD = 1.3
ORT1 (18)
(d)
100µm
ORT1
18.4 ± 0.3 Ma
MSWD = 1.07
EUKL2 (19a)
(e)
100µm
EUKL2
21.7 ± 0.4 Ma
MSWD = 0.56
HOAR1 (20)
(f)
100µm
HOAR1-A
20.4 ± 0.2 Ma
MSWD = 0.80
HOAR1-B
19.9 ± 0.3 Ma
MSWD = 0.95
MOKR1 (23)
(g)
100µm
MOKR1 - B
18.8 ± 0.5 Ma
MSWD = 2.9
Box heights are 2σ
Th (ppm)
U (ppm)
$^{208}Pb/^{232}Th$ age (Ma)

Figure 5.

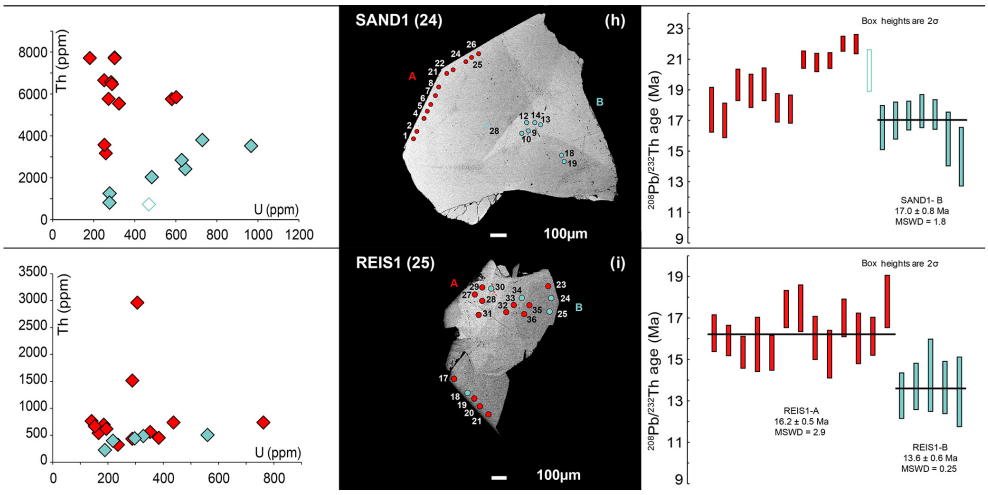


**Figure 5.** Chemical, textural and geochronological information of monazite grains from the eastern TW. On BSE images, colour-filled circles correspond to ion probe spot locations. Note that the square-shape shading in grains 15, 17, 18 and 20 is due to an artefact of composing BSE images with diverse contrast.

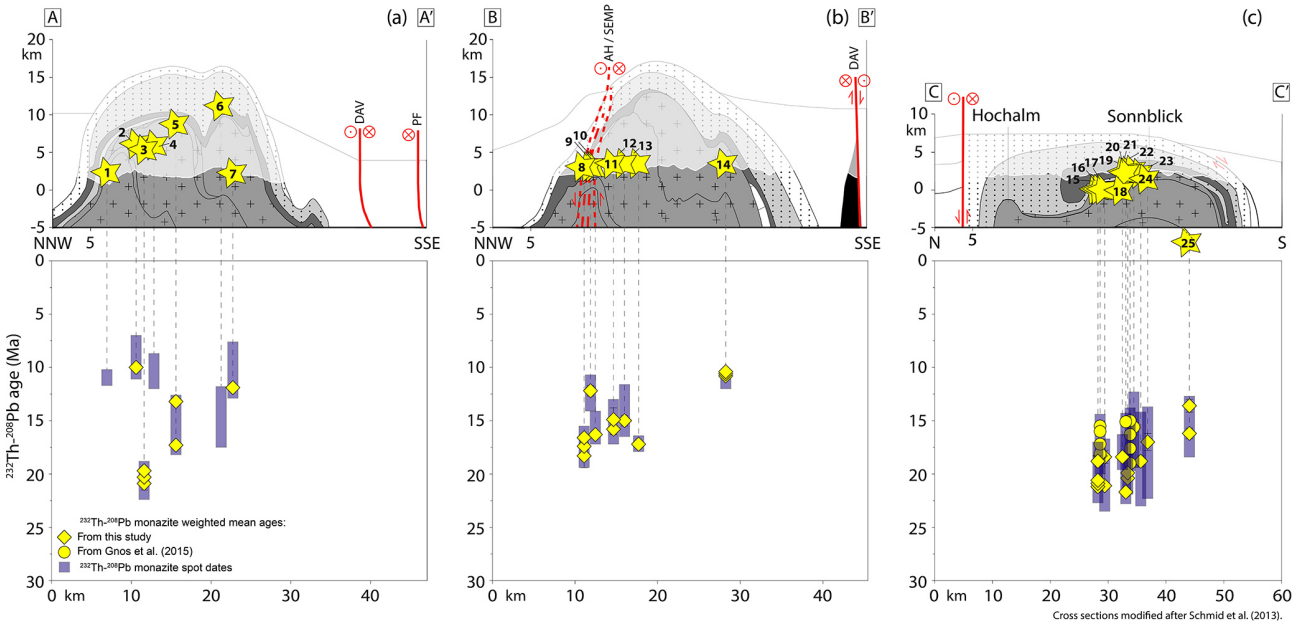


**Figure 6.** Cross sections of **(a)** the western part of the western subdome, **(b)** the central part of the western subdome and **(c)** the western end of the eastern subdome, modified after (Schmid et al., 2013). See Fig. 1 for locations and legend. Sample locations are indicated by yellow stars and identified by sample numbers listed in Table 1. Monazite crystallization ages are present in the lower part of the figure and are linked to each sample by light-grey dashed lines. Weighted mean ages from this study and from Gnos et al. (2015) are presented by yellow diamonds and yellow circles, respectively, and blue bars correspond to the range of single spot dates.

likely linked to the KNF and Mölltal fault (MöF) activity (samples 16, 21, 24 and 25; Fig. 7a and d; e.g. Favaro et al., 2017). In grains located in the western part of the eastern subdome, in the prolongation of the MöF (e.g. Kurz and Neubauer, 1996) (Fig. 1), numerous monazite growth domains yield ages between $15.6 \pm 0.7$ and $15.0 \pm 0.5$ Ma (bracketed by samples 22 and 21 from Gnos et al., 2015; Figs. 1, 6c, 7a and d; green circles in Fig. 7d; Table 4). These ages date the latest known activity of this shear zone to $\sim 15$ Ma. Whereas younger ages, associated with reactivation of fault zones are widespread in the central and western TW, tectonic movements seem to cease in the eastern TW after this time (Fig. 8c).

The youngest monazite growth domain ages, principally recorded in the western subdome, range from $13.2 \pm 0.3$ to $10.0 \pm 0.2$ Ma (samples 5 and 2; Table 4), indicating steps

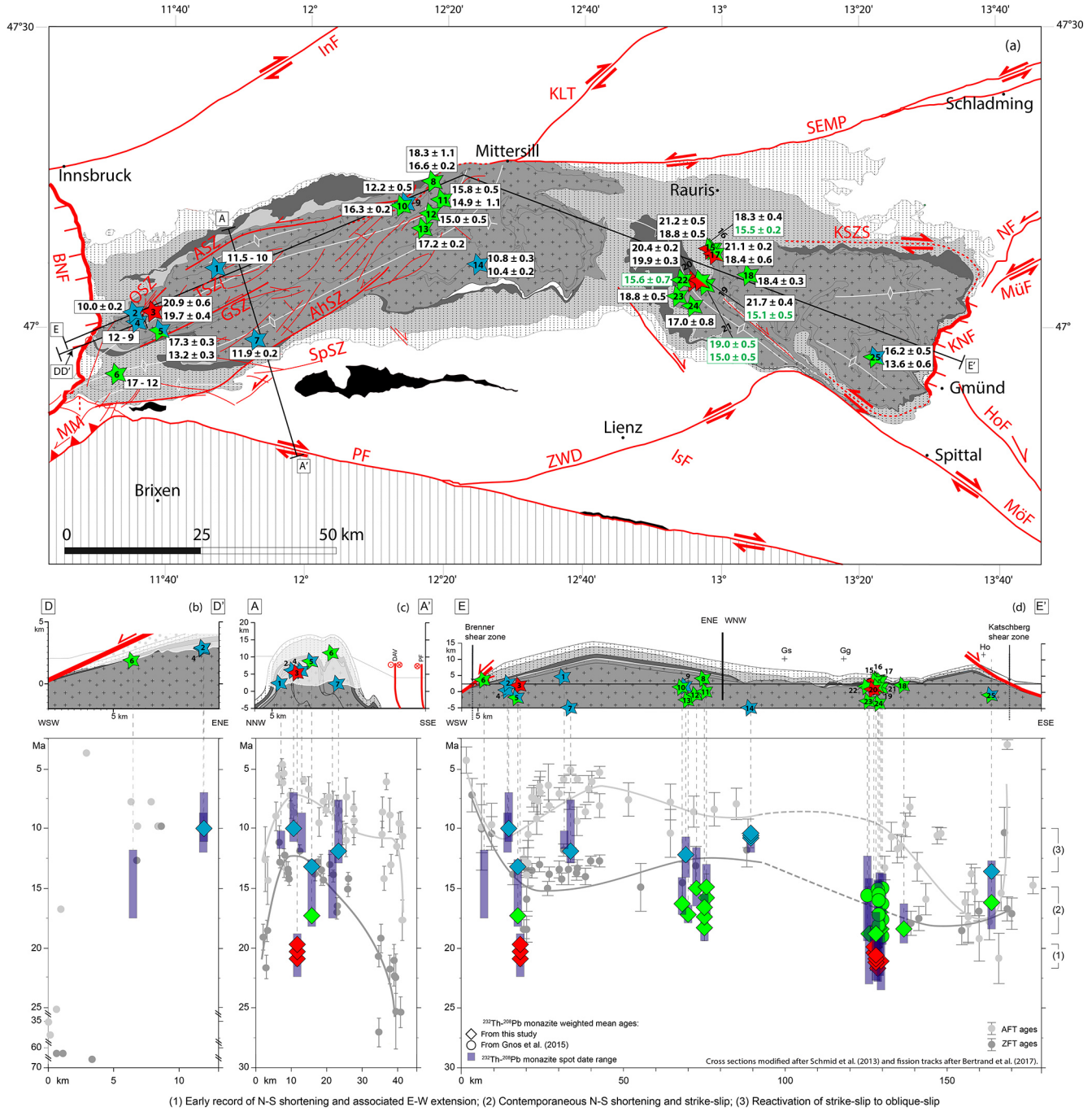


**Figure 7.** **(a)** Map of the TW from Fig. 1 with sample locations coloured as function of deformation episodes (coloured stars). See Fig. 1 for legend. **(b)** DD' NE–SW cross section across the BNF, **(c)** AA' NW–SE cross section perpendicular to the axial plane of the western subdome and **(d)** EE' longitudinal cross section parallel to the main axial plane of the TW metamorphic dome, modified after Bertrand et al. (2017). In the upper part, coloured and numbered stars correspond to sample locations and are linked to corresponding Th-Pb monazite ages by dashed vertical lines. Sample numbers refer to Table 1. In the lower part, monazite weighted mean ages from this study and from Gnos et al. (2015) are labelled by coloured diamond and circles, respectively, and the range of single spot dates is depicted by blue bars. The colour code used for diamonds and circles follows deformation episodes explained in the discussion. Note that most error bars are smaller than the size of the diamonds and circles. Zircon and apatite fission track ages are from the Bertrand et al. (2017) compilation; light- and dark-grey dots with error bars are displayed for comparison. Square brackets shown to the right delimit the main periods of monazite growth discussed in the text: (1) early record of N–S shortening and associated E–W extension, (2) contemporaneous N–S shortening and strike slip, (3) reactivation of strike slip to oblique slip.

of reactivation of the different sinistral strike-slip to oblique-slip movements along different faults (phase 3 and blue symbols in Fig. 7). Based on our monazite crystallization data, the oldest activities of this younger phase are recorded near the GSZ (sample 5) and in the prolongation of the AhSZ (samples 7 and 9). The youngest activities are recorded in association with the ASZ, OSZ and TSZ in Fig. 7a–c (samples 1, 2 and 4), and in the central TW in an area located south of the main fault systems (sample 14; Fig. 7a). In addition to faults activity at ∼ 12 Ma (Fig. 8), coeval strike-slip activity has also been documented in many areas of the central and western Alps (e.g. Bergemann et al., 2017, 2019; Berger et al., 2013; Gasquet et al., 2010; Grand'Homme et al., 2016a; Pleuger et al., 2012; Ricchi et al., 2019).

In summary, in the western TW, monazite ages (Fig. 1) constrain the activities of the ASZ (18–12 Ma, samples 8 and 9), AhSZ (17–12 Ma, samples 13 and 7), TSZ/OSZ (11.5–10 Ma, samples 1 and 2; older ages of sample 3 are probably related to extensional unroofing) and GSZ (17–13 Ma). In the eastern part, the MöF is active between 19 and 15 Ma.

### 5.2 Comparison with shear zone dating

A number of attempts to date shear zone activity in the TW using Ar-Ar, Rb-Sr and Sm-Nd techniques have been made in the past, which were, however, based on mineral separation techniques without a clear structural control on the dated grains (e.g. Blanckenburg et al., 1989; Glodny et al., 2008; Pollington and Baxter, 2010, 2011; Urbanek et al., 2002). An exception to this is the $^{40}Ar$ / $^{39}Ar$ study of Schneider et al. (2013) on syn-kinematic phengite and K-feldspar which will be used in the following as a comparison (Table 2). Fissure monazite ages largely corroborate this work, similarly showing the longevity of different shear zones in the TW. The ages confirm that even though most of the dated monazite samples are only located in the damage zone in the vicinity of the core of the shear zones, fluid-filled fissures provide a sensitive system where tectonic activity triggers fluid-enhanced dissolution–precipitation reactions at lower greenschist to sub-greenschist facies conditions.

While Schneider et al. (2013) obtained crystallization age ranges of 33–15 Ma for the ASZ, 24–12 Ma for the TSZ and 20–7 Ma for the GSZ (Table 2), our data confirm fluid activity, and thus possible tectonic activity, at 18–12, 11.5–10 and 17–13 Ma, respectively (Fig. 7). However, the oldest dates from Schneider et al. (2013) might also be interpreted as older grains that have been aligned in the new foliation (Fig. 8). The data presented here indicate that all of the shear zones where potentially active at least until ∼ 13–12 Ma, and the Tuxer and/or Olperer shear zones even until ∼ 7 Ma, as suggested by younger dates observed in grain 2 (Figs. 3b, 6a and 7, Tables 3 and 4). However, the fissure monazite data do not date the initiation of the GSZ (Selverstone et al., 1991) nor the earliest activity of the TSZ (greenschist to amphibolite facies; Selverstone et al., 1984, 1991) or the ASZ

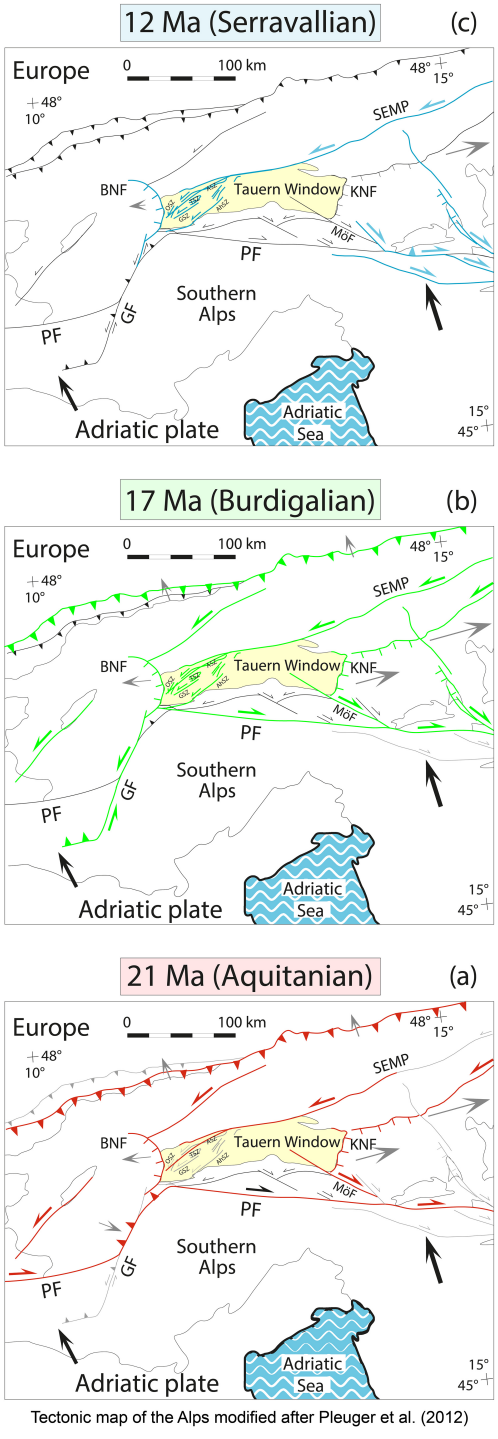


**Figure 8.** Tectonic map of the Alps based on Pleuger et al. (2012) showing active Cenozoic faults at ∼ 21 (in red), 17 (in green) and 12 Ma (in blue), respectively. Note that after 17 Ma the Giudicarie fault (GF) becomes active and hence the Periadriatic fault (PF) and the Mölltal fault (MöF, dextral fault at the southeastern corner of the TW) become inactive. Sinistral strike-slip faulting starts at ∼ 19 Ma and is affecting the western and central parts of the TW until at least 7 Ma. Future active faults are depicted in grey and inactive faults in black.

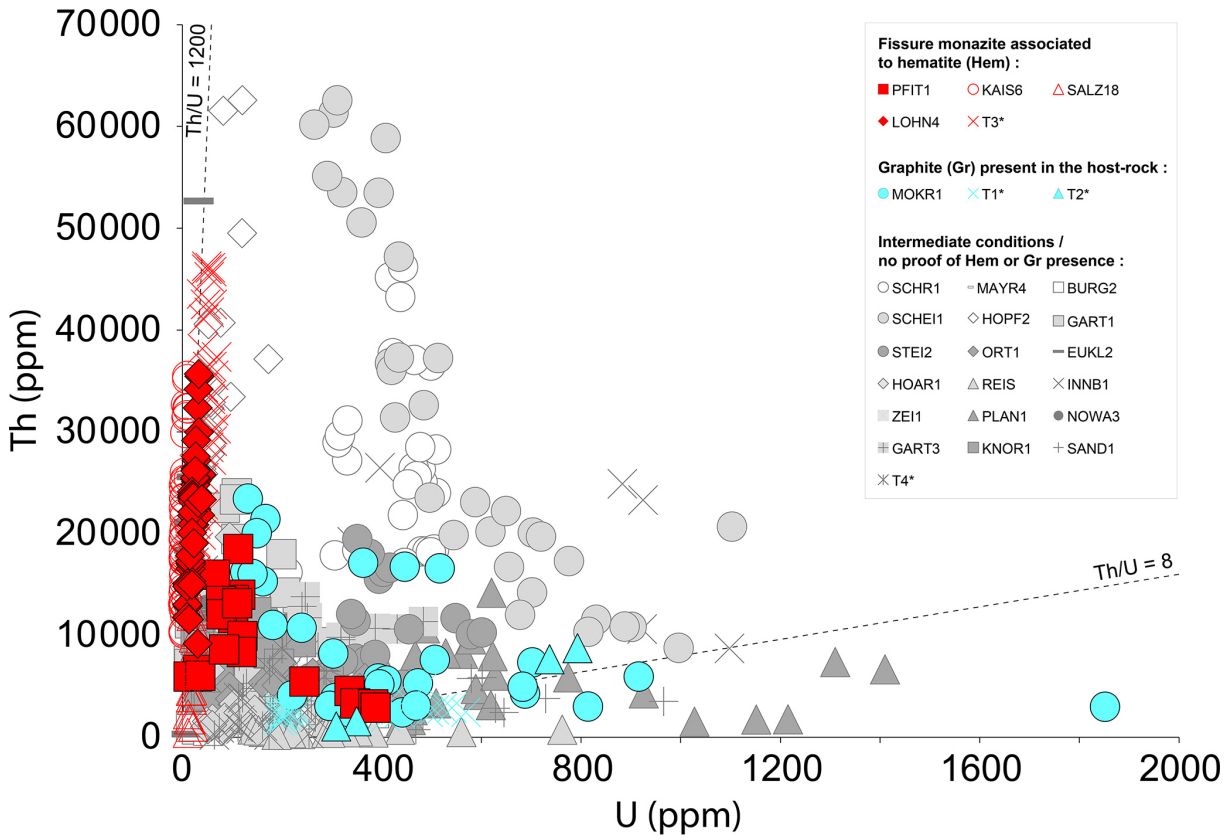


**Figure 9.** Th as function of U content obtained for all the monazite grains analysed in this study. Samples indicated by an asterisk are from Gnos et al. (2015). Fissure monazite grains associated with hematite (oxidizing conditions) are labelled in red, whereas grains hosted in graphite-bearing rocks (reducing conditions) are labelled in blue. Samples with intermediate composition and/or for which we have no information on the presence of hematite or graphite in the fissure environment are labelled in grey.

(greenschist facies; Cole et al., 2007), since their formation already started at amphibolite facies conditions. As Alpine fissures only form under greenschist facies conditions, the oldest monazite crystallization ages are younger than the data obtained by Schneider et al. (2013). This indicates that shear zone activity started earlier than the fissure monazite record. As the monazite age range of the younger fault activity is comparable to the data of Schneider et al. (2013) but is not the same for individual shear zones, it seems likely that all shear zones of the western TW were active as recently as 8–7 Ma.

### 5.3 Comparison with fission track data

There is a wealth of zircon fission track (ZFT) data that can assist in describing the exhumation and low-grade tectonic activity in the TW (Bertrand, 2014; Bertrand et al., 2017; Dunkl et al., 2003; Fügenschuh et al., 1997; Mancktelow et al., 2001; Most, 2003; Pomella et al., 2011; Steenken et al., 2002; Stöckhert et al., 1999; Viola et al., 2001; Wölfler et al., 2008) and apatite fission track (AFT) data (Bertrand, 2014; Bertrand et al., 2017; Coyle, 1994; Di Fiore, 2013; Foeken et al., 2007; Fügenschuh et al., 1997; Grundmann and Morteani, 1985; Hejl, 1997; Mancktelow et al., 2001; Most, 2003; Pomella et al., 2011; Staufenberg, 1987; Steenken et al., 2002; Viola et al., 2001; Wölfler et al., 2008, 2012).

Three cross sections, DD' (perpendicular to the BNF), AA' (perpendicular to the western limb of the western subdome) and EE' (parallel to the main axial plane of the TW), are presented in Fig. 7, redrawn after Bertrand et al. (2017) and Schmid et al. (2013). Zircon and apatite fission track data compiled by Bertrand et al. (2017) are displayed in the lower part of Fig. 7b–d and compared to fissure monazite ages. As described in Bertrand et al. (2017) (first model), fission track data along the AA' cross section (Fig. 7c) nicely display a dome-like shape, with younger ages recorded near the subdome axial plane, where cooling was slower. By contrast, along the EE' longitudinal cross section (Fig. 7d), ZFT and AFT are younger on the western and eastern borders of the TW where the two major extensional faults, the BNF and KNF, are respectively located. Perpendicular to the BNF (DD' cross section, Fig. 7b), the fission tracks record cooling ages younging from the footwall toward the plane of the normal fault (from 10 to 4 Ma for AFT; second model

of Bertrand et al., 2017). Along the EE' cross section, the youngest monazite ages (15–10 Ma) lie between zircon and apatite fission track data (grey and blue symbols), whereas the older ages (> 17 Ma) do not follow the cooling trend and are equal to or older than the ZFT data. This means that at least the fissure monazites recording older ages crystallized somewhere above ZFT closure temperatures of ∼ 240–280 °C (Bernet, 2009; Bernet and Garver, 2005; Reiners, 2005; Yamada et al., 1995) (Fig. 7d).

### 5.4 Monazite Th/U as monitor of oxidizing and reducing conditions

Extreme low and high Th/U ratios described in fissure monazite by Gnos et al. (2015) (T1, T2 and T3 samples in Fig. 9) are also observed in some grains from this study (red and blue labels in Fig. 9). Hydrothermal monazite from the TW associated with hematite in fissure typically displays very high Th/U ratios of around 1200 (Fig. 9, red labels; Table 1), whereas grains obtained from graphite-bearing host rocks show very low Th/U ratios around 8 (Fig. 9, blue labels; Table 1). This attests for oxidizing and reducing fluid conditions in the fissure environment, respectively.

The Th/U in monazite grains PFIT1 and MOKR1 would instead record a dynamic oxidation environment due to variable fluid conditions. In PFIT1 monazite, the Th/U decreases from core to rim, whereas within MOKR1 the opposite evolution is observed (Fig. 9). Thus, in the first case, the fissure environment evolves toward reducing conditions, whereas in the second case there is an evolution towards more oxidizing conditions. Many of the other grains indicate intermediate oxidizing conditions and they could not be assigned to one of the two categories defined above, as the presence of either hematite or graphite is uncertain (Fig. 9; grey labels).

## 6 Conclusions

Th-Pb ages of fissure monazite provide an extended record of exhumation of the TW during the Miocene. The investigated monazites crystallized at temperatures < 400 °C in the presence of hydrothermal fluids that circulated in open fissures formed through tectonic movements. The Th-Pb ages recorded by fissure monazites are in general agreement with previously published geochronological data and range between $21.7 \pm 0.4$ and $10.0 \pm 0.2$ Ma. Spot dates suggests that monazite crystallization in the metamorphic and structural TW dome occurred over a period of ∼ 16 Myr. The combination of structural and geochronological information allows relating monazite growth to tectonic movements that affected the TW. The three major growth episodes identified in this study, by dating monazite growth domains, are interpreted to be associated with N–S shortening associated with the E–W extension (22–20 Ma), contemporaneous N–S shortening and sinistral strike-slip movements (19–15 Ma) and reactivation of strike-slip/normal faulting (14–10 Ma). Overall, fissure monazite age recording indicates that in the TW Cenozoic faults show increased activity at ∼ 21, ∼ 17 and ∼ 12 Ma, probably due to reorganization of plate movements occurring at those times. Comparison of Th-Pb fissure monazite crystallization ages with existing crystallization and cooling ages (e.g. AFT, ZFT, white mica from fault zones) shows that the latest stages of monazite crystallization occurred at temperatures between apatite and zircon fission track "closure" temperatures. This enlarged dataset also supports previous observations on fissure monazite chemistry displaying extremely high Th/U ratios (∼ 1200) under oxidizing conditions in association with hematite.

*Data availability.* The data used in this study are available in Tables 3 and 4.

*Supplement.* The supplement related to this article is available online at: https://doi.org/10.5194/se-11-437-2020-supplement.

*Author contributions.* Fissure monazite samples were organized by EG and FW. Monazite samples for dating were selected by ER, CAB, EG and AB according to tectonic settings and fault activity of the study area. ER prepared the manuscript during her PhD project under the supervision of EG, with contributions from all coauthors. Sample preparation and BSE imaging were performed by ER and CAB. Data acquisition and reduction at the SwissSIMS and NordSIMS facility was, respectively, carried out by ER and CAB under the supervision of DR and MJW.

*Competing interests.* The authors declare that they have no conflict of interest.

*Acknowledgements.* We thank Sepp Brugger, Kurt Novak, Franz Gartner, Peter Hellweger, Adolf Meyer, Sebastian Planken-Steiner, Johann Rappold, Josef Rathgeb, Alexandre Salzmann, Maria Schaffhauser, Andreas Steiner, and Ermin Welzl for providing samples for this study. Urs Klötzli and Jan Pleuger are thanked for their helpful comments.

*Financial support.* This research has been supported by the Swiss National Science Foundation (grant no. 200020-165513). The NordSIMS facility received funding from the Swedish Research Council (infrastructure grant no. 2014-06375) and the Swedish Museum of Natural History; this is NordSIMS publication no. 636.

*Review statement.* This paper was edited by Bernhard Grasemann and reviewed by Jan Pleuger and Urs Klötzli.

## References


Aleinikoff, J. N., Schenck, W. S., Plank, M. O., Srogi, L. A., Fanning, C. M., Kamo, S. L., and Bosbyshell, H.: Deciphering igneous and metamorphic events in high-grade rocks of the Wilmington complex, Delaware: Morphology, cathodoluminescence and backscattered electron zoning, and SHRIMP U-Pb geochronology of zircon and monazite, Bull. Geol. Soc. Am., 118, 39–64, https://doi.org/10.1130/B25659.1, 2006.

Ayers, J. C., Miller, C., Gorisch, B., and Milleman, J.: Textural development of monazite during high-grade metamorphism: Hydrothermal growth kinetics, with implications for U,Th-Pb geochronology, Am. Mineral., 84, 1766–1780, https://doi.org/10.2138/am-1999-11-1206, 1999.

Bergemann, C. A., Gnos, E., Berger, A., Whitehouse, M., Mullis, J., Wehrens, P., Pettke, T., and Janots, E.: Th-Pb ion probe dating of zoned hydrothermal monazite and its implications for repeated shear zone activity: An example from the Central Alps, Switzerland, Tectonics, 36, 671–689, https://doi.org/10.1002/2016TC004407, 2017.

Bergemann, C. A., Gnos, E., Berger, A., Whitehouse, M. J., Mullis, J., Walter, F., and Bojar, H. P.: Constraining long-term fault activity in the brittle domain through in situ dating of hydrothermal monazite, Terra Nov., 30, 440–446, https://doi.org/10.1111/ter.12360, 2018.

Bergemann, C. A., Gnos, E., and Whitehouse, M. J.: Insights into the tectonic history of the Western Alps through dating of fissure monazite in the Mont Blanc and Aiguilles Rouges Massifs, Tectonophysics, 750, 203–212, https://doi.org/10.1016/j.tecto.2018.11.013, 2019.

Bergemann, C. A., Gnos, E., Berger, A., Janots, E., and Whitehouse, M. J.: Dating tectonic activity in the Lepontine Dome and Rhone-Simplon Fault regions through hydrothermal monazite-(Ce), Solid Earth, 11, 199–222, https://doi.org/10.5194/se-11-199-2020, 2020.

Berger, A., Gnos, E., Janots, E., Whitehouse, M., Soom, M., Frei, R., and Waight, T. E.: Dating brittle tectonic movements with cleft monazite: Fluid-rock interaction and formation of REE minerals, Tectonics, 32, 1176–1189, https://doi.org/10.1002/tect.20071, 2013.

Bernet, M.: A field-based estimate of the zircon fission-track closure temperature, Chem. Geol., 259, 181–189, https://doi.org/10.1016/j.chemgeo.2008.10.043, 2009.

Bernet, M. and Garver, J. I.: Fission-track analysis of detrital zircon, Rev. Mineral. Geochem., 58, 205–237, 2005.

Bertrand, A.: Exhuming the core of collisional orogens, the Tauern Window (Eastern-Alps), A geochronological, modelling and structural study, PhD tesis, Freie Univ. Berlin, 2014.

Bertrand, A., Rosenberg, C., and Garcia, S.: Fault slip analysis and late exhumation of the Tauern Window, Eastern Alps, Tectonophysics, 649, 1–17, https://doi.org/10.1016/j.tecto.2015.01.002, 2015.

Bertrand, A., Rosenberg, C., Rabaute, A., Herman, F., and Fügenschuh, B.: Exhumation mechanisms of the Tauern Window (Eastern Alps) inferred from apatite and zircon fission track thermochronology, Tectonics, 36, 207–228, https://doi.org/10.1002/2016TC004133, 2017.

Blanckenburg, F. v., Villa, I. M., Baur, H., Morteani, G., and Steiger, R. H.: Time calibration of a PT-path from the Western Tauern Window, Eastern Alps: the problem of closure temperatures, Contrib. Mineral. Petrol., 101, 1–11, https://doi.org/10.1007/BF00387196, 1989.

Cherniak, D. J., Watson, E. B., Grove, M., and Harrison, T. M.: Pb diffusion in monazite: A combined RBS/SIMS study, Geochim. Cosmochim. Ac., 68, 829–840, https://doi.org/10.1016/j.gca.2003.07.012, 2004.

Cole, J., Hacker, B., Ratschbacher, L., Dolan, J., Seward, G., Frost, E., and Frank, W.: Localized ductile shear below the seismogenic zone: Structural analysis of an exhumed strike-slip fault, Austrian Alps, J. Geophys. Res.-Sol. Ea., 112, 1–15, https://doi.org/10.1029/2007JB004975, 2007.

Coyle, D. A.: The application of apatite fission-track analysis to problem in tectonics, PhD thesis, La Trobe Univ. Bundoora, Victoria, Australia, 1994.

Di Fiore, G.: Evoluzione Morfotettonica delle aree alpine "Sempione" e "Brennero" attraverso studi termocronologici di bassa temperatura, PhD thesis, Università di Bologna, 2013.

Dunkl, I., Frisch, W., and Grundmann, G.: Zircon fission-track thermochronology of the south-eastern part of the TW and the adjacent Austroalpine margin, Eastern Alps, Eclogae Geol. Helv., 96, 209–217, 2003.

Favaro, S., Handy, M. R., Scharf, A., and Schuster, R.: Changing patterns of exhumation and denudation in front of an advancing crustal indenter, Tauern Window (Eastern Alps), Tectonics, 36, 1053–1071, https://doi.org/10.1002/2016TC004448, 2017.

Fitz-Diaz, E., Cottle, J. M., Vidal-Reyes, M. I., and van der Pluijm, B.: In situ Th/Pb dating of monazite in fibrous veins: Direct dating of veins and deformation in the shallow upper crust of the Mexican Orogen, J. Struct. Geol., 124, 136–142, https://doi.org/10.1016/j.jsg.2019.04.004, 2019.

Foeken, J. P. T., Persano, C., Stuart, F. M., and ter Voorde, M.: Role of topography in isotherm perturbation: Apatite (U−Th)/He and fission track results from the Malta tunnel, Tauern Window, Austria, Tectonics, 26, https://doi.org/10.1029/2006TC002049, 2007.

Fügenschuh, B., Seward, D., and Mancktelow, N.: Exhumation in a convergent orogen: the western Tauern Window, Terra Nov., 9, 213–217, https://doi.org/10.1111/j.1365-3121.1997.tb00015.x, 1997.

Gardés, E., Jaoul, O., Montel, J. M., Seydoux-Guillaume, A. M., and Wirth, R.: Pb diffusion in monazite: An experimental study of $Pb^{2+} + Th^{4+} <=> 2Nd^{3+}$ interdiffusion, Geochim. Cosmochim. Ac., 70, 2325–2336, https://doi.org/10.1016/j.gca.2006.01.018, 2006.

Gardés, E., Montel, J. M., Seydoux-Guillaume, A. M., and Wirth, R.: Pb diffusion in monazite: New constraints from the experimental study of $Pb^{2+} <=> Ca^{2+}$ interdiffusion, Geochim. Cosmochim. Ac., 71, 4036–4043, https://doi.org/10.1016/j.gca.2007.06.036, 2007.

Gasquet, D., Bertrand, J. M., Paquette, J. L., Lehmann, J., Ratzov, G., Ascenção De Guedes, R. A., Tiepolo, M., Boullier, A. M., Scaillet, S., and Nomade, S.: Miocene to Messinian deformation and hydrothermal activity in a pre-Alpine basement massif of the French western Alps: New U-Th-Pb and argon ages from the Lauzière massif, Bull. Soc. Geol. Fr., 181, 227–241, https://doi.org/10.2113/gssgfbull.181.3.227, 2010.

Glodny, J., Ring, U., and Kühn, A.: Coeval high-pressure metamorphism, thrusting, strike-slip, and extensional shear-

ing in the Tauern Window, Eastern Alps, Tectonics, 27, https://doi.org/10.1029/2007TC002193, 2008.

Gnos, E., Janots, E., Berger, A., Whitehouse, M., Walter, F., Pettke, T., and Bergemann, C. A.: Age of cleft monazites in the eastern Tauern Window: constraints on crystallization conditions of hydrothermal monazite, Swiss J. Geosci., 108, 55–74, https://doi.org/10.1007/s00015-015-0178-z, 2015.

Grand'Homme, A., Janots, E., Bosse, V., Seydoux-Guillaume, A. M., and Ascenção De Guedes, R. A.: Interpretation of U-Th-Pb in-situ ages of hydrothermal monazite-(Ce) and xenotime-(Y): evidence from a large-scale regional study in clefts from the western alps, Mineral. Petrol., 110, 787–807, https://doi.org/10.1007/s00710-016-0451-5, 2016a.

Grand'Homme, A., Janots, E., Seydoux-Guillaume, A. M., Guillaume, D., Bosse, V., and Magnin, V.: Partial resetting of the U-Th-Pb systems in experimentally altered monazite: Nanoscale evidence of incomplete replacement, Geology, 44, 431–434, https://doi.org/10.1130/G37770.1, 2016b.

Grand'Homme, A., Janots, E., Seydoux-Guillaume, A. M., Guillaume, D., Magnin, V., Hövelmann, J., Höschen, C., and Boiron, M. C.: Mass transport and fractionation during monazite alteration by anisotropic replacement, Chem. Geol., 484, 51–68, https://doi.org/10.1016/j.chemgeo.2017.10.008, 2018.

Grundmann, G. and Morteani, G.: The young uplift and thermal history of the central Eastern Alps (Austria/Italy), evidence from apatite fission track ages, Jahrb. Geol. Bundesanst, 128, 197–216, 1985.

Hejl, E.: "Cold spots" during the Cenozoic evolution of the Eastern Alps: Thermochronological interpretation of apatite fission-track data, Tectonophysics, 272, 159–173, https://doi.org/10.1016/S0040-1951(96)00256-9, 1997.

Janots, E., Berger, A., Gnos, E., Whitehouse, M., Lewin, E., and Pettke, T.: Constraints on fluid evolution during metamorphism from U–Th–Pb systematics in Alpine hydrothermal monazite, Chem. Geol., 326, 61–71, 2012.

Janots, E., Grand'Homme, A., Bernet, M., Guillaume, D., Gnos, E., Boiron, M.-C., Rossi, M., Seydoux-Guillaume, A.-M., and De Ascenção Guedes, R.: Geochronological and thermometric evidence of unusually hot fluids in an Alpine fissure of Lauzière granite (Belledonne, Western Alps), Solid Earth, 10, 211–223, https://doi.org/10.5194/se-10-211-2019, 2019.

Kurz, W. and Neubauer, F.: Deformation partitioning during updoming of the Sonnblick area in the Tauern Window (Eastern Alps, Austria), J. Struct. Geol., 18, 1327–1337, https://doi.org/10.1016/S0191-8141(96)00057-0, 1996.

Ludwig, K. R.: User's manual for a geochronological toolkit for Microsoft Excel (Isoplot/Ex version 3.0), Berkeley Geochronol. Cent. Spec. Publ., 4, 1–70, 2003.

Luth, S. W. and Willingshofer, E.: Mapping of the post-collisional cooling history of the Eastern Alps, Swiss J. Geosci., 101, 207–223, https://doi.org/10.1007/s00015-008-1294-9, 2008.

Mancktelow, N. S., Stöckli, D. F., Grollimund, B., Müller, W., Fügenschuh, B., Viola, G., Seward, D., and Villa, I. M.: The DAV and Pediatriatic fault systems in the Eastern Alps South of the Tauern window, Int. J. Earth Sci., 90, 593–622, https://doi.org/10.1007/s005310000190, 2001.

Most, P.: Late Alpine cooling histories of tectonic blocks along the central part of the Transalp-Traverse (Inntal-Gadertal): Constraints from geochronology, PhD thesis, University of Tübingen, p. 97, 2003.

Mullis, J.: P-T-t path of quartz formation in extensional veins of the Central Alps, Schweiz. Miner. Petrogr. Mitt, 76, 159–164, https://doi.org/10.5169/seals-57694, 1996.

Mullis, J., Dubessy, J., Poty, B., and O'Neil, J.: Fluid regimes during late stages of a continental collision: physical, chemical, and stable isotope measurements of fluid inclusions in fissure quartz from a geotraverse through the Central Alps, Switzerland, Geochim. Cosmochim. Ac., 58, 2239–2267, 1994.

Pleuger, J., Mancktelow, N., Zwingmann, H., and Manser, M.: K-Ar dating of synkinematic clay gouges from Neoalpine faults of the Central, Western and Eastern Alps, Tectonophysics, 550, 1–16, https://doi.org/10.1016/j.tecto.2012.05.001, 2012.

Pollington, A. D. and Baxter, E. F.: High resolution Sm-Nd garnet geochronology reveals the uneven pace of tectonometamorphic processes, Earth Planet. Sc. Lett., 293, 63–71, https://doi.org/10.1016/j.epsl.2010.02.019, 2010.

Pollington, A. D. and Baxter, E. F.: High precision microsampling and preparation of zoned garnet porphyroblasts for Sm-Nd geochronology, Chem. Geol., 281, 270–282, https://doi.org/10.1016/j.chemgeo.2010.12.014, 2011.

Pomella, H., Klötzli, U., Scholger, R., Stipp, M., and Fügenschuh, B.: The Northern Giudicarie and the Meran-Mauls fault (Alps, Northern Italy) in the light of new paleomagnetic and geochronological data from boudinaged Eo-/Oligocene tonalites, Int. J. Earth Sci., 100, 1827–1850, https://doi.org/10.1007/s00531-010-0612-4, 2011.

Putnis, A.: Mineral Replacement Reactions, Rev. Miner. Geochem., 70, 87–124, https://doi.org/10.2138/rmg.2009.70.3, 2009.

Reiners, P. W.: Zircon (U−Th)/He Thermochronometry, in: Reviews in Mineralogy and Geochemistry, vol. 58, 151–179, 2005.

Ricchi, E., Bergemann, C. A., Gnos, E., Berger, A., Rubatto, D., and Whitehouse, M. J.: Constraining deformation phases in the Aar Massif and the Gotthard Nappe (Switzerland) using Th-Pb crystallization ages of fissure monazite-(Ce), Lithos, 342/343, 223–238, https://doi.org/10.1016/j.lithos.2019.04.014, 2019.

Rosenberg, C. L. and Berger, A.: On the causes and modes of exhumation and lateral growth of the Alps, Tectonics, 28, https://doi.org/10.1029/2008TC002442, 2009.

Rosenberg, C. L. and Garcia, S.: Estimating displacement along the Brenner Fault and orogen-parallel extension in the Eastern Alps, Int. J. Earth Sci., 100, 1129–1145, https://doi.org/10.1007/s00531-011-0645-3, 2011.

Rosenberg, C. L. and Schneider, S.: The western termination of the SEMP Fault (eastern Alps) and its bearing on the exhumation of the Tauern Window, Geol. Soc. Lond. Spec. Publ., 298, 197–218, 2008.

Rosenberg, C. L., Schneider, S., Scharf, A., Bertrand, A., Hammerschmidt, K., Rabaute, A., and Brun, J. P.: Relating collisional kinematics to exhumation processes in the Eastern Alps, Earth-Sci. Rev., 176, 311–344, https://doi.org/10.1016/j.earscirev.2017.10.013, 2018.

Scharf, A., Handy, M. R., Favaro, S., Schmid, S. M., and Bertrand, A.: Modes of orogen-parallel stretching and extensional exhumation in response to microplate indentation and roll-back subduction (Tauern Window, Eastern Alps), Int. J. Earth Sci., 102, 1627–1654, https://doi.org/10.1007/s00531-013-0894-4, 2013.

Schmid, S. M., Fügenschuh, B., Kissling, E., and Schuster, R.: Tectonic map and overall architecture of the Alpine orogen, Eclogae Geol. Helv., 97, 93–117, https://doi.org/10.1007/s00015-004-1113-x, 2004.

Schmid, S. M., Scharf, A., Handy, M. R., and Rosenberg, C. L.: The Tauern Window (Eastern Alps, Austria): a new tectonic map, with cross-sections and a tectonometamorphic synthesis, Swiss J. Geosci., 106, 1–32, https://doi.org/10.1007/s00015-013-0123-y, 2013.

Schneider, S., Hammerschmidt, K., and Rosenberg, C. L.: Dating the longevity of ductile shear zones: Insight from $^{40}Ar/^{39}Ar$ in situ analyses, Earth Planet. Sc. Lett., 369–370, 43–58, https://doi.org/10.1016/j.epsl.2013.03.002, 2013.

Selverstone, J.: Evidence for east-west crustal extension in the Eastern Alps: Implications for the unroofing history of the Tauern Window, Tectonics, 7, 87–105, 1988.

Selverstone, J., Spear, F. S., Franz, G., and Morteani, G.: High-pressure metamorphism in the SW tauern window, Austria: P-T paths from hornblende-kyanite-staurolite schists, J. Petrol., 25, 501–531, https://doi.org/10.1093/petrology/25.2.501, 1984.

Selverstone, J., Morteani, G., and Staude J.-M: Fluid channelling during ductile shearing: transformation of granodiorite into aluminous schist in the Tauern Window, Eastern Alps, J. Metamorph. Geol., 9, 419–431, 1991.

Seydoux-Guillaume, A. M., Montel, J. M., Bingen, B., Bosse, V., de Parseval, P., Paquette, J. L., Janots, E., and Wirth, R.: Low-temperature alteration of monazite: Fluid mediated coupled dissolution-precipitation, irradiation damage, and disturbance of the U-Pb and Th-Pb chronometers, Chem. Geol., 330/331, 140–158, https://doi.org/10.1016/j.chemgeo.2012.07.031, 2012.

Sharp, Z. D., Masson, H., and Lucchini, R.: Stable isotope geochemistry and formation mechanisms of quartz veins; extreme paleoaltitudes of the Central Alps in the Neogene, Am. J. Sci., 305, 187–219, 2005.

Spencer, C. J., Kirkland, C. L., and Taylor, R. J. M.: Geoscience Frontiers Strategies towards statistically robust interpretations of in situ U e Pb zircon geochronology, Geosci. Front., 7, 581–589, https://doi.org/10.1016/j.gsf.2015.11.006, 2016.

Stacey, J. S. and Kramers, J. D.: Approximation of terrestrial lead isotope evolution by a two-staged model, Earth Planet. Sc. Lett., 26, 207–221, 1975.

Staufenberg, H.: Apatite fission-track evidence for postmetamorphic uplift and cooling history of the Eastern Tauern Window and the surrounding Austroalpine (Central Eastern Alps, Austria), Jahrb. Geol. Bundesanst, 130, 571–586, 1987.

Steenken, A., Siegesmund, S., Heinrichs, T., and Fügenschuh, B.: Cooling and exhumation of the Rieserferner Pluton (Eastern Alps, Italy/Austria), Int. J. Earth Sci., 91, 799–817, https://doi.org/10.1007/s00531-002-0260-4, 2002.

Stöckhert, B., Brix, M. R., Kleinschrodt, R., Hurford, A. J., and Wirth, R.: Thermochronometry and microstructures of quartz-a comparison with experimental flow laws and predictions on the temperature of the brittle-plastic transition, J. Struct. Geol., 21, 351–369, https://doi.org/10.1016/S0191-8141(98)00114-X, 1999.

Urbanek, C., Frank, W., Grasemann, B., and Decker, K.: Eoalpine versus Tertiary deformation: dating of heterogeneously partitioned strain (Tauern Window, Austria), in Abstract volume, edited by: PanGeo Austria, 183–184, 2002.

Viola, G., Mancktelow, N. S., and Seward, D.: Late oligocene-neogene evolution of Europe-Adria collision: New structural and geochronological evidence from the Giudicarie fault system (Italian Eastern Alps), Tectonics, 20, 999–1020, https://doi.org/10.1029/2001TC900021, 2001.

Wölfler, A., Dekant, C., Danišík, M., Kurz, W., Dunkl, I., Putiš, M., and Frisch, W.: Late stage differential exhumation of crustal blocks in the central Eastern Alps: Evidence from fission track and (U-Th)/He thermochronology, Terra Nov., 20, 378–384, https://doi.org/10.1111/j.1365-3121.2008.00831.x, 2008.

Wölfler, A., Stüwe, K., Danišík, M., and Evans, N. J.: Low temperature thermochronology in the Eastern Alps: Implications for structural and topographic evolution, Tectonophysics, 541, 1–18, https://doi.org/10.1016/j.tecto.2012.03.016, 2012.

Yamada, R., Tagami, T., Nishimura, S., and Ito, H.: Annealing kinetics of fission tracks in zircon?: an experimental study, Chem. Geol., 122, 249–258, 1995.